

IMPACT PROOF PRELIMINARY DESIGN FOR THE
MARINE BIOLOGY STATION IN DICHATO

2016/2017

PART III
APPENDIX



Table of Contents

A	General background information	5
A.1	Geography, population and industry of Chile	5
A.2	The physics of earthquakes and tsunamis	5
A.3	History of seismic events in Chile	6
A.4	History of regional tsunami events.....	9
A.5	General seismic design philosophy.....	9
A.6	Chilean seismic design practice and codes: past vs. present.....	10
A.7	Chilean construction practice.....	11
A.8	The Maule Earthquake and Tsunami of February 27, 2010.....	12
B	Geotechnical background information	17
B.1	Geological regional history	17
B.2	Geology At Dichato Bay.....	17
B.3	Regional mining activity.....	17
B.4	Geotechnical ground mass characterisation.....	18
B.5	Foundation design	24
C	Site observations Coliumo Bay	26
C.1	Dichato, November 11, 2016	26
C.2	Coliumo, November 26, 2016	28
C.3	Dichato, December 1, 2016.....	30
D	Evaluation of Alternatives	36
D.1	Multi-Criteria Analysis	36
D.2	Weight factors	37
D.3	Costs	38
E	Dimensioning: Jetty.....	40
E.1	Dimensioning according to rules of thumb	40
E.2	Jetty foundation piles	41
F	Dimensioning: Breakwater	49
F.1	First Determination Design Storm	49
F.2	SWANONE.....	52
F.3	Requirements.....	53
G	Design: Jetty.....	57

G.1	Evaluating Marco Aislado Configuration.....	57
G.2	Material properties	58
G.3	Input ETABS.....	59
G.4	Load cases.....	63
G.5	Correction loads for final design	71
G.6	Foundation Piles.....	72
G.7	Structural Checks	80
H	Design: Breakwater	98
H.1	Determination design storm	98
H.2	Wave modelling	105
H.3	BREAKWAT3.0.....	112
H.3.2	Model input	114
H.4	Plaxis 2D	116
I.	Design: Pavement.....	124
I	Stone and sand analysis.....	127
I.1	Dichato revetment grading analysis.....	127
I.2	Dichato sand grading analysis.....	130
J	Extreme Impact Evaluation: Tsunami Loads	131
J.1	Computation of forces.....	131
J.2	Numerical tsunami simulation	134
J.3	Assumptions.....	136
J.4	Results	137
J.5	Load combinations	138
K	Extreme Impact Evaluation: Geohazards	139
K.1	Slope failure	139
L	Structural Drawings	145
L.1	3D Impressions	145
	References.....	149

A GENERAL BACKGROUND INFORMATION

A.1 GEOGRAPHY, POPULATION AND INDUSTRY OF CHILE

The Republic of Chile is a modern, industrialized country (NEHRP Consultants, 2012) extending 4300 kilometres along the southern half of the Pacific coast of South America. A mere 175 kilometres in width, its topography consists of a central plain between coastal mountains in the west and the Andes mountain range in the east. Current estimates of the population lie around 17 million, with 89% living in urban areas. The Chilean economy is among the most stable of South America, and its GDP is composed mainly of industry, including mineral production; agriculture, including beef, fish and wine; and services and tourism (Central Intelligence Agency, 2013). However, a report by the Organization for Economic Co-Operation and Development (OECD) states that amongst developed countries: “Chile is the OECD country with the greatest difference between the rich and the poor, as well as the 4th poorest country”, in a 2011 report on inequality (Immervoll, 2011).

A.2 THE PHYSICS OF EARTHQUAKES AND TSUNAMIS

Chile is located along the subduction zone of the Nazca Plate. This plate converges with the South American plate at a rate of approximately 8 cm per year, generating interplate type thrust earthquakes. When the overriding South American plate ‘sticks’ to the subducting Nazca plate, it bulges, see Figure A-1. This movement may continue for decades or centuries, slowly accumulating stresses. During an earthquake, the leading edge of the overriding plate is freed and springs seawards, releasing energy. For a large earthquake, this results in a rupture zone along a fault rather than a single point as hypocentre.

Tsunamis are wave phenomena closely related to tectonic movements and are generated by sudden releases of energy, in the form of submarine seismic events, landslides, and volcanic activity, amongst others. In the case of a seismic event, the wave height is determined by the magnitude of the earthquake, as the sea floor and correspondingly the sea surface is moved upwards by the release of the overriding plate. In the case of the Nazca plate subduction the sea surface displaces creating a wave with a period of 10 to 90 minutes. Figure A-1 illustrates various phases in tsunami generation as a result of an earthquake in a subduction zone.

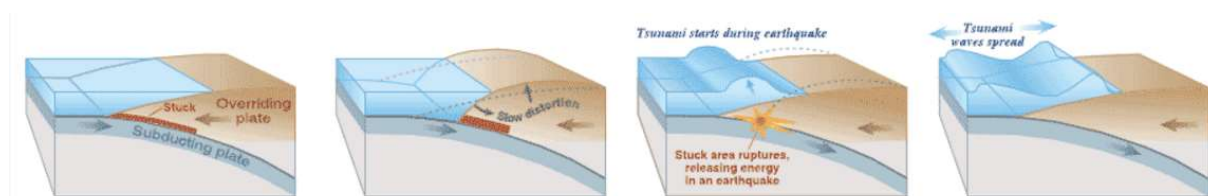


Figure A-1: Generation of tsunami wave due to interplate type earthquake

The general phases in tsunami physics are 1) generation 2) propagation and 3) inundation. The generation of the wave is governed by seismic parameters according to Figure A-2 (Okada, 1985), as well as the following equations for earthquake magnitude M_0 in relation to sea bed displacement D_0 and the shear modulus of the interplate fault zone μ :

$$M_0 = \mu L W D_0$$

$$M_w = \frac{2}{3} [\log(M_0) - 9.1]$$

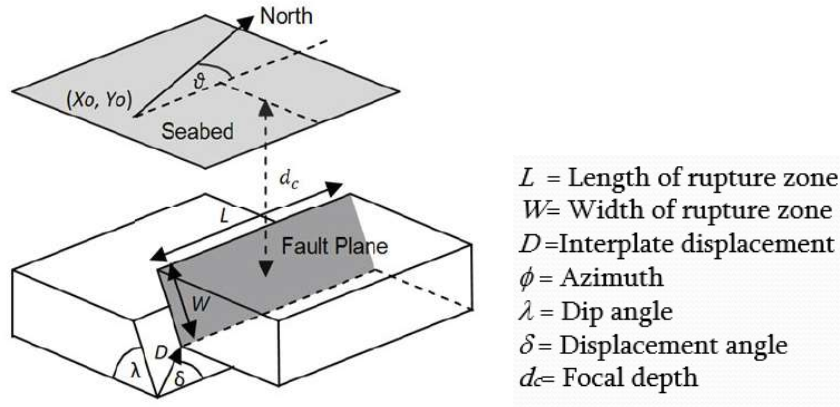


Figure A-2: Seismic parameters influencing tsunami generation

Once the wave has been generated, the propagation is governed by diffraction, refraction and reflection resulting from local bathymetry. Finally, the inundation phase depends highly on the local (onshore) topography.

A.3 HISTORY OF SEISMIC EVENTS IN CHILE

Chile is characterized by the largest level of seismicity in the world, with strong ($M_w > 8.5$) earthquakes roughly every 80 years (Lagos, et al., 2012). The major earthquakes affecting the coastal regions are generally aligned and concentrated offshore from Concepción southward, with the major epicentres producing a predictable pattern of seismic and tsunami effects.

The first systematic seismological recordings in Chile began after the 1906 earthquake and devastating consequential fire which destroyed the town of Valparaíso (Moreno, Rosenau, & Oncken, 2010). Melnick et al (2009) has delineated three rupture segments in the region as shown in Figure A-3.

Seismic gaps are defined as those segments along active convergent or transform plate boundaries that have not experienced a repeat of a large interplate earthquake for more than a few decades and are thus considered likely sites for future large events. The concept of seismic gaps provides the foundation for long-term earthquake forecasting (Nishenko, 1985). From Figure A-4 it may be observed that especially around latitudes between 25 and 30 degrees there is a seismic gap of almost 100 years, and a large event may be expected within the next decade. For the Concepción area, the gaps between large events range from 20 to 100 years.

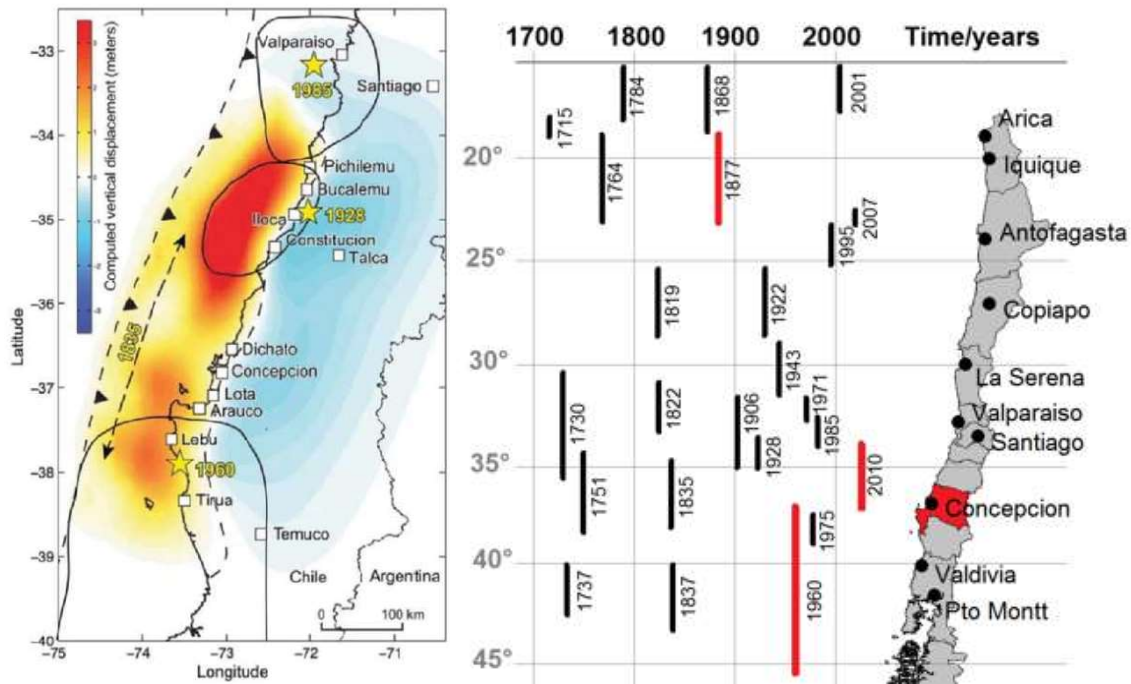


Figure A-3: Surface displacements predicted by forward modelling the rupture slip distribution. Colour ramp shows vertical displacements (uplift/subsidence); barbed line shows subduction zone trench; dashed line indicates location of hinge line between areas of uplift and subsidence. Yellow stars are the epicentres of past quakes, with their approximate rupture zones outlined with thin black lines (Melnick, 2009)

Figure A-4: Seismic events in Chile with latitudinal location of rupture zone and relative size since 1700

Table A-1 gives an overview of historical major earthquakes in the Biobío region and affecting the Greater Concepción area, more specifically (Lomnitz, 2004) (Soloviev & Go, 1975).

Table A-1: Historical major earthquakes and associated tsunamis in Central Chile

Year	Magnitude and intensity (Mw/ MMI)	Location of epicentre	Earthquake damage	Tsunami event
1570	8.3, XI	Concepción	Around 2000 fatalities. All houses destroyed.	Destructive tsunami.
1647	8.5, XI	Santiago	Around 1000 fatalities. Virtually all buildings destroyed.	-
1730	8.7	Valparaíso	Severe damage over a wide area. Only 5 fatalities, many could flee in time due to strong foreshock.	Destructive tsunami, wave run-up of 16m in Concepción.
1835	8.1	Concepción	Devastated Concepción, up to 95% of stone-built constructions destroyed. Around 500 fatalities.	Destructive tsunami. Three separate waves, run-up of 7m – 24m, destroyed

				harbour of Talcahuano.
1906	8.2	Valparaíso	Severe damage in all of Central Chile. 3882 fatalities	-
1960	8.1-8.3, IX	Concepción	Part of foreshock sequence before largest earthquake ever recorded, Valdivia 1960. 125 fatalities, 30% of buildings destroyed.	-
1985	8.0, IX	Algarrobo	Major damage across Central Chile, 177 fatalities. Many destructive landslides.	-
2010	8.8, IX	Offshore Maule, Biobío	525 fatalities.	Destructive tsunami.

Historically, seismicity has played a major part in indigenous culture. The Mapuche, the native people of the Chilean coastal regions, have myths which highlight their special connection to seismic events. One such a myth is that of Kai Kai and Treng Treng (Precolombino, 2016).

“A long time ago, two enormous serpents lived in Mapuche territory. Kai Kai was the serpent of the sea and Treng Treng was the serpent of the land. One time, Kai Kai rose up from the sea and cried kai, kai, kai, louder and louder, shriller and shriller. The serpent’s cries caused a great rain to fall. And the rains turned into a storm and then a torrent, flooding the Earth. To save themselves, the Mapuche people ran to the mountaintops. Just when they could ascend no more, they heard a voice coming from deep within the earth, calling treng, treng, treng. It was the divine serpent come to help them.

And thus began the battle between Kai Kai and Treng Treng. As Kai Kai howled louder and louder, Treng Treng caused the earth to shake, and it rose up higher and higher. Releasing his defeat, Kai Kai sank back into the depths of the sea, and has never been seen again.”

And since that time, whenever the sea floods the land, or during times of heavy rain, the Mapuche hear Kai Kai’s cry. Luckily, Treng Treng is on the watch, and before Kai Kai can harm the Mapuche people, he warns them by shaking the earth. Therefore, the earthquake allows the people to seek refuge on higher land before the induced tsunami wave comes ashore. The evacuation mentality is therefore deeply embedded in Chilean society, and the low death toll amongst locals in coastal towns throughout many major events reflects this.

A.4 HISTORY OF REGIONAL TSUNAMI EVENTS

Historically tsunami research in Chile has been limited for two reasons: 1) only 8 large tsunami events in 500 years discounts a probabilistic approach and 2) the capital Santiago is located inland and has produced a nationwide focus on earthquake rather than tsunami research. However, since the destructive tsunami of 2010 this latter phenomenon has seen a turn-around.

See Table A-1 for an overview of tsunamis affecting Concepción. The earthquakes of 1657 and 1751 with an offshore epicentre near Concepción produced large tsunamis which severely affected the town, with the latter event leading to a relocation of the city (Udias, 2012). In its new location, Concepción is relatively protected from tsunami impact, but it has been re-erected in poor soil conditions which has a negative influence on structural performance during seismic loading.

A.5 GENERAL SEISMIC DESIGN PHILOSOPHY

Seismic activity induces dynamic loads within a structure because of inertia forces, which act in opposite direction to the acceleration of earthquake excitations (Ishiyama, Takada, Fukushima, & Inoue, 2006). The term *action* is often used in literature instead of *load* to indicate the varying nature of seismic action in time and space, and other influences on structure deformation. The magnitude of the induced motion in a structure is a function of: depth of earthquake and distance of structure from epicentre, type of structure, type of foundation, soil stratigraphy underneath the structure, wave path between the source and the site (Pender, 1995).

Response spectra are used to determine the response of a structure to seismic ground motion, for different site (soil) conditions. Often it is illustrated as a plot of spectral acceleration versus the period T of the structural movement (short for low-rise structures) (Chavez, Khemici, Khater, & Keshishian, 2010). In order to move from an elastic to an inelastic, true, response, several factors must be taken into account: 1) the classification of the building under consideration, or importance factor 2) the amplification factor which is seismic period and soil type dependant 3) the maximum effective acceleration, depending on the soil type and 4) a reduction factor to take into account the ductility of the resisting structural system and the over-strength of some of these systems (Lagos, Kpufer, Lindenberg, & Bonelli, 2012).

Some main philosophies on earthquake-resistant building engineering include the lightness of construction material, the cohesion of the building (the connections between structural elements) and the regularity of the design, to avoid stress concentrations and local failure (Heerkens, 2014). One aspect of the cohesion is the connection of the structure to the foundation. In general, only one type of foundation ought to be used for the same structure (NPR9998, 2015). In contrast to structural design, geotechnical design is often clouded by uncertainties of soil behaviour. However, during earthquakes, the soil classification affects the period of vibration of the structures, and the seismic load on a building may vary up to 80%, due to amplification through clay (Vucetic, 1992).

A.6 CHILEAN SEISMIC DESIGN PRACTICE AND CODES: PAST VS. PRESENT

Since the 1970s Chile has followed the recommendations of seismic requirements published by the Structural Engineering Association of California (SEAOC) in 1961 (Chavez, Khemici, Khater, & Keshishian, 2010). However, unlike other South American countries, the Chilean code does not follow the American Uniform Building Code as closely since the strong earthquake of 1985 (NEHRP Consultants, 2012). Damage was extensive in this earthquake, but taller concrete buildings in Valparaíso and Viña del Mar performed well due to dense shear wall patterns in floor plates. These buildings thus had enough strength and redundancy to perform well, but lacked seismic detailing. To overcome this latter issue, the U.S. ACI 318, Building Code Requirements for Reinforced Concrete (ACI 1983), was slowly embodied into Chilean seismic design practice in NCh433.Of96 *Earthquake Resistant Design of Buildings* (INN, 1996) and NCh430.Of2008, *Reinforced Concrete Design and Analysis Requirements* (INN, 2008).

The general safety philosophy of the Chilean seismic code is to maintain Life Safety by avoiding collapse during severe earthquakes, and to avoid non-structural damage during moderate earthquakes, i.e. there are two design cases (Chavez, Khemici, Khater, & Keshishian, 2010), of which the ultimate limit state case is based on a return period of 475 years. However, due to the short interval between large earthquakes (roughly 80 years) the seismic design practice has achieved an almost operational performance level (Lagos 2012). For determining the design spectrum, the amplification factor and the reduction factor, the Chilean seismic code differentiates between 3 seismic zones, 5 soil types, and 4 building categories. This is elaborated in Figure A-5 to Figure A-7.

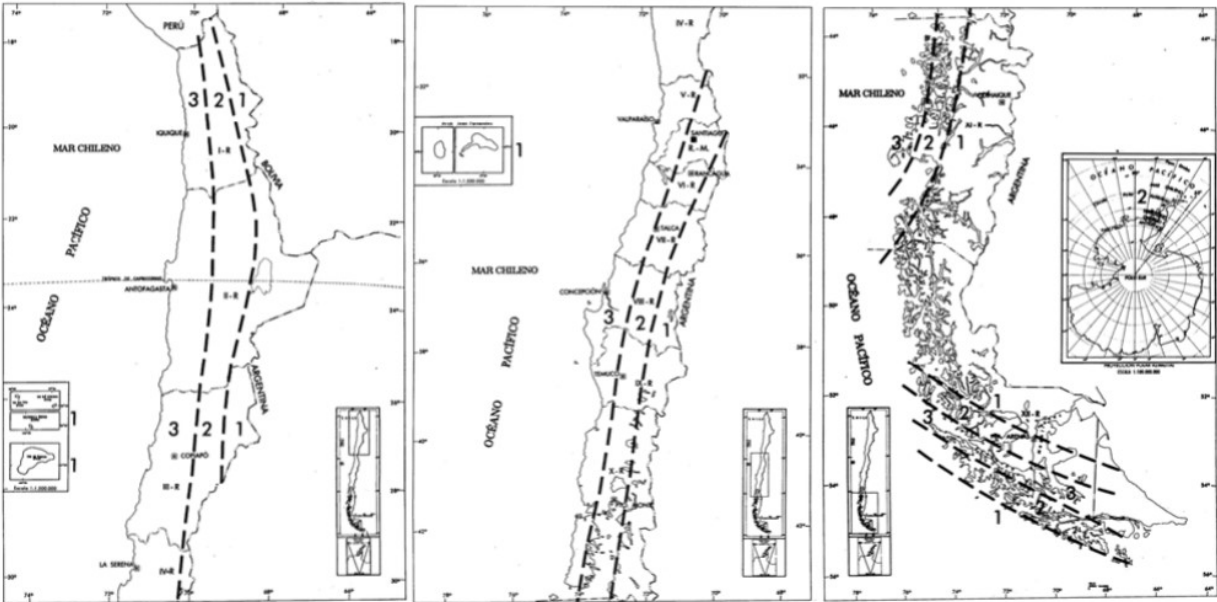


Figure A-5: Seismic zonation map of Northern, Central and Southern Chile (NCh433, INN 1996). Zone 1 encompasses the eastern portion of the country, Zone 2 generally encompasses the central plain, and Zone 3 encompasses the coastal region, which has the highest level of maximum effective soil acceleration A_0 (PGA). See Figure A-7 for values.

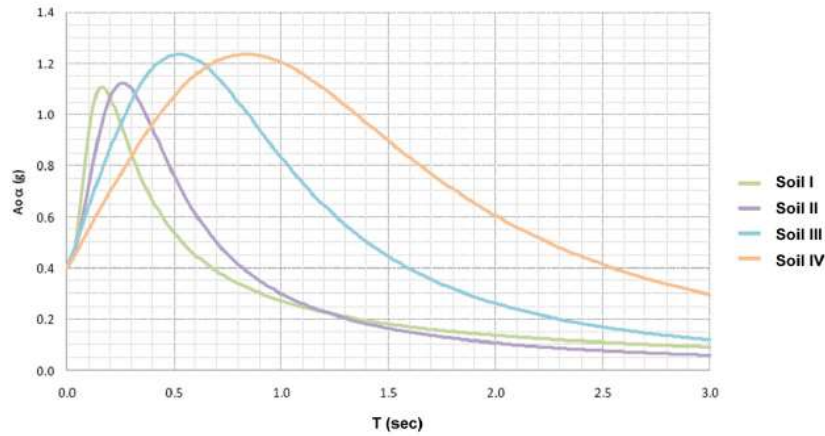


Figure A-6: Elastic Design Spectrum ($R^*=1$) for seismic Zone 3 for different soil types [NCh433.Of96]

Seismic Zoning:		
Seismic Zone	Geographic Area	A_0
Zone 1	Andes Mountains area	0.20 g
Zone 2	Central strip of Chile between the Coastal Mountains and the Andes Mountains	0.30 g
Zone 3	Costal area	0.40 g
Types Soils:		
Soil Type	Description	S T ₀ T' n p
I	Rock	0.90 0.15 0.20 1.00 2.0
II	Dense gravel, and soil with $v_s \geq 400$ m/s in upper 10 m	1.00 0.30 0.35 1.33 1.5
III	Unsaturated Gravel and sand with low compaction	1.20 0.75 0.85 1.80 1.0
IV	Saturated cohesive soil with $q_u < 0.050$ Mpa	1.30 1.20 1.35 1.80 1.0
Building Category: Importance factor		
Building Category	Description	I
A	Governmental, municipal, public service or public use	1.2
B	Buildings with content of great value or with a great number of people.	1.2
C	Buildings not included in Category A or B	1.0
D	Provisional structures not intended for living	0.6

Figure A-7: Determination of factors for design spectrum [NCh433.Of96]

A.7 CHILEAN CONSTRUCTION PRACTICE

The Chilean economy grew immensely in the period between 1990 and 2010, resulting in widespread building development throughout the country. Urban centres in Chile include many tall residential and commercial structures of reinforced concrete bearing wall systems (NEHRP Consultants, 2012). Low-rise buildings are usually constructed with cast-in-place concrete or confined masonry. In this latter case, wood is often used in the southern part of the country where forestation is extensive. Only large industrial facilities and other long-span buildings are typically constructed in steel. Figure A-8 shows floor plans of two of the most common reinforced concrete

high rise buildings in Chile, namely a residential and an office building. These two differ in requirements with regards to open spaces versus partitions for privacy. For residential buildings, the floor system is composed of flat concrete reinforced slabs, with spans of 5 to 8m, supported on shear walls and upturned beams at the perimeter. Vertical and lateral loads are transferred through concrete walls. Office buildings have greater spans and thicker floor slabs.

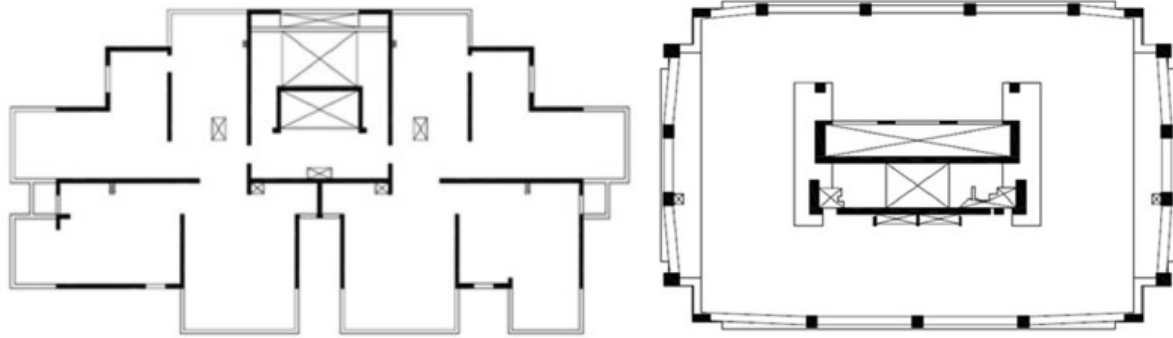


Figure A-8: Typical residential (left) and office (right) floor plans in Chilean high rise RC buildings

With regard to foundation construction practice, in the most densely populated areas of Chile, most buildings are built on mat or continuous footing foundations, due to the high bearing capacity of the rock and the cemented sand and gravel present in these areas (Islam, Jameel, & Zamin Jumaat, 2011). Only close to rivers, where there may be some pockets of clay, buildings are founded on piles, although houses built on stilts are becoming more widespread in coastal towns since the Coastal Reconstruction Plan of 2011-2013.

Overall, in Chile, the relatively low cost of construction labour relative to materials favours the use of distributed structural systems where many elements provide lateral resistance. This means it is possible to design with a high level of redundancy: shorter spans, more vertical load resisting elements, and smaller structural elements with lighter reinforcement. This is less applicable in European countries of the United States, for example (NEHRP Consultants, 2012). Furthermore, the vast majority of buildings are constructed in situ.

A.8 THE MAULE EARTHQUAKE AND TSUNAMI OF FEBRUARY 27, 2010

A.8.1 EARTHQUAKE

The Maule earthquake occurred along the subduction fault between the Nazca and South American plates, with an offshore fault rupture length of 500 km and with of 100 km. It initiated at 3:34 am local time on February 27, 2010, and generated severe ground shaking in the Maule and Biobío regions of Central Chile. The moment magnitude was M_w 8.8, with an epicentre approximately 105 kilometers north-northeast of Concepción, as shown in Figure A-9. The figure also shows that the most of Chile's central plain experienced a Modified Mercalli Intensity of VII, with higher intensities of VIII or even IX at the coast. Concepción experienced a maximum horizontal and vertical acceleration of 0.65g and 0.58g, respectively, lasting for more than 120 seconds in some records (Brzev, 2010).

According to several reports (Brzev, 2010), the earthquake resulted in more than 520 fatalities, 12,000 injuries, and 30 billion USD in damage and economic losses. At least 370,000 houses, as well as highways, roads, ports and airports were damaged. There was widespread disruption of electricity, telecommunications and water supply systems. However, many of these effects were caused by the ensuing tsunami, which struck the coast initially within 30 minutes of the ground shaking. See Figure A-10 and Figure A-12 for photographs of various damage scenarios in the Greater Concepción area.

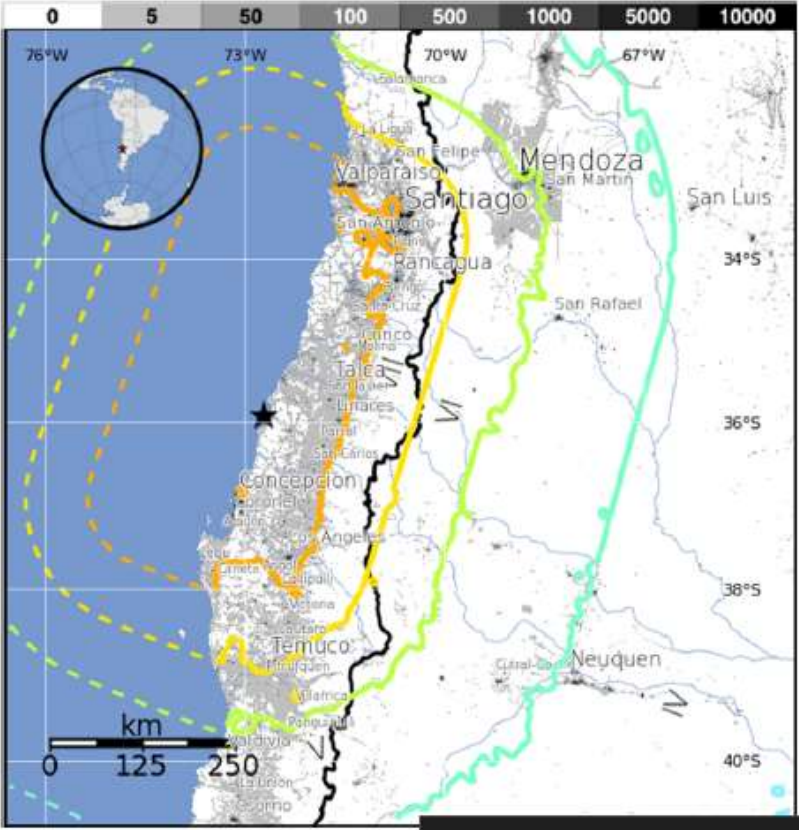


Figure A-9: Isoseismal map of the 2010 Maule earthquake (USGS, 2011)

A.8.2 EFFECT OF EARTHQUAKE ON NATIONAL DESIGN CODES

The large seismicity in Chile, leads to an overall deterministic strategy to assess hazard for building design -using known seismic and building performance data. In low or diffuse seismicity regions, a probabilistic approach is often used. In this sense, the Maule 2010 earthquake presented a unique opportunity to calibrate the behaviour of modern engineered reinforced concrete structures in response to severe earthquake shaking.

The Maule earthquake of February 2010 prompted a re-evaluation of the seismic code in Chile. It only caused the collapse of very few high-rise buildings which had been built since the previous strong earthquake of 1985. 0.2% of over 9-storey buildings collapsed and 2% had to be demolished due to severe damage (Lagos, Kpuffer, Lindenberg, & Bonelli, 2012). However, in Concepción, a 15-storey residential building collapsed and there was widespread seismic damage to high-rise

buildings. The concern was that design and especially detailing of reinforced concrete walls needed to be improved to prevent concrete crushing and rebar buckling under large axial compressive forces and bending action (Archila, 2013).

The following changes were implemented in the national design codes:

- NCh433 (*Earthquake Resistant Design of Buildings*): A new Soil Type classification is introduced, where soil types I, II, III, IV becomes types A, B, C, D and E, respectively, with the addition of a sixth soil type F. A new soil-dependent parameter S is used in the computation of the pseudo-acceleration spectrum, and a new Elastic Displacement Response Spectrum S_{de} is introduced.
- NCh430 (*Reinforced Concrete Design and Analysis Requirements*): Adoption of ACI 318-08 (US) with some minor exceptions for special structural walls, in order to prevent crushing and spalling of concrete and buckling of vertical reinforcement bars.



Figure A-10: (Left) Partially collapsed O'Higgins Tower, Concepción; (Right) Damage to typical unconfined shear wall boundary zone observed in Concepción (ASCE 2010)

A.8.3 TSUNAMI

The tsunami which hit Dichato following the Maule earthquake, with wave height between 5 and 7 m, caused large-scale erosion of the foreshore, as well as lifting up of houses from their foundations. See Figure A-12 for some examples of effects. Figure A-11 shows an inundation map of Coliumo Bay. The tsunami intensity was of category V on the Soloviev scale (1978), indicating a very large tsunami which destroys coastal structures and results in large-scale inland accumulation of debris, floating objects and dead animals. Except for large ships, all vessels are washed onto the shore.

A.8.4 TSUNAMI EFFECT ON COASTAL DISASTER MITIGATION

Chile holds the 9th position worldwide for vulnerability of cities to natural disasters, since 90% of its population resides in large cities, often at the coast. Besides tsunamis and earthquakes, they may suffer the effects of volcano eruptions, floods and landslides. After the Maule 2010 earthquake, the authorities realized that whilst most cities withstood the seismic event well, they were unprepared for the tsunami, especially on an organizational level. 1500 critical buildings, such as schools, hospitals, and industry, were destroyed by the tsunami waves. A committee was erected to deal with urban planning, with a focus on organization and social capital, as opposed to engineering structures to withstand tsunami impact (Baeriswyl, 2015).

The overall philosophy of tsunami impact reduction in Chile is one of *damage control* as opposed to prevention (Santander, 2016). A combination most often applied along the populated Chilean coastline is that of relocating houses further onshore and the construction of an onshore sea wall. Offshore mitigative structures such as breakwaters are rarely implemented, due to the high costs in relation to population sizes of seaside towns, as well as legal obstacles, on a parliamentary level, regarding offshore construction.

A second aspect of the *damage control* philosophy is that of internalizing risk: the capacity of structures to recover within a short time period (i.e. days) after the disaster is upgraded. Measures include building houses on stilts, with the basic necessities located on upper floors, and relocating houses further upslope. See Appendix C for photographs of mitigative measures.

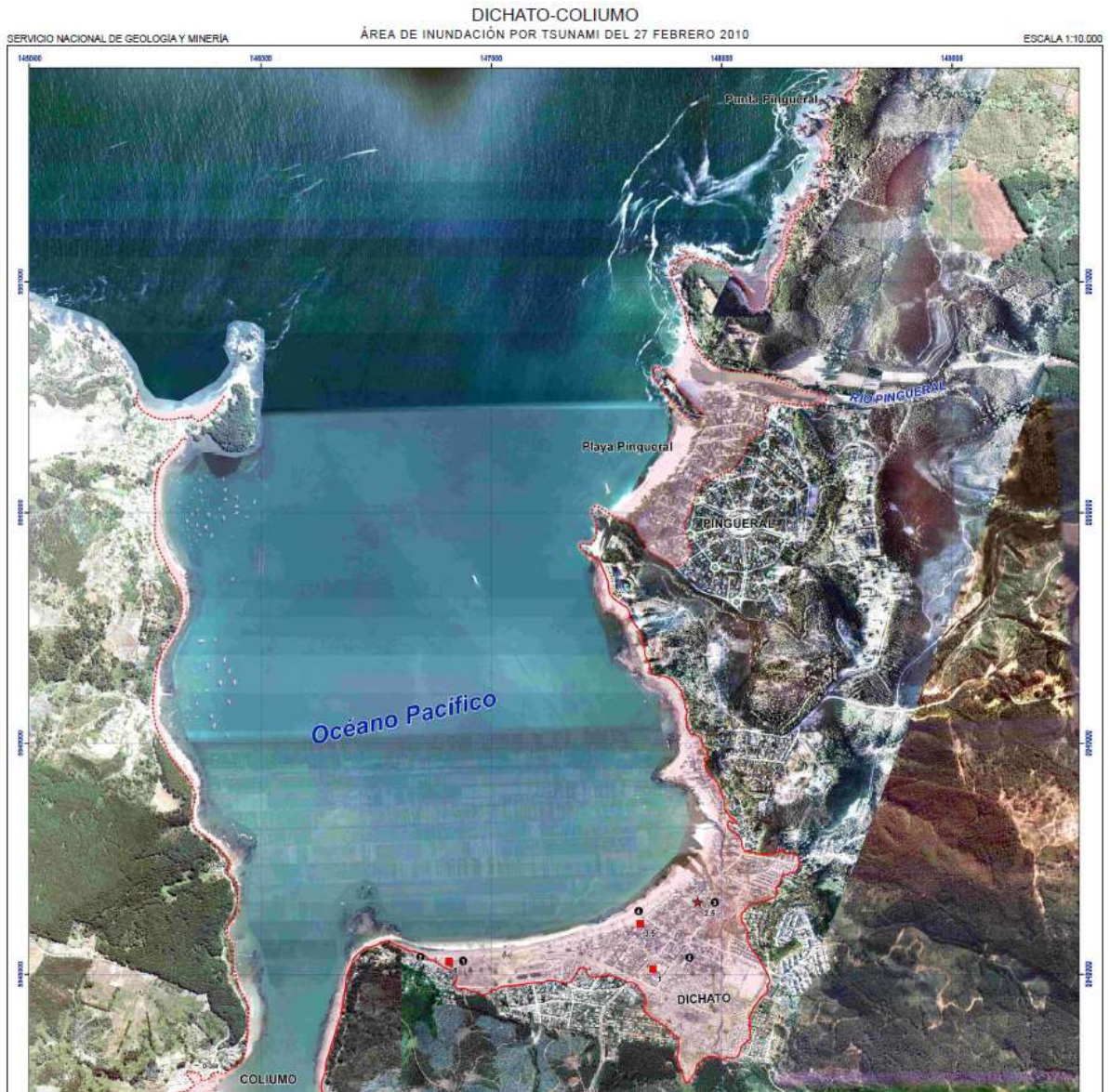


Figure A-11: Inundation of Coliumo Bay (in red) [source: Servicio Nacional de Geología y Minería]



Figure A-12: (Left) Exposure of buried lifeline due to tsunami erosion. (Right) House lifted from foundation and moved inland.

B GEOTECHNICAL BACKGROUND INFORMATION

B.1 GEOLOGICAL REGIONAL HISTORY

The geology of Chile has resulted from the Andean and preceding orogenies, where the Nazca and South-American tectonic plates converge. The country finds itself on an active continental margin. Consequently, volcanoes are widespread and almost the entire country is subject to shallow strike-slip fault induced earthquakes (Moreno, Rosenau, & Oncken, 2010). Regional geologic characteristics reflect long-term cycles of crustal deformation, with coseismic coastal uplift and inland subsidence.

Central Chile may be divided into four primary geologic domains (Melnick, 2009): The Coastal Platform, consisting of Cenozoic marine deposits and terraces, (2) the Coastal Ranges consisting of Permo-Triassic metamorphic rocks and older granitic rocks, (3) the Central Depression, including Cenozoic volcanic rocks overlain by semi-consolidated and unconsolidated alluvial sediments in the Central Valley, and (4) the Main Andean Cordillera, consisting of Mesozoic and Cenozoic volcanic rocks.

B.2 GEOLOGY AT DICHATO BAY

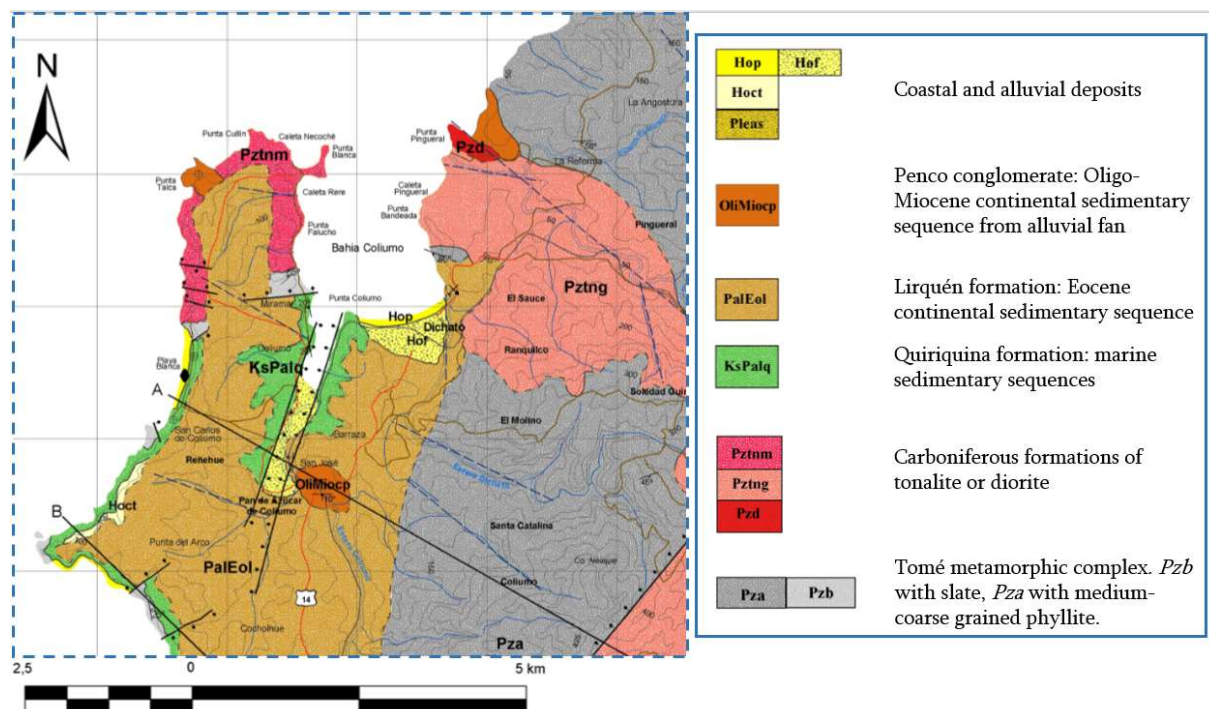


Figure B-1: Geology at Coliumo Bay, showing the Lirquen formation present at Marine Biology Station (*PalEol*)

B.3 REGIONAL MINING ACTIVITY

Mining has been an important source of economic welfare in the Dichato area, historically. Charles Darwin first discovered carbon mantles and fossils here around 1835. Coal exploitation in the mine of Coliumo began in 1856. In the period up until the earthquake of 1939, coal mining flourished around Dichato, where after the activities shifted to the towns of Coronel and Lota (Hackley, 2006).

Other mind minerals to the north of Concepción include copper and iron ore. There are several large open-pit mines to the east and south-east of Concepción, where granite is quarried for use as aggregate for various applications.

B.4 GEOTECHNICAL GROUND MASS CHARACTERISATION

B.4.1 SITE INVESTIGATION: SPTS FEBRUARY 2010

The SPTs performed at Caleta Villarrica in 2010 produced an N-value profile as shown in Figure B-2. Figure B-3 gives photographs of samples from S-1 and S-4, respectively.

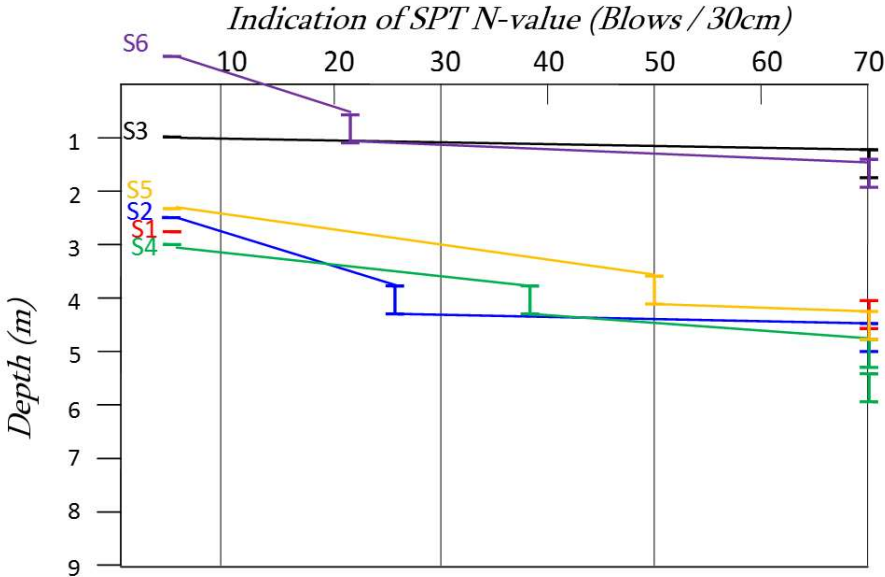


Figure B-2: N-value versus depth for 6 SPTs (Villarrica, 2010)



Figure B-3: Photographs of SPT samples from S-1 (left) and S-4 (right)

B.4.2 SPT RESULTS OF OVERLYING SOIL STRATA

From the SPT records the classification and properties are derived in Table B-1.

Table B-2 gives the associated N values for each sample. The N value is a function packing density and grading of the soil, and is linked to properties such as friction angle and safe bearing pressure (Waltham, 2009).

Table B-1: Classification and mechanical properties resulting from SPTs

SPT No.	Sample No.	Depth below MSL (m)	USCS classification	Specific gravity G_s (kN/m^3)	Moisture content (%)
S-1	1A	5.23-5.45	SM	2.649	32.4
	1B	5.45-5.68	ML	2.652	30.2
S-2	1	5.15-5.60	ML	2.617	32.2
	2	5.90-6.28	ML	2.681	30.8
S-3	1	2.10-2.50	ML	2.673	24.6
S-4	1	5.30-5.75	ML	2.695	31.5
	2	6.25-6.70	ML	2.685	29.9
	3	6.75-7.20	ML	2.652	30.1
S-5	1	5.10-5.55	ML	2.631	29.9
	2	5.60-6.05	ML	2.624	28.6
S-6	1	2.85-3.30	SM	2.624	17.6
	2	3.53-3.98	SM	2.631	19.0

Table B-2: Estimates of geotechnical properties derived from N value

SPT No.	Sample No.	N-value ¹ (blows / 30 cm)	RD	Friction angle ϕ (°)	SBP ² (kPa)
S-1	1A	R (60 in final 4 cm)	> 0.8	≥ 40	> 500
S-2	1	26	0.40-0.45	33-35	200-250
	2	R (70 in 8 cm)	> 0.8	≥ 40	> 500
S-3	1	R (70 in 10 cm)	> 0.8	≥ 40	> 500
S-4	1	38	0.65-0.75	36-38	400-450
	2	104	> 0.8	≥ 40	> 500
	3	105	> 0.8	≥ 40	> 500
S-5	1	50	0.75-0.85	38-40	450-500
	2	80	> 0.8	≥ 40	> 500
S-6	1	22	0.45-0.55	32-34	150-200
	2	77	> 0.8	≥ 40	> 500

¹ R indicates rejection point: rock is reached (>50 blows in 30 cm)

² Safe Bearing Pressure, a guideline value for maximum loads that may safely be imposed on undisturbed ground.

B.4.3 SITE INVESTIGATION: GEOPHYSICAL SURVEY NOVEMBER 2016

Local soil conditions may vary wildly between sites, and modify and often amplify the perceived surface movement of an earthquake. The level of amplification depends on the dynamic properties of the soil at the site, including the propagation velocities of shear waves. After the Maule earthquake of 2010, the need to revise the Chilean seismic soil classification system arose. Consequently, the measurement of the average shear wave velocity of the top 30m of the subsurface (v_{s30}) was incorporated into the code, and declared mandatory for buildings with a certain minimum height or surface area and built on certain soil types. A standardized method was set up by the National Soil Mechanics Committee to determine this parameter (Tokimatsu & Hiroshi, 2004).

Surface dispersion wave methods are based on the following principles: in a homogeneous medium, the propagation or phase velocity of Rayleigh waves is constant, whereas in a horizontally stratified medium the velocity depends on the wavelength, see Figure B-4. This property is known as dispersion, and the graph showing the variation of phase velocity with frequency is the dispersion curve. Geophysical methods based on surface wave analysis use the dispersive characteristic to characterize soils based on the profile of shear wave velocities. Smaller wavelengths correspond to properties of the surface layer, whilst longer wavelengths correspond to deeper layers (Humire Guarachi, Saez Robert, & Leyton Florez, 2015).

To carry out the surface wave analysis, geophones are installed in a regular pattern on site. First, a passive test is carried out, measuring the environmental vibrations. Next, an active test is carried out where the recorded surface waves are caused by a controlled dynamic source -in this case the blow of a hammer.

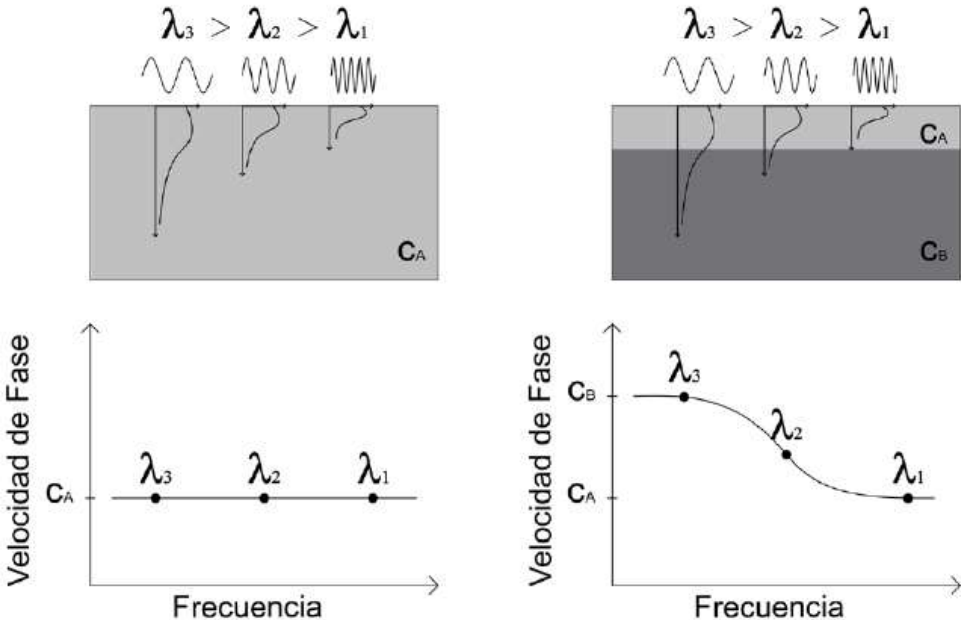


Figure B-4: Phase velocity (V) for different wavelengths in a homogeneous medium (left) and a stratified medium (right). Source: Strobbia (2003).

The geometry of the geophone set-up for the passive test is shown in Figure B-5. Figure B-6 and Figure B-7 give the environmental vibrations and the active test vibrational offset in time at each geophone, respectively. Using a Nakamura method, which combines 3 components of microtremors (North-South, East-West and Up-Down, see Figure B-8), Figure B-8 shows the determination of the fundamental (peak) frequency of the soil of the shallow subsurface, at 0.5 Hz.

The results of the Nakamura test are cross-correlated with the passive and active test to give the final result: a dispersion curve (Figure B-9) and a depth profile of the shear wave velocities (Figure B-10) showing some stratification of the subsurface. The top 3m indicate a sandy soil ($v_{s30} \approx 180$ m/s), followed by 20m of soft rock belonging to the Curanilahue formation ($v_{s30} \approx 500$ m/s). Below 25m the harder Quiriquina formation is found, with $v_{s30} > 800$ m/s). See Appendix B for photographs of the survey.

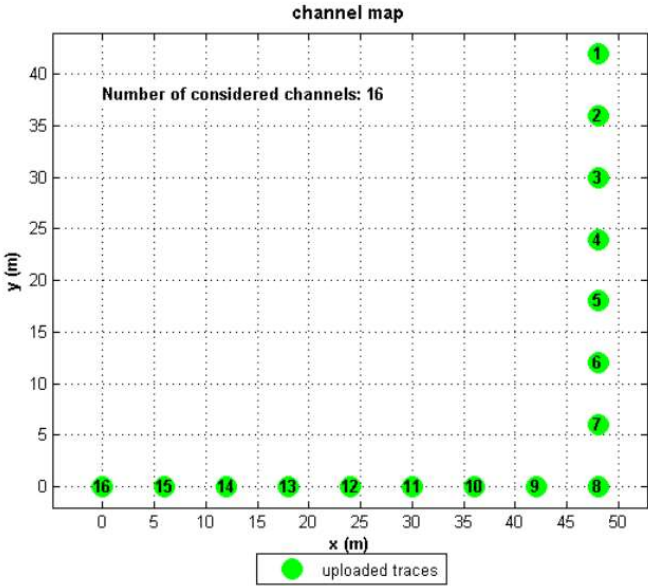


Figure B-5: Spatial set-up of 16 geophones on site

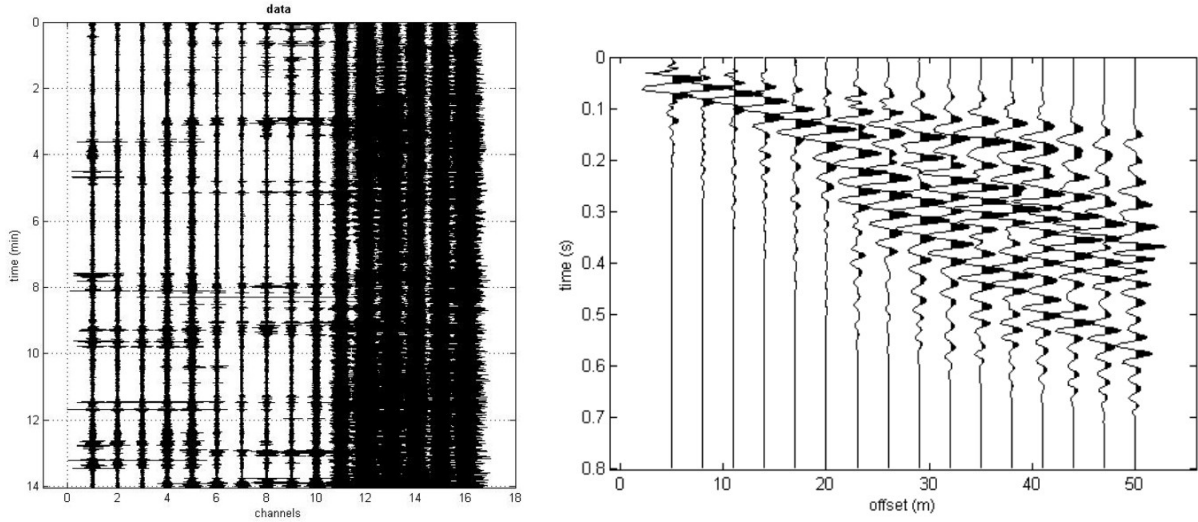


Figure B-6: Vibrations at each geophones from passive test Figure B-7: Propagation of shear wave from active test

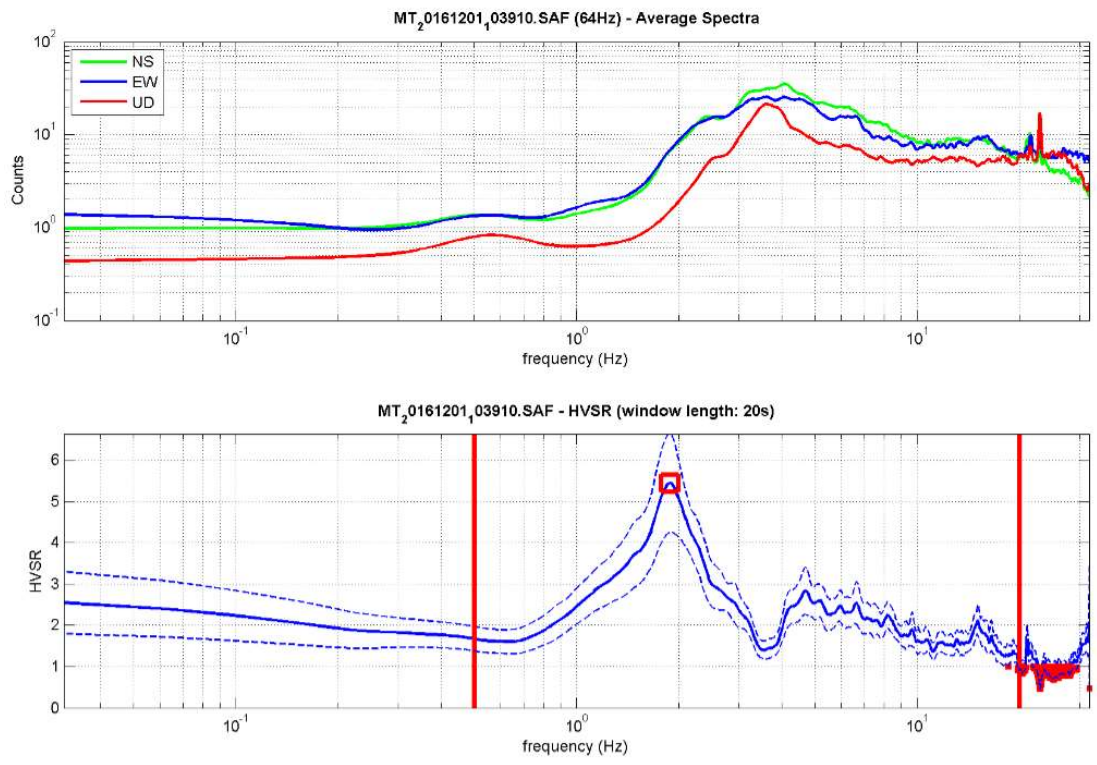


Figure B-8: Results of Nakamura test

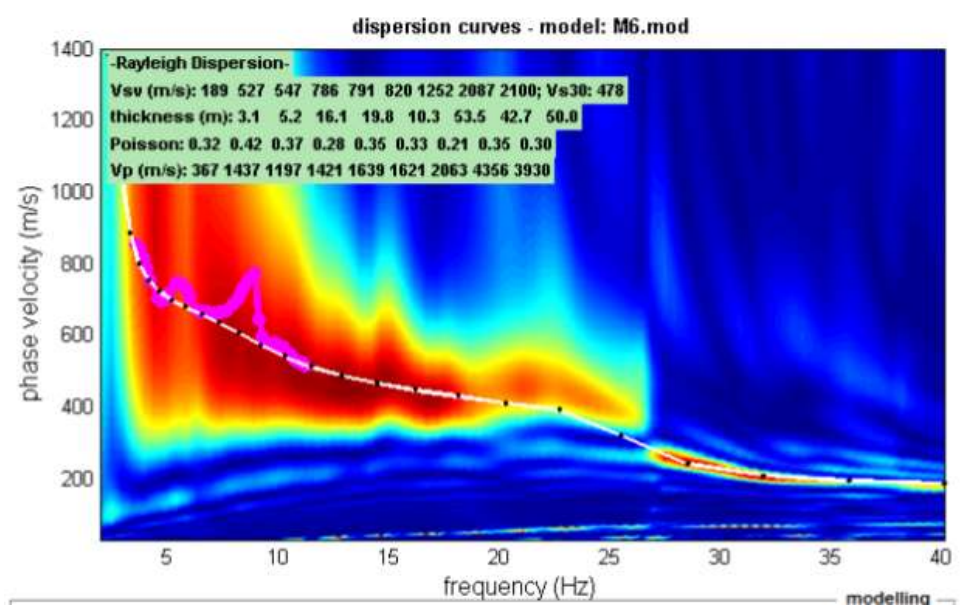


Figure B-9: Dispersion curve (pink line corresponds to passive test)

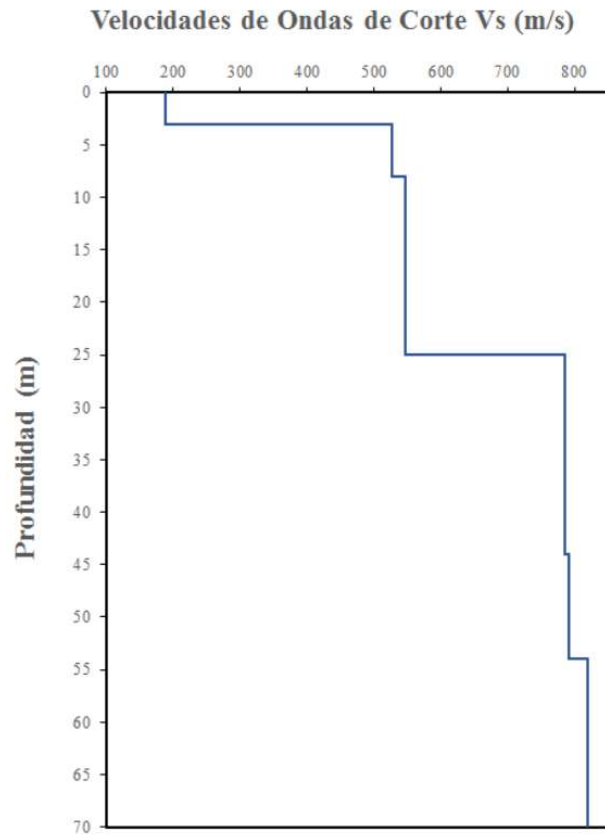


Figure B-10: Depth profile of shear wave velocities

B.5 FOUNDATION DESIGN

B.5.1 SEISMIC DESIGN CONSIDERATIONS FOR SHALLOW AND PILED FOUNDATIONS

Although any offshore structure is likely to be designed on piles, onshore structures may also be founded on shallow foundations. Piled foundations tend to be more susceptible to earthquake-related damage than shallow foundations, see Figure B-11 for an illustration. The piles must be tested for two earthquake loads: 1) inertial loading from the overlying structure and 2) kinematic loading due to lateral ground motion. Liquefaction may result in a loss of strength of the soil, and must be taken into account.

The stability of the piles must be tested in two cases. Firstly, during the earthquake, calculating 1) the vertical bearing capacity 2) the horizontal bearing capacity and 3) buckling, taking into account the dynamic loads from the overlying structure, the reduced soil shear strength due to accumulation of pore pressure, and lateral earthquake loads. Secondly, the piles must be stable after the earthquake, in terms of 1) vertical bearing capacity, 2) settlement 3) horizontal bearing capacity and 4) buckling, taking into account the reduced shear strength of the soil and the settlement due to densification. Of course, this latter phenomenon involves soil-pile-structure interaction. Pile grouping has some effects and stiff or deep foundations may dampen the vibrations of tall structures relative to the surface vibrations. In terms of general guidelines for designing foundations for earthquake-resistant buildings, NPR9998 suggests taking into account the development of over-strength i.e. the foundation preventing the structure from moving elastically with the earthquake-induced ground motion. To allow for the motions of the structure to be absorbed fully elastically, the code recommends vibration isolation in the connection of the foundation to the structure.

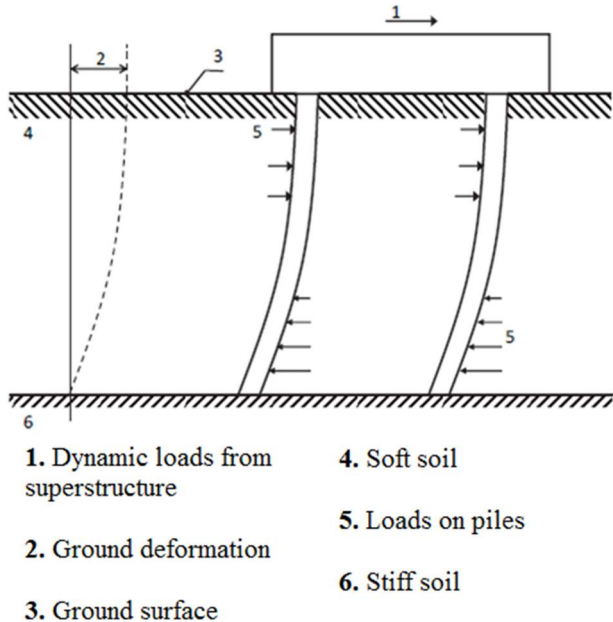


Figure B-11: Illustration of inertial and kinematic loading on piles during seismic loading [Pappin, 1991]

B.5.2 DESIGN CONSIDERATIONS FOR FOUNDATIONS AT HARBOUR COMPLEX

At the harbour site, the existing rock and soil types may be classified according to the Chilean soil type classification as follows (NCh2369.Of2003 (table 5.3):

Table B-3: Estimates of geotechnical properties derived from N value

Soil or rock unit	Description	Estimated v_s (m/s)	Soil type
SM	Silty sand	<200	C (III)
ML	Low plasticity silt	200-300	C (III)
Sedimentary rock	Sandstone from Curanilahue formation	300-500	B (II)
Underlying rock	Sedimentary rock from Quiriquina formation	> 500	A (I)

C SITE OBSERVATIONS COLIUMO BAY

C.1 DICHATO, NOVEMBER 11, 2016

On the 26th of November, the Impact Proof Chile team visited various locations along Coliumo Bay for a first insight into earthquake and tsunami impacts at coastal towns. Map 1 shows the bay with the locations of the towns of Dichato and Coliumo, as well as the points of interest labelled A-D (see photographs below).



Map 1: Coliumo Bay with labels of photograph locations

C.1.1 TSUNAMI MITIGATIVE MEASURES

Points A-C in and around Dichato mark locations where mitigation measures against tsunami impact have been implemented.



Figure C-1: Sea wall along Dichato boulevard (1.5m height)



Figure C-2: Start of tsunami retention park

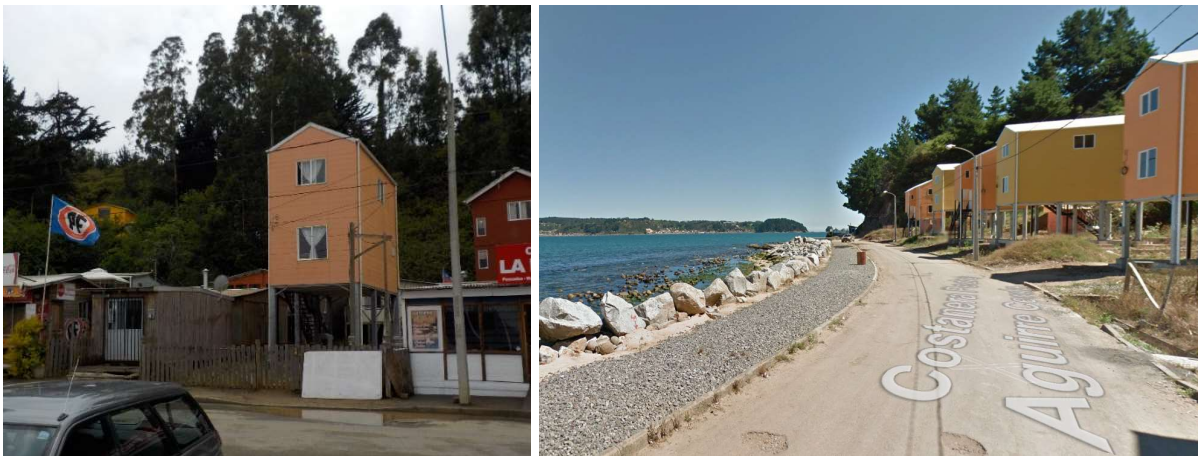


Figure C-3: (Left) House on stilts near Caleta Villarrica. (Right) Scour protection against tsunami erosion next to stilted houses.



Figure C-4: Tsunami hazard zone warning sign

C.2 COLIUMO, NOVEMBER 26, 2016

C.2.1 REFERENCE PROJECT: FISHERMEN'S JETTY

A jetty was constructed after the Maule earthquake of 2010 in Coliumo as a mooring facility for local fishing boats. It is marked on Map 1 as point of interest *D*.



Figure C-5: Coliumo L-shaped jetty for fishermen's boats with two (yellow) cranes



Figure C-6: Jetty with concrete deck and steel piles, some battered to resist lateral loads



Figure C-9: Connection steel piles to wooden fender with rubber strip to absorb kinetic energy of vessel

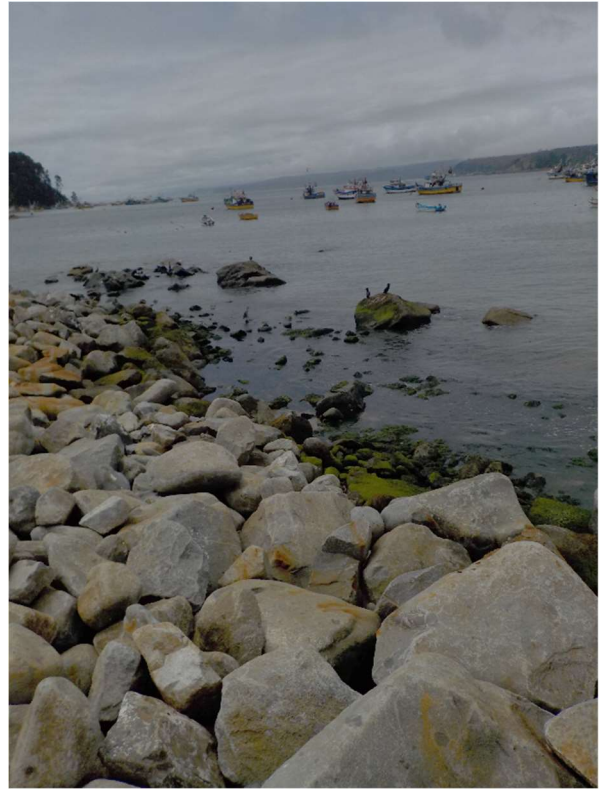


Figure C-10: Granite rubble mound against jetty



Figure C-7: Rigid column-beam connection



Figure C-8: Dilation joints

C.3 DICHATO, DECEMBER 1, 2016

C.3.1 GEOPHYSICAL SITE SURVEY

See Appendix B.4 for a description of the geophysical test and the results.



Figure C-11: Geophones (in yellow), installed in L-shape pattern on site



Figure C-13: Geophone recording set-up



Figure C-12: Installing the geophones at 6m c.t.c. distance in L-shaped line



Figure C-14: Interpreting the vibration results

C.3.2 MARINE BIOLOGY STATION BUILDING SURVEY

Map 2 shows the locations of the various buildings, structures and facilities as photographed in Figure Map 2 A to Figure Map 2 H. For a functional description of the current state of all elements of the site, see Chapter 2.2.3: Structural Conditions.



Map 2: Locations of photographed buildings and facilities on site



Figure Map 2 A: Concrete remains of shallow foundation for stay-over cabins. Potential redevelopment site



Figure Map 2 B: Building completed in 2014 (Left: Entrance side, Right: Sea-side)



Figure Map 2 C: Educational and research facilities within building (B)



Figure Map 2 D: Remains of old building, currently a single layer. Potential redevelopment site.



Figure Map 2 E: (Left) Unpaved road along building (D) towards pier

Figure Map 2 F: (Right) Storage facilities behind main buildings

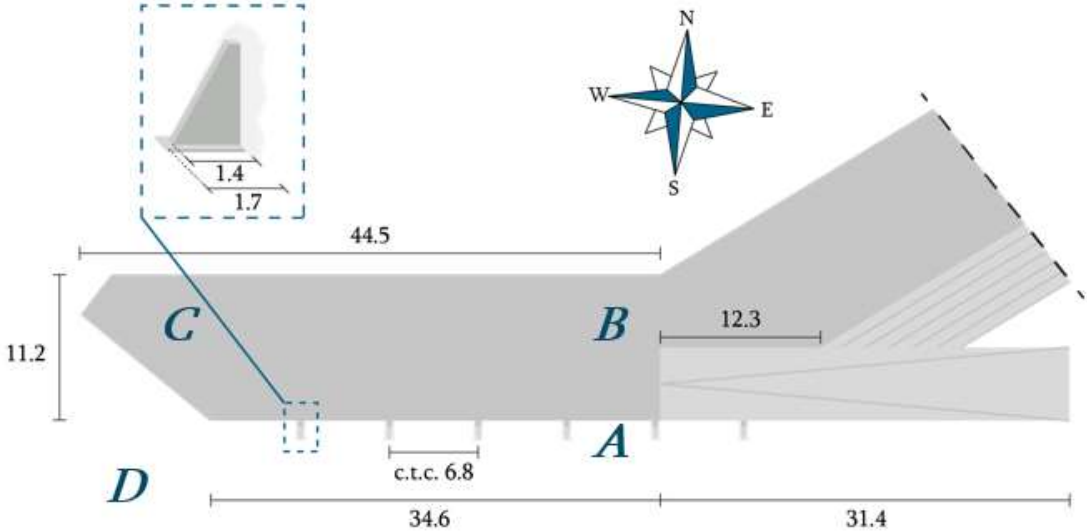


Figure Map 2 G: (Left) Building with research facilities for organisations, including INCAR

Figure Map 2 H: (Right) Single floor storage building for test equipment in between two academic and research facilities

C.3.3 MARINE BIOLOGY STATION PIER

Map 3 illustrates the features and dimensions of the currently existing concrete abutment, which has a length of around 40 m, and a slipway of 31.4 m long, used to move small boats such as the one in Figure Map 3 B to and from the water. See Figure Map 3 A to Figure Map 3 D for photographs of the elements labelled in Map 3.



Map 3: Overview of features and dimensions of existing concrete abutment



Figure Map 3 A: Abutment sea-side with concrete protrusions and foundation rock outcrops



Figure Map 3 B: Concrete abutment with slipway on right and Marine Biology Station buildings in background

Figure Map 3 C: Narrow end of concrete abutment



Figure Map 3 D: Existing piles from previous jetty

Figure 3. 1: Marine Biology Station research vessel, Kay Kay II



Figure 3. 2: Examples of equipment to be loaded onto Kay Kay II (maximum 1000 kg)

D EVALUATION OF ALTERNATIVES

D.1 MULTI-CRITERIA ANALYSIS

Table D-1: Legend for Multi-Criteria Analysis

	Score	Risk
1	Bad	Big
2	Unfavourable	Moderate
3	Neutral	Small
4	Favourable	None

Table D-2: Multi-Criteria Analysis

		(B)	(C)	(D)	(E)
Aspect	<i>External interface</i>				
	· Environment	2	3	2	4
	· Stakeholders	1	4	2	3
	· Aesthetics	2	3	2	4
	<i>Flexibility</i>				
	· Possibility to extend	2	3	2	4
	<i>Design</i>				
	· Simplicity design	3	3	2	2
	· Simplicity wave defence	3	3	2	3
	· Simplicity foundation	2	3	2	3
	<i>Construction</i>				
	· Building time	3	2	2	2
	· Available space building material	4	2	1	3
	· Available space building equipment	3	2	1	2
	<i>Prestige</i>				
	· Prestige of design for client	1	2	4	4
	<i>Maintenance</i>				
	· Sustainability	1	2	4	2
· Possibility for maintenance	2	3	3	3	
· Possibility for maintenance after extreme event	3	1	4	4	
<i>Safety</i>					
· During extreme event	2	2	4	3	
· Safety during operation	2	3	4	3	
Risk	<i>Technical</i>				
	· Design errors	3	3	2	1
	· Failure during construction	1	3	4	3
	<i>Organisation</i>				
	· Project time	3	2	1	2
· Logistics	3	2	1	3	
Total (sum of each score * associated weight)		223	252	285	285

D.2 WEIGHT FACTORS

Table D-3: Weighting factors

WF x 100, sum = 100	2.95	1.47	0.25	3.44	8.35	8.35	7.86	0.49	2.46	2.46	4.42	8.35	3.93	8.85	6.39	9.34	7.86	5.90	2.46	4.42
Weight factor (WF), sum = 1	0.0295	0.0147	0.0025	0.0344	0.0835	0.0835	0.0786	0.0049	0.0246	0.0246	0.042	0.0835	0.0393	0.0885	0.0639	0.0934	0.0786	0.0590	0.0246	0.0442
Enhanced weight, sum = 407	12	6	1	14	34	34	32	2	10	10	18	34	16	36	26	38	32	24	10	18
Weight	6	3	0	7	17	17	16	1	5	5	9	17	8	18	13	19	16	12	5	9
Logistics	1	0	0	0	1	1	1	0	0	0	0	1	0	1	1	1	1	1	0	1
Project time	0	1	0	1	1	1	1	0	0	0	1	1	0	1	1	1	1	1	0	1
Failure during construction	0	0	0	0	1	1	1	0	0	0	0	1	0	1	1	1	1	1	0	0
Design errors	0	0	0	0	1	1	1	0	0	0	0	1	0	1	0	1	1	1	0	0
Safety during operation	0	0	0	0	0	0	0	0	0	0	0	0	0	0	0	1	1	1	0	0
Safety during extreme event	0	0	0	0	1	1	0	0	0	0	0	1	0	1	0	1	1	1	0	0
Pos. for main. after extreme event	0	0	0	0	0	0	0	0	0	0	0	0	1	1	0	1	1	0	0	0
Possibility for maintenance	0	0	0	1	1	1	1	0	0	0	1	0	1	1	1	1	1	1	0	1
Sustainability	0	0	0	0	1	1	1	0	0	0	0	1	0	1	1	1	1	1	0	0
Prestige of design for client	0	0	0	0	1	1	1	0	0	0	1	1	0	1	1	1	1	1	0	1
Available space building equipment	1	0	0	0	1	1	1	0	1	1	1	1	1	1	1	1	1	1	1	1
Available space building material	1	0	0	0	1	1	1	0	1	1	1	1	1	1	1	1	1	1	1	1
Building time	1	1	0	1	1	1	1	0	1	1	1	1	1	1	1	1	1	1	1	1
Simplicity foundation	0	0	0	0	1	1	1	0	0	0	0	1	0	1	1	1	1	1	0	0
Simplicity wave defence	0	0	0	1	1	1	1	0	0	0	0	1	0	1	1	1	1	1	0	0
Simplicity design	0	0	0	1	1	1	1	0	0	0	0	1	0	1	1	1	1	1	0	0
Possibility to extend	1	1	0	1	1	1	1	0	1	1	1	1	0	1	1	1	1	1	0	1
Aesthetics	1	1	0	1	1	1	1	0	1	1	1	1	1	1	1	1	1	1	1	1
Stakeholders	1	0	0	1	1	1	1	0	1	1	1	1	1	1	1	1	1	1	0	1
Environment	1	0	0	1	1	1	1	0	1	1	1	1	1	1	1	1	1	1	0	1
Environment	1	0	0	1	1	1	1	0	1	1	1	1	1	1	1	1	1	1	0	1
Stakeholders	0	1	0	1	1	1	1	0	1	1	1	1	1	1	1	1	1	1	0	1
Aesthetics	0	1	0	1	1	1	1	0	1	1	1	1	1	1	1	1	1	1	0	1
Possibility to extend	1	1	0	1	1	1	1	0	1	1	1	1	0	1	1	1	1	1	0	1
Simplicity design	1	1	0	1	1	1	1	0	1	1	1	1	0	1	1	1	1	1	0	1
Simplicity wave defence	1	1	0	1	1	1	1	0	1	1	1	1	0	1	1	1	1	1	0	1
Simplicity foundation	1	1	0	1	1	1	1	0	1	1	1	1	0	1	1	1	1	1	0	1
Building time	0	0	0	0	0	0	0	0	0	0	0	0	0	0	0	0	0	0	0	0
Available space building material	0	1	1	1	1	1	1	0	1	1	1	1	1	1	1	1	1	1	1	1
Available space building equipment	0	1	1	1	1	1	1	0	1	1	1	1	1	1	1	1	1	1	1	1
Prestige of design for client	1	1	1	1	1	1	1	0	1	1	1	1	0	1	1	1	1	1	0	1
Sustainability	1	1	1	1	1	1	1	0	1	1	1	1	0	1	1	1	1	1	0	1
Possibility for maintenance	1	1	0	0	0	0	0	0	0	0	0	0	1	0	0	0	0	0	0	0
Pos. for main. after extreme event	1	1	1	1	1	1	1	0	1	1	1	1	1	1	1	1	1	1	0	1
Safety during extreme event	1	1	1	1	1	1	1	0	1	1	1	1	0	1	1	1	1	1	0	1
Safety during operation	1	1	1	1	1	1	1	0	1	1	1	1	1	1	1	1	1	1	0	1
Design errors	1	1	1	1	1	1	1	0	1	1	1	1	0	1	1	1	1	1	0	1
Failure during construction	1	1	1	1	1	1	1	0	1	1	1	1	0	1	1	1	1	1	0	1
Project time	1	0	1	1	1	1	1	0	1	1	1	1	0	1	1	1	1	1	0	1
Logistics	0	1	1	1	1	1	1	0	1	1	1	1	0	1	1	1	1	1	0	1

D.3 COSTS

Table D-4: Cost estimates per alternative

	Element	#	Unity	CPL/ unity	Costs (CPL)	Costs (€)
Null option (A)	n/a	-	-	-	-	-
	Element	#	Unity	CPL/ unity	Costs (CPL)	Costs (€)
Simple option (B)	Foundation – concrete	1	m ³	80,000	80,000	116
	Foundation – reinforcement	0.01	m ³	4,056,000	40,560	59
	Foundation – formwork	16	m ²	6,699	107,184	155
	Foundation – pouring	1	day(s)	100,000	100,000	145
	Mooring stairs – purchase	1	#	14,000,000	14,000,000	20,290
	Mooring stairs – placing (7 men + crane)	3	day(s)	2,140,000	6,420,000	9,304
	Dredging	1	#	4,900,000	4,900,000	7,101
	Installations – purchase	1	lumpsum	4,000,000	4,000,000	5,797
	Installations – placing (5 men)	5	day(s)	100,00	500,000	725
	Crane – purchase (1000 kg)	1	#	1,380,000	1,380,000	2,000
	Crane – placing (2 men + crane)	1	day(s)	2,040,000	2,040,000	2,957
	Total	-	-	-	\$ 33,567,744	€ 48,649
	Element	#	Unity	CPL/ unity	Costs (CPL)	Costs (€)
Traditional option (C)	Foundation – concrete	12	m ³	80,000	960,000	1,391
	Foundation – reinforcement	0,12	m ³	4,056,000	486,720	705
	Foundation – formwork	48	m ²	6,699	321,552	466
	Foundation – pouring (5 men)	1	day(s)	100,000	100,000	145
	Piles – purchase	12	#	302,082	3,624,984	5,254
	Piles – driving	12	#	60,000	720,000	1,043
	Beams – purchase	16	#	362,498	5,799,974	8,406
	Beams – placing (5 men + crane)	5	day(s)	2,100,000	10,500,000	15,217
	Deck – formwork	198	m ²	6,699	1,326,402	1,922
	Deck – reinforcement	0.45	m ³	4,056,000	1,825,200	2,645
	Deck – concrete	45	m ³	80,000	3,600,000	5,217
	Deck – pouring (5 men)					
	Mooring stairs – purchase	1	#	14,000	14,000	20,290
	Mooring stairs – placing (7 men + crane)	3	day(s)	2,140	6,420	9,304
	Installations – purchase	1	lumpsum	4,000,000	4,000,000	5,797
	Installations – placing (5 men)	5	day(s)	100,000	500,000	725
	Crane – purchase (1000 kg)	1	#	1,380,000	1,380,000	2,000
	Crane – placing (2 men + crane)	1	day(s)	2,040,000	2,040,000	2,957
	Armour stones	2100	m ³	20,000	42,000,000	60,870
	Breakwater – placing	20	day(s)	2,000,000	40,000,000	2,899
Total	-	-	-	\$ 139,604,832	€ 147,253	

	Element	#	Unity	CPL/ unity	Costs (CPL)	Costs (€)
Impact proof option (D)	Foundation – sheet piles	72	m	76,000	5,472	7,930
	Foundation – anchors/struts	20	#	100,000	2,000,000	2,899
	Foundation – concrete	900	ton	80,000	72,000,000	104,348
	Foundation - pouring (5 men)	5	day(s)	100,000	500,000	725
	Beams – purchase	3	#	362,498	1,087,495	1,576
	Beams – placing (5 men + crane)	1	day(s)	2,100,000	1,050,000	1,522
	Deck – formwork	15	m ²	6,699	100,485	146
	Deck – reinforcement	0,15	m ³	4,056,000	608,400	882
	Deck – concrete	9	m ³	2,100,000	18,900,000	27,391
	Deck - pouring (5 men)	1	day(s)	100,000	100,000	145
	Mooring stairs – purchase	1	#	14,000,000	14,000,000	20,290
	Mooring stairs – placing (7 men + crane)	3	day(s)	2,140,000	6,420,000	9,304
	Installations – purchase	1	lumpsum	4,000,000	4,000,000	5,797
	Installations – placing (5 men)	5	day(s)	100,000	500,000	725
	Crane – purchase (1000 kg)	1	#	1,380,000	1,380,000	2,000
	Crane – placing (2 men + crane)	1	day(s)	2,040,000	2,040,000	2,957
	Armour stones	1800	m ³	20,000	36,000,000	52,174
	Breakwater – placing	10	day(s)	2,000,000	20,000,000	28,986
	<i>Total</i>	-	-	-	\$ 186,158,380	€ 269,795
	Element	#	Unity	CPL/ unity	Costs (CPL)	Costs (€)
Future float option (E)	Foundation – concrete	12	m ³	80,000	960,000	1,391
	Foundation – reinforcement	0,12	m ³	4,056,000	486,720	705
	Foundation – formwork	48	m ²	6,699	321,552	466
	Foundation - pouring (5 men)	1	day(s)	100,000	100,000	145
	Piles – purchase	12	#	302,082	3,624,984	5,254
	Piles – driving	12	#	60,000	720,000	1,043
	Floating deck – deck	180	m ²	220,000	39,600,000	57,391
	Floating deck – fix mechanism	12	#	300,000	3,600,000	5,217
	Floating deck – ramp	1	#	3,500,000	3,500,000	5,072
	Installations – purchase	1	lumpsum	4,000,000	4,000,000	5,797
	Installations – placing (5 men)	5	day(s)	100,000	500,000	725
	Crane – purchase (1000 kg)	2	#	1,380,000	2,760,000	4,000
	Crane – placing (2 men + crane)	1	day(s)	2,040,000	2,040,000	2,957
	Armour stones	2100	m ³	20,000	42,000,000	60,870
	Breakwater – placing	20	day(s)	2,000,000	40,000,000	2,899
<i>Total</i>	-	-	-	\$ 144,213,256	€ 209,004	

E DIMENSIONING: JETTY

E.1 DIMENSIONING ACCORDING TO RULES OF THUMB

E.1.1 CONCRETE DECK

The deck consists over a two-way spanning slab of reinforced concrete, supported by a grid of steel beams with a centre-to-centre distance of 6 m. The concrete will be approximately 30 m by 6 m. The most common floor thicknesses (d) for conventional spans (L) of 4 to 8 m, are between 100 and 250 mm. The rules of thumb make a distinction between end- and mid-fields. For the relatively small structure of the jetty, only end-fields are present. The rule of thumb belonging to this type of structure is:

$$L/d = 28$$

According to this rule of thumb, the thickness of the deck should be $d = 5000/28 = 179$ mm. To be sure at this point in the design, we choose a slight overestimated thickness of 250 mm.

E.1.2 STEEL BEAMS

A steel grid is applied underneath the concrete deck with a centre-to-centre distance of 6 m. The steel beams form the transition from the concrete deck to the steel piles carrying the construction. A welded H-profile is chosen as a starting point. This profile is commonly used in structures with a span (L) between 4 and 12 meters. The conventional height (d) of this type of beam lies between 100 and 500 mm. The rule of thumb for an open steel profile like this is as follows:

$$L/d = 18$$

As L equals 5000 mm, according to this rule of thumb, the height of the beam should be $d = 5000/18 = 278$ mm. Therefore, a H300x300x105.5-profile is chosen. This profile has a height which is equal to its width, namely 300 mm (Acero, 2000).

E.1.3 STEEL PILES

For the steel piles supporting the structure, a closed round profile is chosen for its structurally efficient and aesthetically pleasing shape as well as its possibility to be filled with concrete. To determine the diameter (D) of the piles, in structures with heights (L) up to 8 meters, the rule of thumb is as follows:

$$20 \leq L/D \leq 35$$

For the jetty, the length of the piles is about 6.0 meters. According to the rule of thumb, the diameter (D) of the pile should be between $D = 6000/35 = 171$ mm and $6000/20 = 300$ mm. In agreement with this range, a closed profile is chosen with a diameter of 262 mm and a wall thickness of 6 mm. This profile is produced using submerged arc welding (Acero, 2000).

E.2 JETTY FOUNDATION PILES

E.2.1 PILE CROSS-SECTION

For the piles a steel (A-53) round hollow tube is selected with the properties given in Table E-1 (Acero, 2000). Steel pipes are used as piles given their proven applicability in weak sandstone in similar projects, and generally present fewer corrosion problems than in the case of H piles. They may be filled with concrete to ensure the connection to the superstructure, as well as allowing a connection to the sedimentary seabed rock through the open-tipped end of the pile.

Table E-1: Cross-sectional dimensions and properties of steel pile tube

Dimension	Unit	Value
Diameter, d	mm	262
Thickness, t	mm	5
Area, A	mm ²	4825
Moment of inertia, I	mm ⁴	40e6
Elastic Modulus steel, E	MPa	2.10e5
Self-weight G	kg/m	37.88

E.2.2 LOADS AND REACTION FORCES

The governing pile forces result from a first ETABS iteration with the deck, beam and pile dimensions as resulting from the rule of thumb dimensioning phase. Table E-2 gives the maximum and minimum axial forces in each pile, both for straight ‘C’ piles and inclined ‘D’ piles. See Figure E-1 for a visualisation of the pile locations.

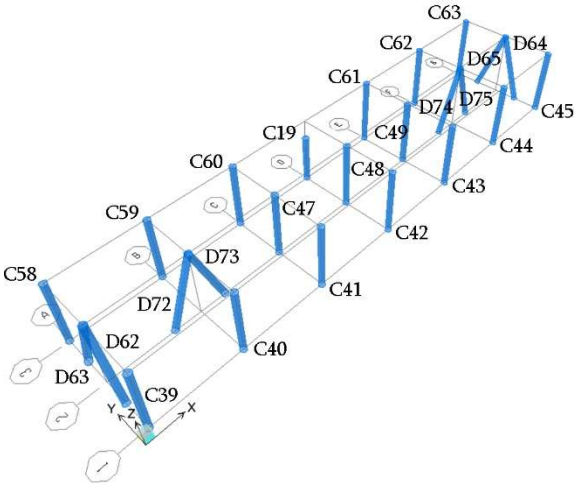


Figure E-1: Pile locations

Table E-2: Governing pile forces from first ETABS computation

Governing pile (straight)	$E_{ax,max}$	$E_{ax,min}$		Governing pile (inclined)	$E_{ax,max}$	$E_{ax,min}$
C19	-34.57	-3.42		D62	-523.36	397.58
C39	-98.27	-47.89		D63	-527.34	412.16
C40	-111.21	-55.71		D64	-498.05	418.61
C41	-114.87	-59.59		D65	-498.2	418.94
C42	-114.9	-67.48		D66	-13.06	29.63
C43	-107.15	-67.62		D67	-14.75	26.49
C44	-119.51	-60.62		D68	-18.58	29.74
C45	-59.56	-25.84		D69	-14.98	35.8
C47	-175.92	-95.39		D70	-15.36	14.01
C48	-173.01	-89.91		D71	-7.19	3.44
C49	-191.98	-105.19		D72	-431.71	280.31
C58	-65.75	-31.05		D73	-442.5	279.6
C59	-125.95	-65.62		D74	-438.77	279.85
C60	-77.76	-31.91				
C61	-74.64	-23.59				
C62	-129.35	-67.69				
C63	-61.53	-28.87				

Table E-3: Load cases corresponding to governing pile forces

Governing pile (straight)	$E_{ax,max}$ load case	$E_{ax,min}$ load case		Governing pile (inclined)	$E_{ax,max}$ load case	$E_{ax,min}$ load case
C19	CB21	CB48		D62	CB37	CB36
C39	CB21	CB46		D63	CB36	CB47
C40	CB21	CB46		D64	CB38	CB45
C41	CB21	CB46		D65	CB35	CB48
C42	CB21	CB1		D66	CB42	CB33
C43	CB21	CB1		D67	CB41	CB34
C44	CB21	CB45		D68	CB42	CB33
C45	CB21	CB45		D69	CB42	CB33
C47	CB21	CB46		D70	CB35	CB48
C48	CB21	CB47		D71	CB36	CB47
C49	CB21	CB47		D72	CB34	CB41
C58	CB21	CB47		D73	CB31	CB44
C59	CB21	CB47		D74	CB34	CB41
C60	CB21	CB47				
C61	CB21	CB48				
C62	CB21	CB48				
C63	CB21	CB48				

E.2.3 EMBEDMENT DEPTH PILES

Fixing the pile at a virtual point of fixity allows for it to be considered a cantilever structure. The depth of this point, D_f , depends on the soil properties, pile width, lateral loadings and pile head boundary conditions. Following the Japanese code for *Technical standards and commentaries for port and harbour facilities in Japan* (OCAD, 2009), the point of fixity may be determined as follows

$$D_f = \frac{1}{\beta} \quad (1)$$

Where

$$\beta = \sqrt[4]{\frac{K_{ch}d}{4EI}} \quad (2)$$

Using an estimation for the lateral subgrade reaction coefficient of the soil K_{ch} based on the SPT N-value ($N=70$ for the sedimentary rock), we obtain the following value: $K_{ch} = 0.15N = 10.5 \text{ MN/m}^3$. Using the steel pile profile values from Table E-1, $D_f = 105 \text{ cm}$.

However, the embedment depth of the pile, L , extends beyond the virtual point of fixity according to

$$L = \frac{1.5}{\beta} \tan^{-1} \left(\frac{1-\beta h}{1+\beta h} + \pi \right) \quad (3)$$

Where h is the distance between the ground surface level and where the pile connects to the superstructure, which is taken as 2m in this preliminary design. The resulting required embedment depth is $L = 2.10 \text{ m}$. However, from experience with the sedimentary rock around Coliumo Bay, it has proven difficult to embed piles beyond 2m. The piles however may still be considered fixed as in Chilean construction practice generally $8 \cdot D$ is assumed sufficient embedment depth. Furthermore, the inclined piles are assumed to require rock anchoring to be able to resist pull-out loads. As a first estimation, it is sufficient to consider D_f and L the same for both the vertical and inclined piles.

E.2.4 VERTICAL PILE AXIAL BEARING CAPACITY

The bearing capacity of the vertical piles, considering the type of weak rock in which they are embedded only 2.0 m, assumed to be only end-point bearing capacity. The pile resistance in compression is based on the bearing capacity of the soil q and the pile tip area A :

$$R_{ax;ult} = Aq_{ult} \quad (4)$$

Where q was previously determined to be 102.2 kg/cm^2 based on laboratory testing of compressional strength. This results in a compressional resistance value per pile of $R_{ax;ult} = 550 \text{ kN}$.

E.2.4.1 Lateral bearing capacity

There is much ongoing research into lateral loading resistance of vertical piles. Upwards loads, lateral loads and moments generally act on piles due to forces such as wind, waves and earthquakes. A pile resists lateral load by mobilising the passive pressure of the surrounding soil, depending on the stiffness of the soil and the pile and the fixity of the ends of the pile. Therefore, it is a typical soil-structure interaction problem.

Vertical piles may resist lateral loads via shear and bending. The allowable lateral load on such piles is usually determined from one of two methods: 1) calculating ultimate lateral resistance or 2) calculating acceptable deflection at the working lateral load. A common method is Broms, using a distinction between short or rigid piles and long or elastic piles; and between free-head or fixed-head piles.

However, using inclined or raked piles, it is assumed that all lateral loads are resisted by the horizontal component of the axial force in the inclined piles, see Figure E-2. The implicit assumption here is that raked foundation does not deflect laterally, which is not necessarily true. Therefore, it

is good practice to use vertical piles to resist only vertical loads and inclined piles to resist only lateral loads.

In this case, the lateral bearing capacity of the inclined pile is

$$R_{h;ult} = R_{ax;ult} \sin \theta \quad (5)$$

With batter angle θ . Thus, per raked pile of axial bearing capacity 480 kN and batter angle 20° , the lateral resistance amounts to 188 kN.

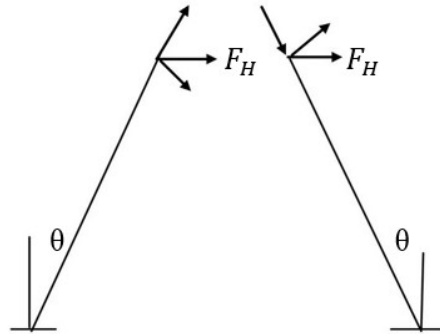


Figure E-2: Force distribution in negative batter pile (left), loaded in tension, and positive batter pile (right), loaded in compression.

E.2.5 RESISTANCE AGAINST PULL-OUT: TENSION PILE

The system of two raked piles means that one is loaded in tension, whilst the other is loaded in compression, as displayed in Figure E-2. It is assumed that no vertical pile will be loaded in tension, as all horizontal forces are taken by the inclined piles. However, to calculate the pull-out resistance of the inclined pile, $R_{p;ult;inc}$, it is first necessary to obtain that of a vertical pile, $R_{p;ult;vert}$, since the relation between vertical and inclined pile pull-out capacity is

$$R_{p;ult;inc} = R_{p;ult;vert} \{ \cos \theta / (\cos \theta + \tan \theta) \} \quad (6)$$

According to Awad and Ajoub (Awad & Ayoub, 1976).

For pile pull-out resistance, it is necessary to conduct two checks: 1) to ensure a single pile does not pull out from the ground mass in which it is embedded and 2) to ensure a block of soil between piles is not uplifted.

1) Shaft friction criterion

The shaft frictional resistance against pull-out may be determined from the tip resistance in the soft sedimentary rock q , previously determined to amount to 10220 kN/m^2 ; and a correction factor α_t of 0.008 for tensional loads (Tol, 2006).

$$q_{r;ult} = \alpha_t q \quad (7)$$

Gives $q_{r;ult} = 82$ kPa. To calculate the total skin friction along the shaft of the pile embedded 2.5m (with shaft surface area $O_p L$) in the soft rock:

$$R_{p;ult;vert;1} = O_p L q_{r;ult} \quad (8)$$

This results in a frictional resistance of 135 kN. Considering the self-weight of the pile at 37.9 kg/m, which also resists pull-out, the total resistance $R_{p;ult;vert}$ amounts to 137 kN.

2) Clump criterion

For this a pile configuration schematization as in Figure E-3 is considered. The figure shows that the soil in between piles may absorb tension only once, therefore the zones of influence may not overlap. Taking a wet unit weight γ of the soft sedimentary rock of 22 kN/m³, an embedded pile length L of 2 m, and a minimum equivalent distance s_{eq}^2 between the tensional piles of 6m

$$R_{p;ult;vert;2} = \gamma L s_{eq}^2 \quad (9)$$

Gives $R_{p;ult;vert;2} = 1584$ kN.

The shaft friction resistance is clearly the governing case for pull-out resistance at a mere 137 kN as opposed to 1584 kN for clump pull-out. Finally, the vertical pull-out capacity must be converted to pull-out capacity for the battered pile, which results in a reduction according to equation (6) with $R_{p;ult;inc} = 99$ kN for a 20° batter angle, and $R_{p;ult;inc} = 116$ kN for a 10° batter angle. Clearly, a more upright configuration gives greater pull-out resistance here.

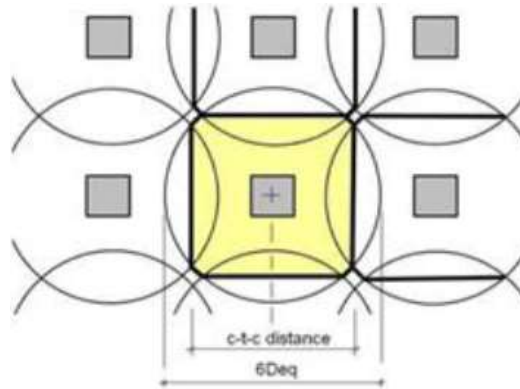


Figure E-3: Schematization of soil mass in between piles for calculating clump criterion (round piles in this case)

E.2.6 RESISTANCE AGAINST BUCKLING: COMPRESSION PILE

The positive batter pile is loaded in compression, and part of this pile is not supported laterally by soil as it is partly in water and open air. The ultimate buckling resistance however is determined by the governing load phase: the pile driving. See section *Construction considerations: pile buckling during driving* for a calculation on the ultimate buckling capacity of the governing (most slender) pile, using Euler's formula and the American code for steel structures, AISC 360-05.

E.2.7 RESISTANCE FACTORS

For both the vertical and horizontal loads on the piles, the appropriate safety factors have been applied in load combination calculations. For the resistant forces, a resistance factor ϕ of 0.55 is applied as suggested in (AASHTO, 1998), which is used as geotechnical code in Chile, and applies to driven pile foundations. This results in the following design values for the pile ultimate capacities:

Table E-4: Design values for pile capacities

Capacity		Batter angle °	Design value (kN)
Axial bearing capacity	$R_{ax;ult;d}$	-	303
Horizontal bearing capacity	$R_{h;ult;d}$	20	104
Pull-out capacity	$R_{p;ult;d}$	20	55

E.2.8 FACTORS OF SAFETY AGAINST FAILURE

Table E-5: Unity checks for pile configuration dimensioning

Check	Governing pile	Load (kN)	Resistance (kN)	F.O.S
Vertical pile bearing resistance	C49	$E_{v;ult}$	$R_{ax;ult;d}$	
		192	303	1.6
Inclined pile vertical bearing resistance	D63	495 ³	303	0.61
Inclined pile horizontal bearing resistance	D63	$E_{h;ult;}$	$R_{h;ult;d}$	
		180 ⁴	104	0.58
Pull-out capacity	D64, D65	$E_{ax;ult;tension}$	$R_{p;ult;d}$	
		418	55	0.13

Vertical piles are assumed to carry only vertical load so will not be subjected to horizontal forces. The factors of safety for the vertical bearing capacity of the vertical pile is sufficient. However, both the vertical and horizontal bearing capacity of the governing inclined pile is insufficient. To achieve a F.O.S >1.0, a minimum pile diameter of 350mm, so we take a Chilean steel tube profile from (Acero, 2000) of 362x6mm for piles D62, D63, D64, D65, D72, D73, D74 and D75. the pull-out capacity of a single inclined pile to the maximum tensional axial load is highly insufficient. It is impossible to embed the piles any deeper than 2.0m. Even if the inclined piles were to be placed at an angle of 10°, the required pile diameter to resist pull-out would be more than 600mm. Therefore, it is recommended to rock anchor the inclined piles to resist pull-out.

³495kN*cos(20)

⁴527kN*sin(20)

E.2.8.1 Required pile dimensions

For economic and logistic reasons, it is favourable to order as many of the same elements in bulk as possible. However, on the other hand it is also economical to minimize the pile diameter for an optimum FOS. Therefore, the pile dimensions are determined separately for the vertical and inclined piles. Since the piles are steel, altering the length is not a problem, as extra length may be added by welding and the tubes may be cut to decrease the length, conversely.

Due to the corrosion of steel piles in an aggressive marine environment, 4mm is added to the thickness t of the pipe, as in common practice in Chilean harbour and pier design. See *Part II: Design, Chapter 6.3.2: Construction Considerations* for more information on corrosion.

Table E-6: Foundation dimensioning results

Pile type	Batter angle	No. of piles	D x t (mm)	Pile length (m)
Vertical piles	-	17	262 x 6	6
Inclined piles	20	8 (4x2)	362 x 6	6.4

F DIMENSIONING: BREAKWATER

F.1 FIRST DETERMINATION DESIGN STORM

To get to wave heights for the ULS and the SLS, use is made of some statistics. Wave statistics for 23 years are downloaded from WaveClimate.com (BMT Argoss, 2016). In this data, measured every 3 hours (with a total of 67208 measurements); wave height, wave direction, wave period and also wind data are included. For the purpose of a design storm, the period and wave height are of importance.

All the wave data is plotted into a table in bins. The bins are divided in wave height (steps of 0.2m) and wave direction (steps of 22.5 degrees). The bins of the wave height are of the biggest importance and are used in the next steps. The directional bins are plotted to determine the main directions of the highest waves. The result is Table F-1.

The column in the right is the number of observed wave heights per bin. The next step is a probability of exceedance (Q) and a probability of any wave height being equal or less than a certain wave height (P).

$$P = P(H'_s \leq H_s)$$

$$Q = H'_s > H_s = 1 - P$$

Table F-1: Main direction waves

	lower	upper	348,75	11,25	33,75	56,25	78,75	101,25	123,75	146,25	168,75	191,25	213,75	236,25	258,75	281,25	303,75	326,25	348,75	ClassObs	
0,2	0,4	0	0	0	0	0	0	0	0	0	0	0	0	0	0	0	0	0	0	0	0
0,4	0,6	0	0	0	0	0	0	0	0	0	0	0	2	10	0	0	0	0	0	0	12
0,6	0,8	0	0	0	0	0	0	0	0	0	0	2	23	19	4	1	0	0	0	0	49
0,8	1,0	0	0	0	0	0	0	0	0	0	0	5	104	100	30	0	2	0	0	0	241
1,0	1,2	0	0	0	0	0	0	0	0	0	2	24	272	247	65	11	1	1	1	1	623
1,2	1,4	0	0	0	0	0	0	0	2	4	75	706	540	122	24	3	1	1	1	1	1477
1,4	1,6	0	0	0	0	0	0	2	2	2	108	1300	866	217	27	4	2	2	2	2	2530
1,6	1,8	0	0	0	0	0	0	4	1	1	163	2038	1091	316	44	18	0	0	0	0	3676
1,8	2,0	1	1	0	0	0	0	5	2	1	310	2565	1313	306	81	28	11	11	11	11	4624
2,0	2,2	3	0	0	0	0	0	0	0	1	4	455	3247	1503	308	87	27	11	11	11	5646
2,2	2,4	1	0	0	0	0	0	0	0	0	3	540	3643	1352	311	97	49	34	34	34	6030
2,4	2,6	4	0	0	0	0	0	0	0	0	4	563	3777	1297	299	112	59	31	31	31	6146
2,6	2,8	4	1	0	0	0	0	0	0	0	0	645	3686	1137	264	114	50	23	23	23	5924
2,8	3,0	6	0	0	0	0	0	0	0	0	0	705	3374	1044	277	103	55	37	37	37	5601
3,0	3,2	14	1	0	0	0	0	0	0	0	0	679	2871	913	282	120	64	27	27	27	4971
3,2	3,4	5	0	0	0	0	0	0	0	0	0	639	2461	776	244	122	57	34	34	34	4338
3,4	3,6	4	1	0	0	0	0	0	0	0	0	592	1911	595	221	101	55	30	30	30	3510
3,6	3,8	7	0	0	0	0	0	0	0	0	0	515	1512	480	154	77	55	28	28	28	2828
3,8	4,0	4	0	0	0	0	0	0	0	0	0	383	1185	351	133	72	48	21	21	21	2202
4,0	4,2	5	0	0	0	0	0	0	0	0	0	282	817	278	124	47	48	20	20	20	1621
4,2	4,4	3	1	0	0	0	0	0	0	0	0	194	652	211	90	58	45	18	18	18	1272
4,4	4,6	0	0	0	0	0	0	0	0	0	0	131	457	171	79	42	39	16	16	16	935
4,6	4,8	1	0	0	0	0	0	0	0	0	0	93	352	154	69	31	26	16	16	16	742
4,8	5,0	2	0	0	0	0	0	0	0	0	0	41	270	150	64	29	28	12	12	12	596
5,0	5,2	1	0	0	0	0	0	0	0	0	0	26	159	107	56	32	21	5	5	5	407
5,2	5,4	4	0	0	0	0	0	0	0	0	0	25	97	90	50	23	18	7	7	7	314
5,4	5,6	6	0	0	0	0	0	0	0	0	0	5	88	73	36	15	10	2	2	2	235
5,6	5,8	2	0	0	0	0	0	0	0	0	0	4	53	58	25	9	4	10	10	10	165
5,8	6,0	2	0	0	0	0	0	0	0	0	0	1	37	39	18	5	12	4	4	4	118
6,0	6,2	0	0	0	0	0	0	0	0	0	0	0	25	40	15	3	9	10	10	10	102
6,2	6,4	0	0	0	0	0	0	0	0	0	0	0	13	23	8	2	10	6	6	6	62
6,4	6,6	1	0	0	0	0	0	0	0	0	0	0	11	14	6	3	2	0	0	0	37
6,6	6,8	0	0	0	0	0	0	0	0	0	0	0	14	27	4	2	3	4	4	4	54
6,8	7,0	1	0	0	0	0	0	0	0	0	0	0	9	26	3	2	2	0	0	0	44
7,0	7,2	1	0	0	0	0	0	0	0	0	0	0	0	12	1	2	0	0	0	0	18
7,2	7,4	1	0	0	0	0	0	0	0	0	0	0	5	9	1	1	0	0	0	0	17
7,4	7,6	1	0	0	0	0	0	0	0	0	0	0	1	11	0	0	0	0	0	0	13
7,6	7,8	1	0	0	0	0	0	0	0	0	0	0	2	7	0	0	0	0	0	0	10
7,8	8,0	3	0	0	0	0	0	0	0	0	0	0	3	3	0	0	0	0	0	0	9
8,0	8,2	0	0	0	0	0	0	0	0	0	0	0	0	3	0	0	0	0	0	0	3
8,2	8,4	0	0	0	0	0	0	0	0	0	0	0	0	2	0	0	0	0	0	0	2
8,4	8,6	0	0	0	0	0	0	0	0	0	0	0	0	2	0	0	0	0	0	0	2
8,6	8,8	0	0	0	0	0	0	0	0	0	0	0	0	1	0	0	0	0	0	0	1
8,8	9,0	0	0	0	0	0	0	0	0	0	0	0	0	1	0	0	0	0	0	0	1
9,0	9,2	0	0	0	0	0	0	0	0	0	0	0	0	0	0	0	0	0	0	0	0
total			93	5	0	0	0	0	11	8	21	7205	37742	15146	4202	1500	852	423			67208

F.1.1 PEAK OVER THRESHOLD ANALYSIS

The above data gives information on exceedance of individual wave conditions. However, for the scope of a certain occurrence of storms, the probability of a certain storm condition needs to be calculated. To get from above data to storm data, a certain value of wave height is set as a 'threshold' value. This value is set to give less importance to long periods of low wave heights. The threshold value is subjectively selected, in this case a value of 5.2m is chosen, after which on average 52 'storms' a year are left from the original data. The wave heights left will be called storm wave heights (H_{ss}). Again, the P and Q will be calculated.

With this data, a Gumbel and Weibull fitting is performed. Extreme value distributions like Gumbel and Weibull are expected to fit the extreme values that are left the best. Both are discussed here.

F.1.2 GUMBEL

The Gumbel distribution:

$$P(H \leq H_{ss}) = e^{-e^{-\frac{H_{ss}-\gamma}{\beta}}}$$

The γ and β are coefficients of the Gumbel distribution. Via a transgression analysis both values can be obtained. The Gumbel distribution can be reduced by taking two times the *log*.

$$G = -\ln(-\ln P) = \frac{H_{ss} - \gamma}{\beta}$$

A reduced Gumbel variable is left which the distribution can be calculated with. A storm height exceedance can be plotted against the reduced Gumbel variable. See Figure F-1. As immediately becomes clear from the figure, the values from the Gumbel distribution overestimate the wave height significantly. The Weibull transgression will be performed to check for a better fitting.

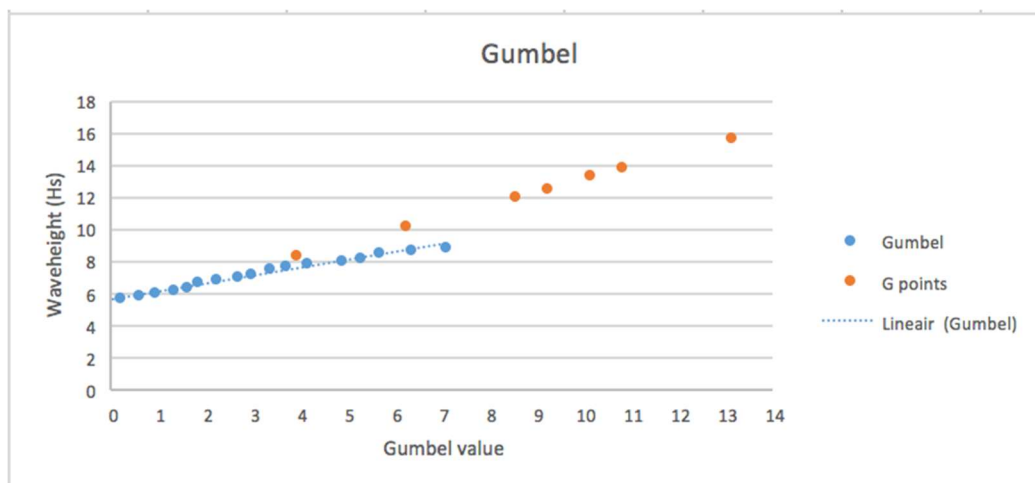


Figure F-1: Gumbel graph

F.1.3 WEIBULL

The Weibull distribution is as follows

$$P(H_{ss}) = Q = e^{-\left(\frac{H_{ss}-\gamma}{\beta}\right)^\alpha}$$

Again, to find the values β and γ the formula needs to be reduced and a regression analysis has to be performed. The value α had to be found by trial and error. The reduced Weibull variable W can be calculated as following:

$$W = (-\ln Q)^{\frac{1}{\alpha}} = \frac{1}{\beta}H_{ss} - \frac{\gamma}{\beta}$$

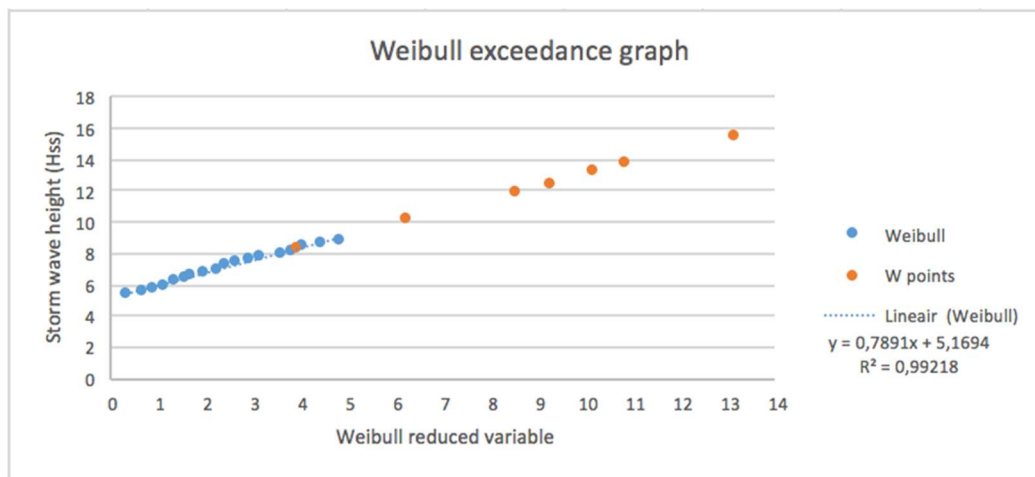


Figure F-2: Weibull graph

The Weibull exceedance graph fits well to the storm wave height values. Wave height with a certain return period can be calculated using the next formula:

$$H_{ss1/\alpha} = \gamma + \beta \left(-\ln \left(\frac{Q_s}{N_s} \right) \right)^{1/\alpha}$$

The outcomes are presented in Table F-2. These values will be used as offshore wave values and translated onshore with software SWAN. These values of the wave heights are rather high in comparison with real measurements. In the next iteration step, a more detailed analysis on the wave direction will be made as well. A split up between the swell from the south west and the storms from the north will be made.

Table F-2: Outcome

annual probability	Return period	Weibull	H_s [m]
18	0,056	1,06	6,00
1	1	3,03	7,56
0,1	10	4,39	8,63
0,01	100	5,65	9,63
0,004	250	6,14	10,01
0,002	500	6,49	10,29
0,001	1000	6,85	10,57

F.2 SWANONE

To get an indication of the wave climate which the breakwater endures, the offshore wave climate has to be transferred to an onshore wave climate. In this design step a very simplified wave model is used. To get a quick insight in onshore waves use is made of SwanOne because of the easy and fast implementation.

SwanOne is an easy to use one-dimensional graphical interface of SWAN. The calculations done by SwanOne are fully 2-D calculations, so SwanOne included refraction, directional spectra and directional spreading. But SwanOne assumes parallel depth contours. In the case of Coliumo bay, interaction with the bathymetry can be expected as an important factor. So by making use of parallel depth contours a large simplification is made. The linear depth contours used for this model are depicted in Figure F-3.



Figure F-3: Linear depth contours SWANONE

Another simplification in the model is the input of the wave spectrum. The input is created via the parameters option within SWANONE. SwanOne converts a deep water wave height (H_{m0}) and a deep water peak period (T_p) to a Jonswap spectrum. The Jonswap spectrum is not a realistic description of the wave climate at the coast of Chile.

$$L = \frac{gT^2}{2\pi} = 375 \text{ m}$$

$$\frac{d}{L} > 0.5 \rightarrow \text{deepwater: } d > 188\text{m}$$

Nevertheless, this very simplified way of modelling serves as input of the first step of the design of the breakwater. And is only meant as first step of the iterative process of designing the breakwater.

The simplified model results in the outcomes presented in Table F-3 and Table F-4.

Table F-3: ULS output SwanOne

ULS		
	Offshore	Onshore
Hs	10	1.96
H2%		2.74
Tp	15.5	15.5
Tm		8.5

Table F-4: SLS output SwanOne

SLS		
	Offshore	Onshore
Hs	6	1.90
H2%		2.7
Tp	14.5	13.8
Tm		8.3

F.3 REQUIREMENTS

In the design of the breakwater, two different cases have to be distinguished. The breakwater needs to protect the jetty from incoming waves. This results in an allowable overtopping or wave transmission at the location of the breakwater, as displayed in Figure F-4. The allowable wave transmission is therefore dependent on the serviceability limit state (SLS). In other words, the allowable downtime for the jetty determines at how many days this transmitted wave height may be exceeded. The stone size however depends on the ULS. This means that the stones may not become unstable before the ultimate limit state is reached.

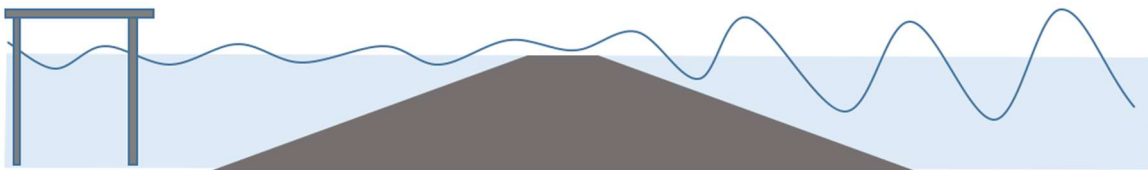


Figure F-4: Wave transmission at breakwater

F.3.1 CREST HEIGHT

The downtime of the jetty is set on 5% per year, which is decided in the program of requirements. This downtime results in an acceptable non-service of 18 days a year. This non-service means that the ship can stay moored if it is moored, but the mooring process itself is impossible according to the guidelines. The guidelines give a limit of 0,30m wave height in the harbour area for ships of this size (Wijdeven, 2015) . The annual probability is 18 days a year, on average 18 days a year there is a maximum wave height of 6m. This value is obtained using a Weibull transgression, see Appendix F.3.

In this phase, the offshore wave height is translated to an onshore wave height using SwanOne, from the TU Delft. This is a strongly simplified case, because of the detailed bathymetry around Dichato and Coliumo Bay. However, for this phase it is important to make some assumptions to get to a design based on rules of thumb. A comprehensive explanation of the wave translation is given in Appendix H.

Table F-5: Translated (SLS) wave heights onshore

SwanOne	Offshore	Onshore
Wave height [Hs] (18 days a year)	6.0 m	1.89 m
Peak period [Ts]	15 s	13.8 s

With help of the software BREAKWAT3.0, developed by Deltares, a rough calculation of the crest height is made, based on the mentioned wave transmission. Some assumptions are made regarding different parameters, listed in the Breakwat screenshot in Figure F-5.

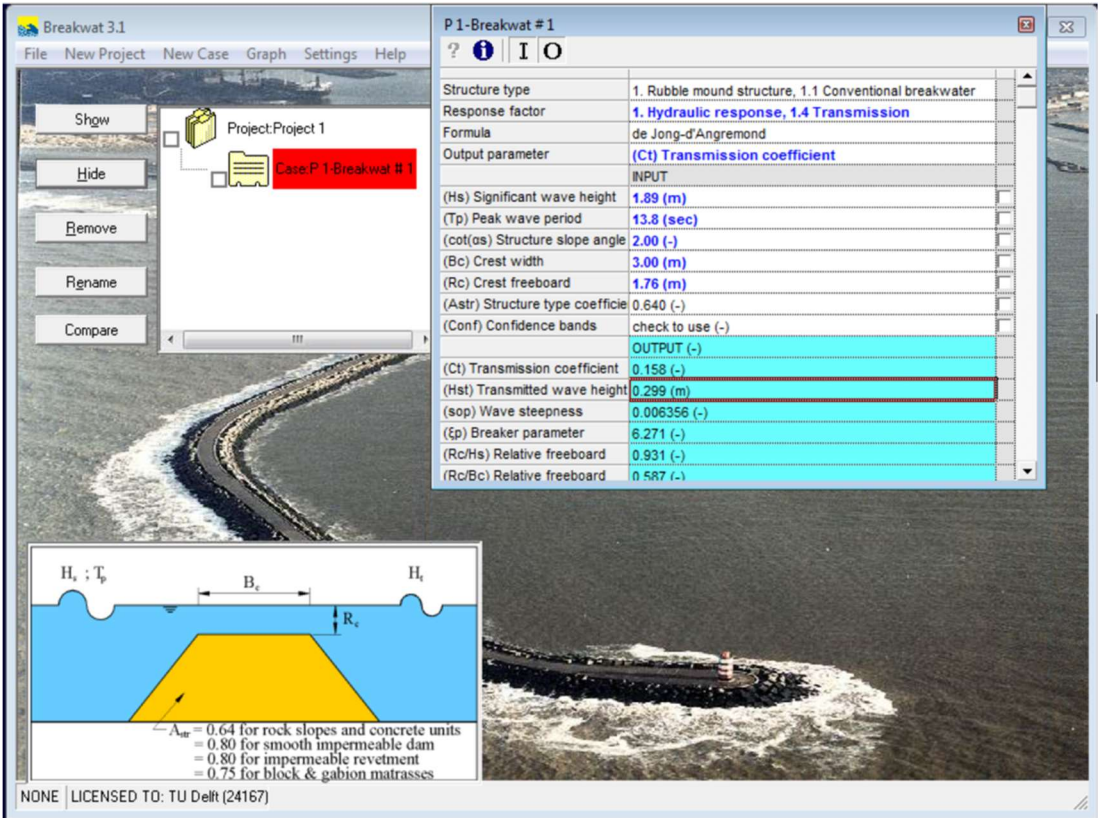


Figure F-5: Breakwat input parameters SLS

The breakwater design is rather simplistic. This is due to the fact that this is just the rough ‘rules of thumb’ calculation, and the case is simplistic in itself. The foundation is made on a rock layer, which is not very usual in breakwater design. Therefore there are no filter layers necessary, as well as no

toe- and scour protection (because there is no outwash of material). Assumed is a slope of 1:2 and a crest width of about 3-4 stones (3m). The height of the breakwater is estimated on **1.76m**.

F.3.2 STONE SIZE

The (ULS) storm wave height is a value based on a probability of failure and the lifetime of the structure. In this case the lifetime is set on 25 years and the probability of failure under normal storm conditions (no tsunami conditions) is 10%. This is a rather average value in the range of 5%-20% (Verhagen, d'Angremond, & van Roode, 2009). These values refer to a design storm of about once every 250 years (237 to be more exact), using the formulas underneath. The ULS storm wave height is meant to design the sizes of the armour stones and equals 10m +MSL. This wave height is obtained via a Weibull transgression, as more in detail discussed in Appendix F.3.

$$p = 1 - e^{-ft}$$

$$f_{designstorm} = -\frac{1}{t} \ln(1 - p)$$

f = Average frequency of the event per year
p = Probability of failure during lifetime
t = Lifetime period

In this phase, the wave height offshore is translated to an onshore value using SwanOne again. The results are listed in Table F-6. Using the software Breakwat the stone size is determined. A weight (W50) of **940 kg** is obtained, with an average diameter of **0.70m**.

Table F-6: Translated (ULS) wave height onshore

SwanOne	Offshore	Onshore
Wave height [Hs]	10,0 m	1.95 m
Mean period [Ts]	10 s	8,5 s

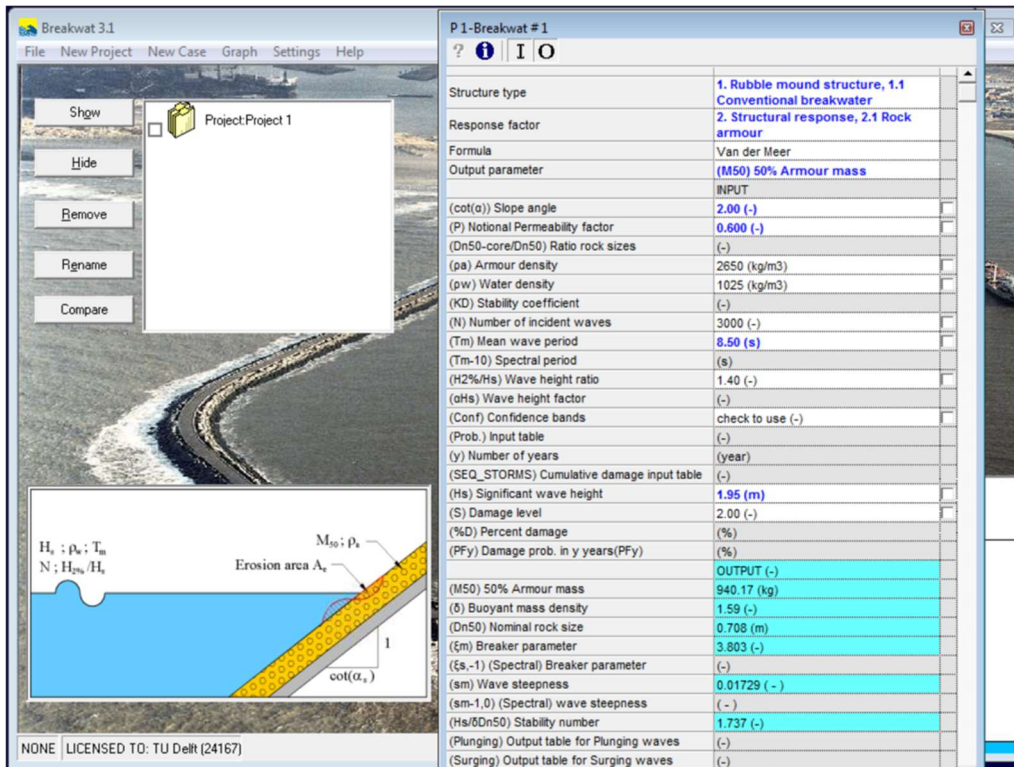


Figure F-6: Breakwat output

The basic (Rule of Thumb) design of the breakwater in summary is given in Table F-7.

Table F-7: Summary of Dimensioning of breakwater

Crest freeboard	1.75 m
High tide	0.45 m
Height breakwater	2.2 m +MSL
Length	40 m
Crest width	3 m
Average height (from seabed)	5.7 m
Slope	1:2
Average cross section	82 m ²
Total volume	4142 m ³
W50	940 kg
Dn50	0.70m

G DESIGN: JETTY

G.1 EVALUATING MARCO AISLADO CONFIGURATION

The Marco Aislado configuration will not be an option for the design of the jetty for a couple of reasons:

First of all, isolated structures are mainly effective in areas in which the most damaging extreme load is earthquake. For the jetty, the damage a tsunami causes will be more relevant, so the use of isolators will only have a small effect.

Secondly, a lot of background information and research is needed before an engineer can adequately design a seismically isolated structure. This takes years of experience and structural understanding. If the seismic isolation is applied inadequately, it will not improve the structural behaviour and can even worsen it.

Furthermore, an extensive study of seismic hazard is required beforehand, which is not possible within the limited timeframe of this project.

Lastly, and probably most importantly, to make the isolated structure work effectively the fundamental period must be above a certain relative high value. The fundamental period of the mass-spring system is dependent on the mass and the stiffness of the structure (Bustos, 2016). The direct relation between the fundamental period and the mass and the stiffness is:

$$T = 2\pi\sqrt{\frac{m}{k}}$$

in which

T	=	the fundamental period	[s]
m	=	the mass	[kg]
k	=	the stiffness	[N/m]

In order to increase the fundamental period of the structure to the required value, the mass would have to be increased so extensively, it is not feasible for a structure as small as this jetty.

G.2 MATERIAL PROPERTIES

Different material types are used in the design of the jetty, the properties of these materials are described in the following tables.

Table G-1: Material properties -Concrete H30 [source: (ETABS, 2016)]

Concrete class	H30	
Type	Isotropic	
Weight per unit volume	24.5	kN/m
Modulus of elasticity	23414	N/mm ²
Poisson's ratio	0.2	-
Shear modulus	9756	N/mm ²
Compressive strength, f_c	24.5	N/mm ²

Table G-2: Material properties -reinforcement A63-42H [source: (ETABS, 2016)]

Reinforcement class	A63-42H	
Tensile strength	440	N/mm ²
Minimum yield strength	280	N/mm ²
Ultimate strain	11.1	%

Table G-3: Material properties -steel A36 [source: (Gerdau AZA S.A., 2010)]

Steel class	A36	
Type	Isotropic	
Weight per unit volume	77	kN/m
Modulus of elasticity	199948	N/mm ²
Poisson's ratio	0.3	-
Shear modulus	76903	N/mm ²
Yield strength, F_y	248	N/mm ²

G.3 INPUT ETABS

G.3.1 DEFINING GRID

A grid is formed by rectangles of 3 times 5 meters in which the structure will be modelled. The height of the grid is 4 meters which is equal to the height of the structure above base level. The grid is shown in Figure G-1.

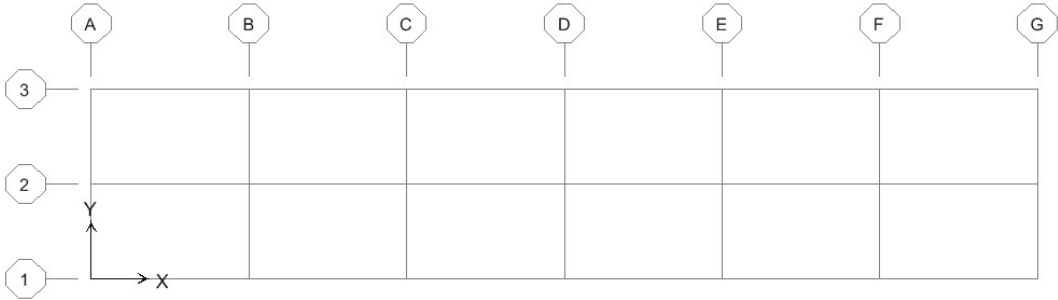


Figure G-1: Basic grid

G.3.2 DEFINING MATERIAL AND SECTION PROPERTIES

Next, the material properties are defined. The chosen strength classes for concrete and steel are H30 and A36, respectively, see Figure G-2 and Figure G-3. The corresponding input material properties are described in Appendix G.1.

The dialog box is titled "Material Property Data" and contains the following fields and options:

- Material Name:** H30
- Display Color:** Color (blue swatch)
- Type of Material:** Isotropic Orthotropic
- Type of Design:** Design (Concrete)
- Analysis Property Data:**
 - Mass per unit Volume: 2.4517
 - Weight per unit Volume: 24.5166
 - Modulus of Elasticity: 23413573.5
 - Poisson's Ratio: 0.2
 - Coeff of Thermal Expansion: 9.900E-06
 - Shear Modulus: 9755655.6
- Design Property Data (ACI 318-08/IBC 2009):**
 - Specified Conc Comp Strength, f'c: 24516.6255
 - Bending Reinf. Yield Stress, fy: 411879.31
 - Shear Reinf. Yield Stress, fys: 411879.31
 - Lightweight Concrete
 - Shear Strength Reduc. Factor: (empty)

Buttons: OK, Cancel

Figure G-2: Material properties -H30 [kN, m]

Material Property Data	
Material Name	A36
Type of Material	<input checked="" type="radio"/> Isotropic <input type="radio"/> Orthotropic
Type of Design	Design: Steel
Analysis Property Data	
Mass per unit Volume	7,8492
Weight per unit Volume	76,9724
Modulus of Elasticity	1,999E+08
Poisson's Ratio	0,3
Coeff of Thermal Expansion	9,900E-06
Shear Modulus	76884615,
Design Property Data	
Minimum Yield Stress, Fy	248211,289
Minimum Tensile Strength, Fu	399895,97
Cost per Unit Weight	2822,5649

Figure G-3: Material properties -A36 [kN, m]

Afterwards, all section properties of the different elements used have to be defined. For the rigid concrete deck, a slab section of material H30 is created with a thickness of 0.25 m of the shell-thin type, see Figure G-4.

Wall/Slab Section	
Section Name	LOS25
Material	H30
Thickness	
Membrane	0,25
Bending	0,25
Type	
<input checked="" type="radio"/> Shell <input type="radio"/> Membrane <input type="radio"/> Plate	
<input type="checkbox"/> Thick Plate	
Load Distribution	
<input type="checkbox"/> Use Special One-Way Load Distribution	
Set Modifiers...	Display Color: ■

Figure G-4: Section properties -concrete deck

For the straight and inclined steel pipes a section of material A36 with an outer diameter of 0.262 m and a wall thickness of 0.006 m is defined. Next, a frame section for the steel beams is created which consists of an H-shaped profile, namely H300x300x105.5 of material A36. Furthermore, the section of the steel frame used for the steel stairs is defined. The section is a tube section of material A36 with a height of 200 mm, a width of 150 mm and a wall thickness of 5 mm. Last, the section for the defence beams is defined as an H-shaped profile of material A36, called H250x200x59.64. See Figure G-5 for all the input data.

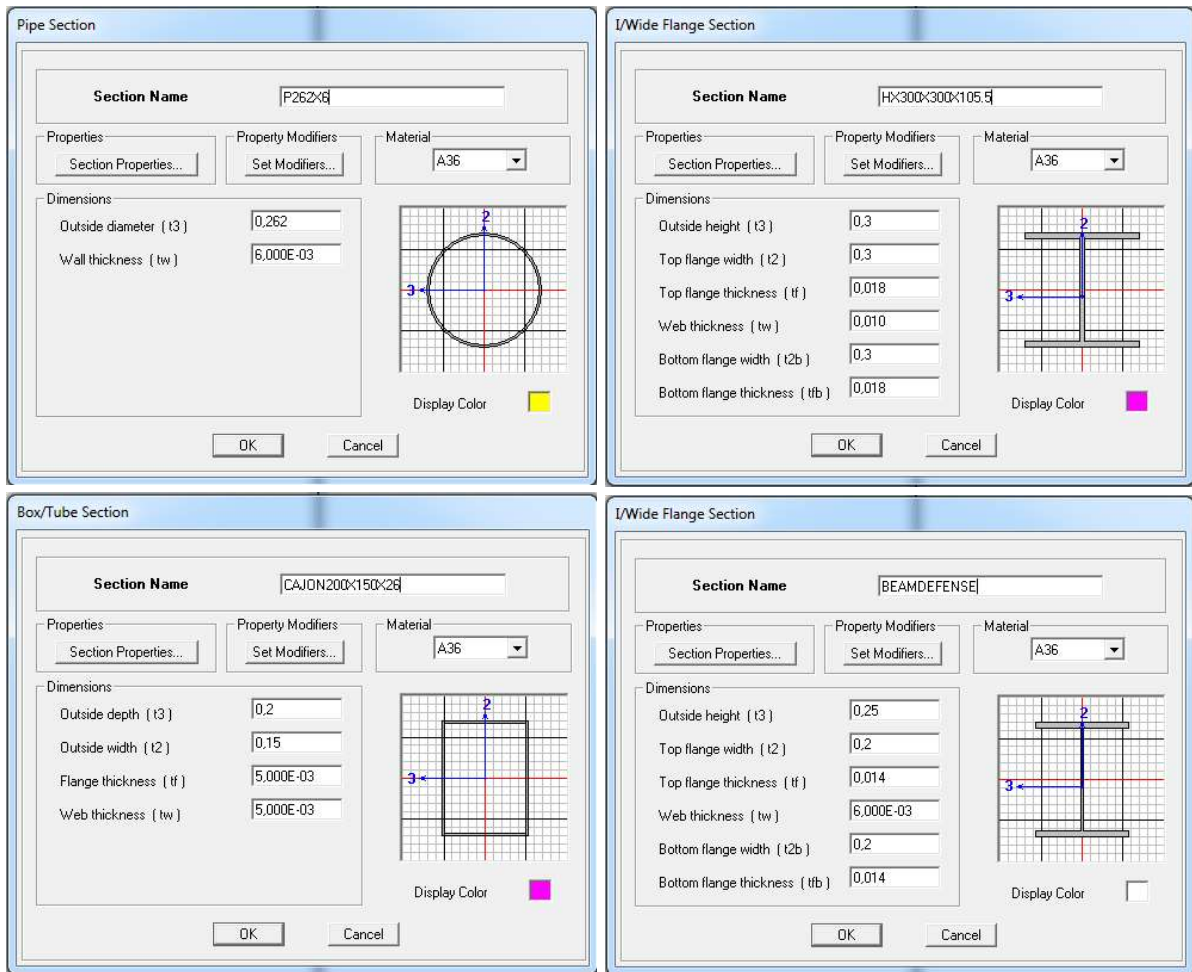


Figure G-5: Section properties -steel elements

G.3.3 DEFINING THE DESIGN

First the rigid concrete deck is created. The concrete deck follows the grid lines plus an additional overhang of 0.5 m at all edges, which results in a total length of 31 meters and a total width of 7 meters. On the side of the concrete abutment, an additional part is needed to guarantee a good connection of the jetty with the abutment. The maximum overhanging length of this deck part is 1.8 m. See Figure G-6. For the deck a mesh is generated, the mesh exists of elements of 0.5 x 0.5 meters.

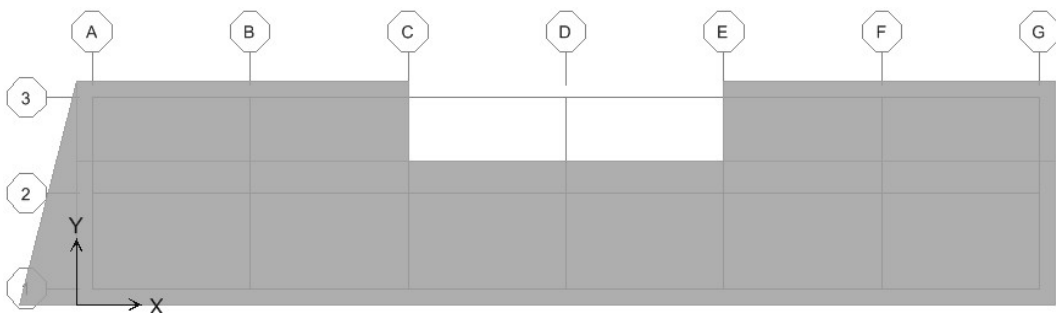


Figure G-6: Design -concrete deck

Next, the piles are created. Both straight and inclined piles are used. The total height above ground level is the same for all piles independent from their structural configuration, namely 4 meters. This length is modelled in ETABS. The support condition for each pile can be modelled as a rigid support which restricts movements and rotations in all directions. The angle between an inclined pile and the vertical axis is 20°.

The straight piles are applied at all grid points except for the piles located at grid point A2, B2, F2, and G2. At grid point A2 and G2 inclined piles are modelled, directed in y-direction. At grid point B2 and F2 inclined piles are modelled, directed in x-direction. See Figure G-7.

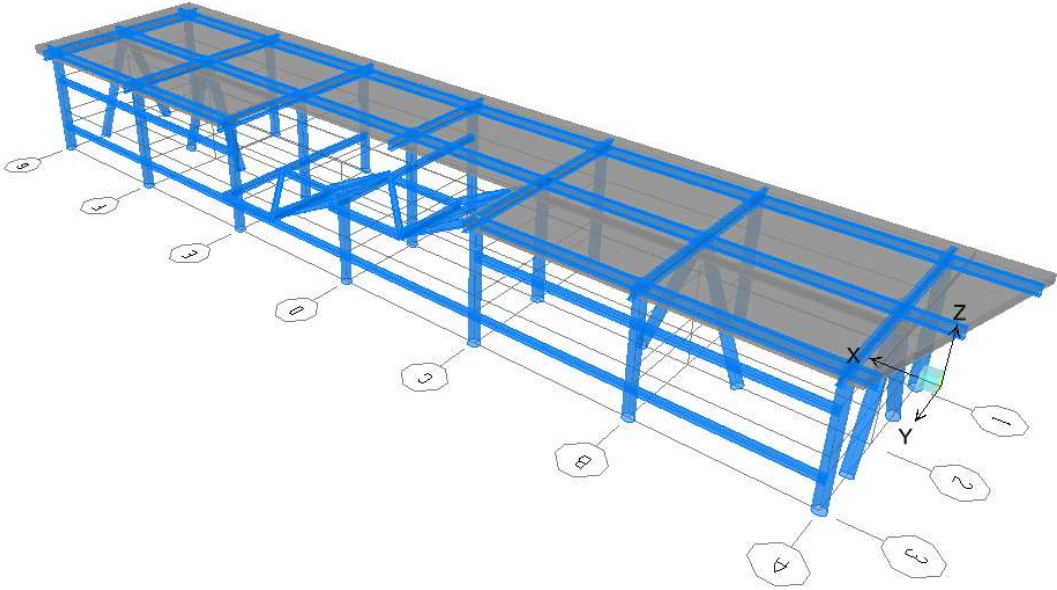


Figure G-7: Design -piles and beams

Next, the beams are modelled. The beams are drawn along the grid lines just underneath the concrete deck. They have a small cantilever at all sides to support the protruding concrete deck. The frame of the stairs is drawn as described in Appendix G.3.3 and finally two beams are drawn on the stairs side of the jetty to which the defenders will be attached.

G.3.4 DEFINING LOAD CASES AND LOAD COMBINATIONS

After completing the structural design in ETABS, all load cases need to be defined, see Figure G-8. The magnitude and location of the loads are described in paragraph G.3. The next step was to formulate all the load combinations, see Figure G-9.

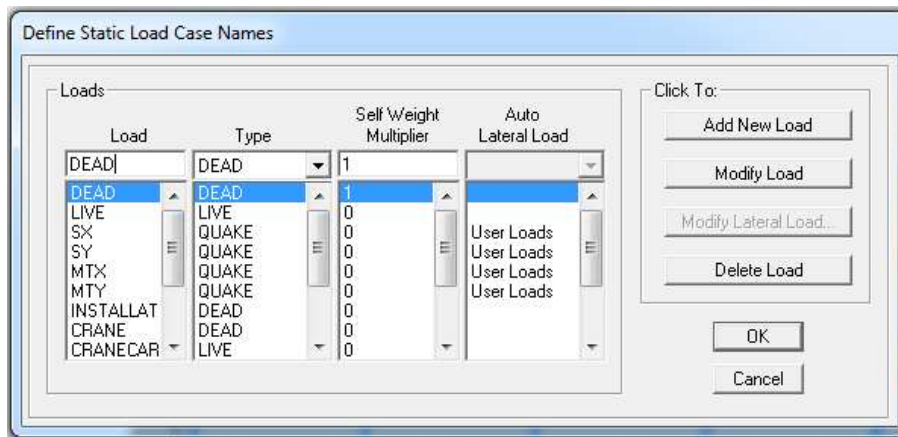


Figure G-8: Load cases

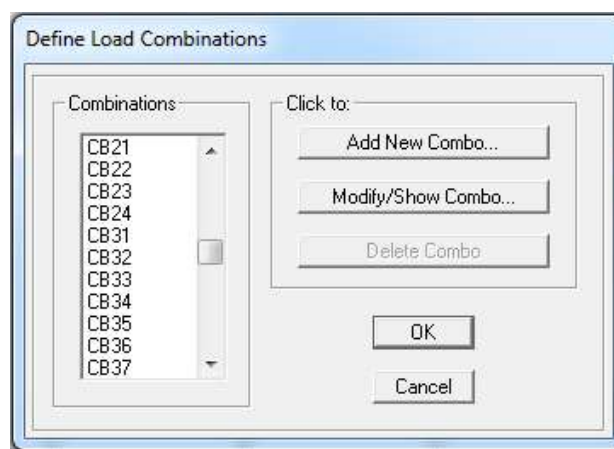


Figure G-9: Load combinations

G.4 LOAD CASES

G.4.1 LOADS ACTING FROM LAND SIDE – PERMANENT LOADS

Loads acting from land side are usually soil-related. In the current design, the jetty is placed completely separate from land and therefore, no permanent loads acting from the land side are to be taken into account.

G.4.2 LOADS ACTING FROM LAND SIDE – LIVE LOADS

In general, the live loads from the land side are caused by the gap filling between the jetty and the land as well as those resulting from pore pressures in the soil and filling. But as mentioned in the previous paragraph, the jetty in this design is a complete independent structure, thus, these live loads are not applicable.

Another live load acting for the land slide is the seismic load. As the jetty is located in an earthquake-prone area, this load is most definitely not negligible. The seismic loads are determined according to the Chilean standards mentioned in Part I: Analysis, Chapter 2.2.3. Both in horizontal and vertical direction coefficients are applied to the self-weight of the structure. As the Chilean standard prescribes, the seismic analysis is carried out using a linear method, called static analysis. (Hidalgo,

1986). An extensive calculation, according to (Hidalgo, 1986) is discussed in the following subsections.

Horizontal seismic loads

The horizontal seismic load is expressed as a horizontal base shear force. To determine this value, firstly, the zone needs to be established. Dichato lies in zone 3 (which is the coastal zone of Chile), in the 8th region, Bío-Bío. With this information, the value of the maximum effective acceleration (A_0) can be derived:

$$A_0 = 0.40g \text{ m/s}^2$$

Next, some parameters relative to the foundation soil have to be determined. The soil present in the Dichato bay is of soil type 2. This results in the following parameters:

$$T' = 0.35 \text{ s}$$

$$n = 1.33$$

The next step is to calculate the seismic coefficient (C), according to the following formula:

$$C = \frac{2.75A_0}{gR} \left(\frac{T'}{T^*} \right)^n \left(\frac{0.05}{\xi} \right)^{0.4}$$

R is the response modification factor. To determine this factor, the Marco Duplas and the Marco Flexural are assumed to be an isostatic seismic resistant structure, which brings the response modification factor up to 3.

The resistant system of the jetty consists of “steel frames with field bolted connections, with or without bracings” (Hidalgo, 1986). The damping ratio (ξ) belonging to this resistant system, is equal to:

$$\xi = 0.03$$

The only thing left to do is determining the fundamental period of vibration in the direction of the analysis (T^*). Two directions have to be considered, namely the x- and y-direction. The periods belonging to these directions are the periods belonging to the first and second mode of the structure. The fundamental periods will be different for all three configurations and are deducted from software (ETABS, 2016) (see

Table G-4). With all determined input, the seismic coefficient for both directions can be calculated, see

Table G-4.

The calculated seismic coefficients (C) need to be lower than a certain maximum value (C_{max}). This value depends on both the response modification factor as well as the damping ratio and is equal to 0.34.

Besides that, the calculated seismic coefficients (C) shall in no case be lower than a certain minimum value (C_{min}) which is equal for all structural configurations:

$$C_{min} = \frac{0.25A_0}{g} = \frac{0.25 \cdot 0.40g}{g} = 0.10$$

Table G-4: Calculation of seismic coefficient (C) and base shear) Q_0

Maximum effective acceleration, A_0	0.40g		m/s ²
Soil dependent parameter, T^*	0.35		s
Soil dependent parameter, n	1.33		-
Response modification factor, R	3		-
Damping ratio, ξ	0.03		-
	x-direction	y-direction	
Fundamental period, T^*	0.29	0.30	s
Seismic coefficient, C	0.57	0.55	-
Minimum seismic coefficient, C_{min}	0.10	0.10	-
Maximum seismic coefficient, C_{max}	0.34	0.34	-
Final seismic coefficient, C	0.34	0.34	-
Importance factor, I	1.00	1.00	-
Weight of the structure, P	1975	1975	kN
Base shear, Q_0	672	672	kN

With the information from

Table G-4, the base shear (Q_0) for both directions can be calculated according to the following formula:

$$Q_0 = CIP$$

I is the coefficient of importance, dependent on the classification of the structure and equipment according to their importance. The jetty is of category C2 which includes “normal structures and equipment, which may be affected by normal easily repairable failures, ...” (Hidalgo, 1986). For a more thorough description, see (Hidalgo, 1986)

The importance coefficient (I) for this category is equal to:

$$I = 1.00$$

P is the total weight of the structure above the base level including self-weight of the jetty and half of the live load on the deck, see Table G-4. The self-weight of the jetty can be obtained from software (ETABS, 2016) as it is equal to the reaction forces resulting from the structure after exposing it to its dead load. The live load is equal to:

$$=0.5[A_{deck} \times v_{deck}] = 0.5[(31 \times 7 + 0.5 \times 1.8 \times 7) \times 5] = 558 \text{ kN}$$

Finally, the base shear (Q_0) can be obtained for each direction and structural configuration. The results are displayed in Table G-4.

So, the shear forces act as a horizontal force in x- or y-direction. It is not necessary to take into account the effect of both horizontal seismic loads acting at the same time. The seismic forces act on the centre of mass of the structure. As the centre of mass is different from the centre of stiffness of the structure, the horizontal force will initiate a torque acting in the horizontal plane due to the eccentricity between the two centre points (Hidalgo, 1986). This torque needs to be considered at the same time as its corresponding shear force. The magnitude of the torque can be calculated as the shear force times the lever arm. The lever arm in respectively x- and y-direction is defined as:

$$\pm 0.10 b_x Z/H; \pm 0.10 b_y Z/H$$

in which

- b_x = the length of the deck in x-direction = 32.8 m
- b_y = the length of the deck in y-direction = 7 m
- Z = the height of the deck above base level = 4 m
- H = the total height of the jetty above base level = 4 m

From these values, the lever arm can be determined after which the torque can be calculated. The results for the torque are displayed in Table G-5.

Table G-5: Calculation of the torque (T)

	x-direction	y-direction	
Lever arm, a	3.28	0.7	m
Base shear, Q_0	672	672	kN
Torque, T	470	2203	kNm

Vertical seismic loads

According to (Hidalgo, 1986) vertical seismic accelerations do not need to be considered because the structure does not meet the mentioned requirements.

G.4.3 LOADS OF AND ON THE JETTY ITSELF – PERMANENT LOADS

The permanent loads of and on the jetty itself include the self-weight of the jetty with all its permanent facilities. These facilities include the crane, mooring stairs and installations.

Self-weight jetty

The self-weight of the structure can be derived from software (ETABS, 2016). The total self-weight of the structure is 1417 kN, ETABS (2016) takes self-weight automatically into account, so it does not have to be applied as an external load.

Self-weight crane

The crane, which will have a permanent placement on the jetty, is a heavy duty free standing jib crane. The self-weight of this crane is 13 kN, this force is assumed to be transferred to the concrete deck through a point load. (Crane Authority, 2009)

Self-weight mooring stairs

The frame of the stairs is drawn in software ETABS (2016), see Figure G-10. The section used for the frame is a steel tube of class A36 with a height of 200 mm, a width of 150 mm and a wall thickness of 5 mm. (Reference Bachelor Thesis) Additionally, the self-weight of the stair steps and plateaus need to be added, which comes down to a area load of 0.5 kN/m². (Steel Flooring Products Co, n.d.) This load is transferred as line loads to the steel frame of the stairs, see Figure G-11.

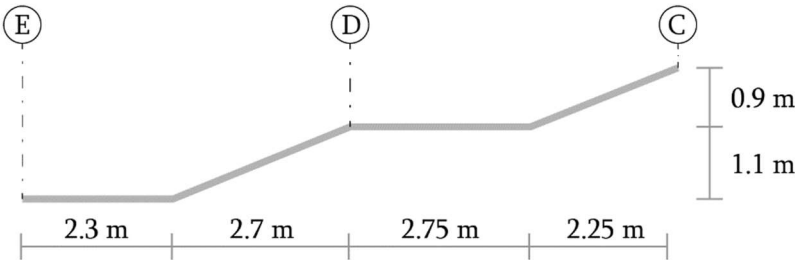


Figure G-10: Frame of mooring stairs

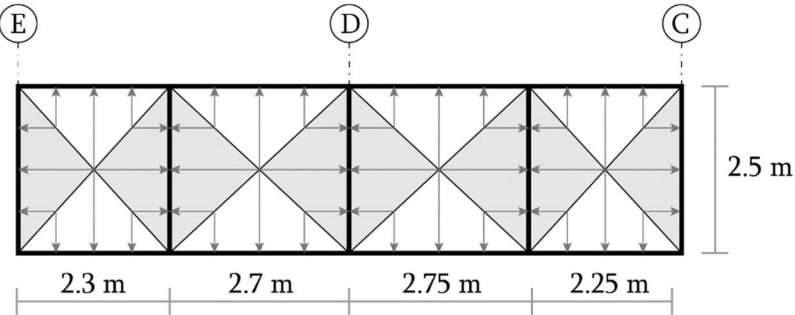


Figure G-11: Load configuration on stairs

Self-weight installations

The self-weight of the installations includes both balustrades at the edges of the deck as well as electricity and water facilities. The self-weight of the balustrade is about 0.3 kN/m (Hekwerkshop.nl, 2013). The contribution of the electricity and water facilities are assumed to be about 0.2 kN/m, which brings the total line load equal to 0.5 kN/m. This vertical distributed line load is applied on all edges of the deck.

G.4.4 LOADS OF AND ON THE JETTY ITSELF – LIVE LOADS

The live loads of and on the jetty itself include variable loads, crane cargo loads, truck loads, and wind loads. Snow loads do not have to be considered in the region of Dichato. Compared to the seismic load combinations, the wind load combinations will never be governing so it is decided to not include them in the analysis. However, the magnitude of the wind loads is calculated and added in this paragraph.

Variable loads

The codes do not include values for the variable loading on jetties. For this reason, the Bachelor Thesis of Munoz (2010) is used as a reference point from which it is assumed that the variable loading is equal to 5.0 kN/m². This variable load includes the truck load. The variable load is applied as an area load on the whole concrete deck.

For the stairs, a smaller variable load is taken because the stairs will not be exposed to high cargo loads or traffic. For this reason, the recommended value from the codes is taken, namely 2.5 kN/m² (Hidalgo, 1986). The variable load act as an area load, but had to be transferred as line loads to the steel frame.

Crane loads

The crane chosen has a loading capacity of 1 ton and a lift range of 6 meters. The live load of the crane is equal to this value, so 10 kN. This force is transferred to the concrete deck as a vertical point load of 10 kN and a bending moment of 60 kNm (= 6 m x 10 kN).

Wind loads: general

The calculation of the wind loads on a structure is dependent on the structure's rigidity, in accordance with the Chilean standard NCh432 (Ibáñez V., 1971). According to NCh432, the two structural configurations can be categorized as "rigid" structures, and will therefore have the same wind loads. A calculation of the wind loads is performed in the next sections.

Horizontal wind loads

The horizontal wind loads acting on the structure will have compression on the windward side, while it will result in tensile stresses both on the leeward side and on lateral surfaces. The resulting distributed loads will increase linearly with height, above the water surface. In Figure G-12, the values of these loads are presented for all structural configurations.

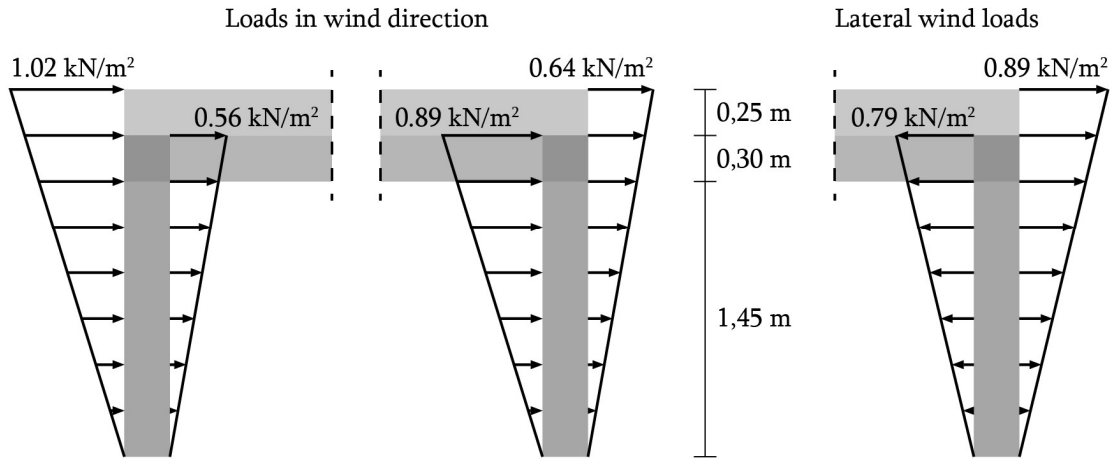


Figure G-12: Horizontal wind loads

The resulting load perpendicular to the jetty is 37.8 kN, while the resulting load parallel to the jetty is 2.8 kN.

Vertical wind loads

The vertical wind loads acting on the deck comprise two load cases, one with downward pressure and one with upward pressure. The loads calculated are presented in Figure G-13. As both cases occur simultaneously, their sum results in a vertical downward pressure of 0.12 and 0.25 kN/m², respectively.

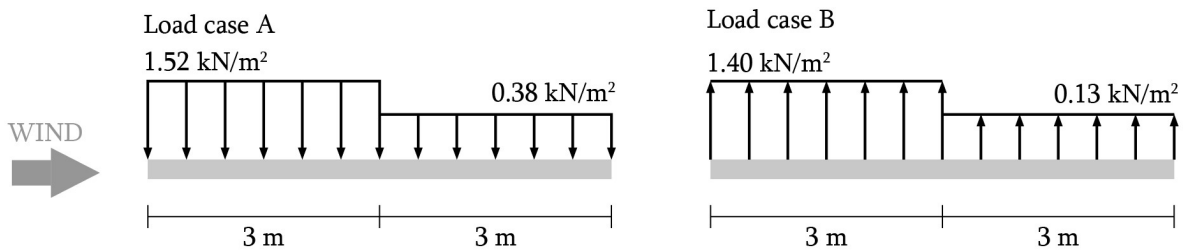


Figure G-13: Vertical wind loads

G.4.5 LOADS ACTING FROM SEA SIDE – PERMANENT LOADS

The jetty is not exposed to any permanent loads acting from the sea side.

G.4.6 LOADS ACTING FROM SEA SIDE – LIVE LOADS

The live loads acting from the sea include wave loads, current loads, bollard pulls, and impact loads. Ice loads do not have to be considered in the region of Dichato. Wave loads have been calculated but they are too small to even consider them. The reason for this low value is the reduction of the wave heights and current load as a result of the placing of the breakwater.

Impact loads

When the vessel hits the jetty, an huge horizontal load acts on the structure, an impact load. The magnitude of this load is equal to -85 kN (Sandoval Munoz, 2010). This load occurs at one of the

defenders which will transfer the load to the two horizontal steel girders which are placed at one side of the jetty. Two extreme cases will be considered, in which the vessel will hit the jetty on the corner, see Figure G-14.

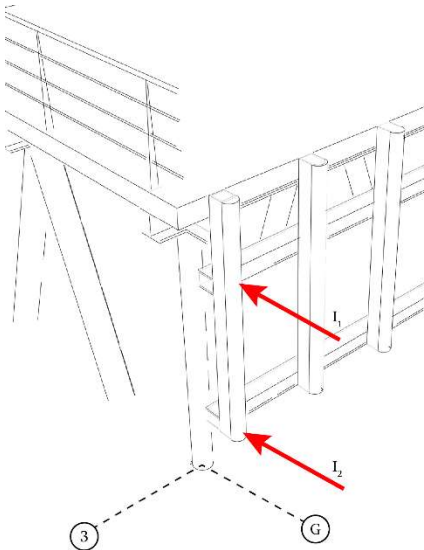


Figure G-14: Impact load schematized on pile G3

Bollard pulls

Two bollard are placed on the concrete deck, located on grid point B3 and F3. See Figure G-15 for a schematization of the load. The load from the bollard can be transferred to a load on the deck by dividing it into a horizontal component, a vertical component, and a moment about the x-axis. The vertical component and the moment are the result of the water height. If the water height is below the level of the stairs, the bollard is exposed to a negative vertical load and a bending moment about the x-axis. The horizontal load is equal to +32.2 kN and the vertical load equals to -8.4 kN. The bollards have a height of 250 mm, which results in a bending moment of $0.25 \times 32.2 = -8.1$ kNm (Sandoval Munoz, 2010).

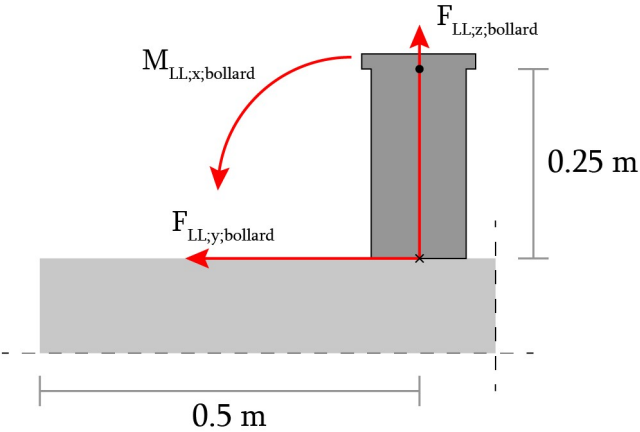


Figure G-15: Bollard pull loads on jetty

G.5 CORRECTION LOADS FOR FINAL DESIGN

For the final design, the optimized design has been determined. Because the dimensions of the elements changed compared to the original dimensioned model, the self-weight of and the horizontal seismic loads on the structure has changed too. The new values are calculated in the following paragraphs.

G.5.1 SELF-WEIGHT

The new total self-weight of the structure is 1354 kN.

G.5.2 SEISMIC LOADS

For the final design, most of the parameters used to calculate the seismic loads stay the same, except for the fundamental period and the self-weight. After changing the fundamental period and the self-weight, the new seismic loads are determined, see

Table G-6 and Table G-7.

Table G-6: Calculation of the seismic coefficient (C) and the base shear (Q₀)

	x-direction	y-direction	
Maximum effective acceleration, A ₀	0.40g		m/s ²
Soil dependent parameter, T ^o	0.35		s
Soil dependent parameter, n	1.33		-
Response modification factor, R	3		-
Damping ratio, ξ	0.03		-
	x-direction	y-direction	
Fundamental period, T*	0.23	0.23	s
Seismic coefficient, C	0.78	0.77	-
Minimum seismic coefficient, C _{min}	0.10	0.10	-
Maximum seismic coefficient, C _{max}	0.34	0.34	-
Final seismic coefficient, C	0.34	0.34	-
Importance factor, I	1.00	1.00	-
Weight of the structure, P	1912	1912	kN
Base shear, Q ₀	650	650	kN

P is the total weight of the structure above the base level including self-weight of the jetty and half of the live load on the deck:

$$P = 1354 + 558 = 1912 \text{ kN}$$

Table G-7: Calculation of the torque (T)

	x-direction	y-direction	
Lever arm, a	3.28	0.7	m

Base shear, Q_0	650	650	kN
Torque, T	455	2133	kNm

G.6 FOUNDATION PILES

Following the dimensioning phase, the resulting pile dimensions adhere to requirements for structural safety and stability. However, the design is enhanced by considering construction aspects and failure mechanisms of the foundation elements.

G.6.1 CONSTRUCTION CONSIDERATIONS

Pile driving equipment

Table G-8: Characteristics of DELMAG D-12 pile driving rig, [source: www.hammersteel.com]

Energy per blow	kg m	3125
Piston weight	kg	1250

The weight W_p of one of the vertical piles of 6m length is $6.0 \times 37.88 = 227.3$ kg. For an inclined pile, it is $6.4 \times 52.68 = 337.2$ kg. It is recommended for this hammer type that the mass of the piston exceeds a third of the weight of the pile. Considering the piston weight of 1250 kg this condition is satisfied for both the vertical and inclined piles.

The transmitted load with each blow is equal to the ultimate bearing capacity of the pile, at 550 kN axially for the vertical piles with diameter 262mm. The Gates formula commonly employed in a dynamic pile driving calculation is

$$R_u = 7\sqrt{E_r} \log(10N_b) - 550 \quad (10)$$

With R_u the ultimate bearing capacity in kN, E_r the energy per blow of the hammer in Joules and N_b the variable of interest: the number of blows per inch at the 'rejection' point. The resulting value for N_b is 0.774 blows per inch, or **32.3 mm/blow**. At this point of embedment, the pile has developed sufficient bearing capacity. A similar calculation may be done for the inclined piles, which gives an N_b value of **13 mm/blow**.

Considering the harbour application, the piles must be driven from a floating pontoon. Furthermore, driving inclined piles adds wear and tear on the piston and cylinder of a hammer. However, according to the chart for Diesel hammers as in Figure G-16, a D12 hammer is able to drive up to 26° (a 1:2 inclination) without a cylinder extension.

Pile buckling during driving

Here, the American code AISC 360-05 *Specification for Structural Steel Buildings* is used. To verify that the thinnest steel profile of the adopted piles (262 x 6 mm), is not too slender, the following check is made on the limiting slenderness parameter for a noncompact element

$$\lambda_r = 0.11 \frac{E}{F_y} > \frac{D}{t} \quad (11)$$

The left-side of this inequality takes into account a Young's modulus of steel of $2.1 \times 10^5 \text{ kg/cm}^2$; and a yield strength F_y of 2400 kg/cm^2 when considering A-53 type steel, and gives a value of $96 \cdot \frac{D}{t}$ with a diameter of 262 mm and a thickness of 6 mm gives 43.7 . Therefore, this check on slenderness is satisfied.

Finally, a check is made on the ultimate compressional strength during pile driving

$$R_{b;ult} = F_{b;ult} \cdot A_g = 0.658^{F_e} \cdot F_y \cdot A_g \quad (12)$$

With

$$F_e = \frac{\pi^2 E}{\left(\frac{kL}{i}\right)^2} = \frac{\pi^2 \cdot 2.1 \times 10^8}{\left(\frac{1.0 \cdot 6.4}{0.0233}\right)^2} = 27471 \text{ kPa} \quad (13)$$

Giving a $R_{b;ult}$ of 6196 kN . AISC recommends a capacity reduction factor Ω of 1.67 . Thus, the check on compressional strength with regards to the rejection point compressional load (550 kN) is

$$\frac{R_{ax;ult}}{R_{b;ult}/\Omega} = \frac{550}{6196/1.67} = 0.15 \ll 1 \quad (14)$$

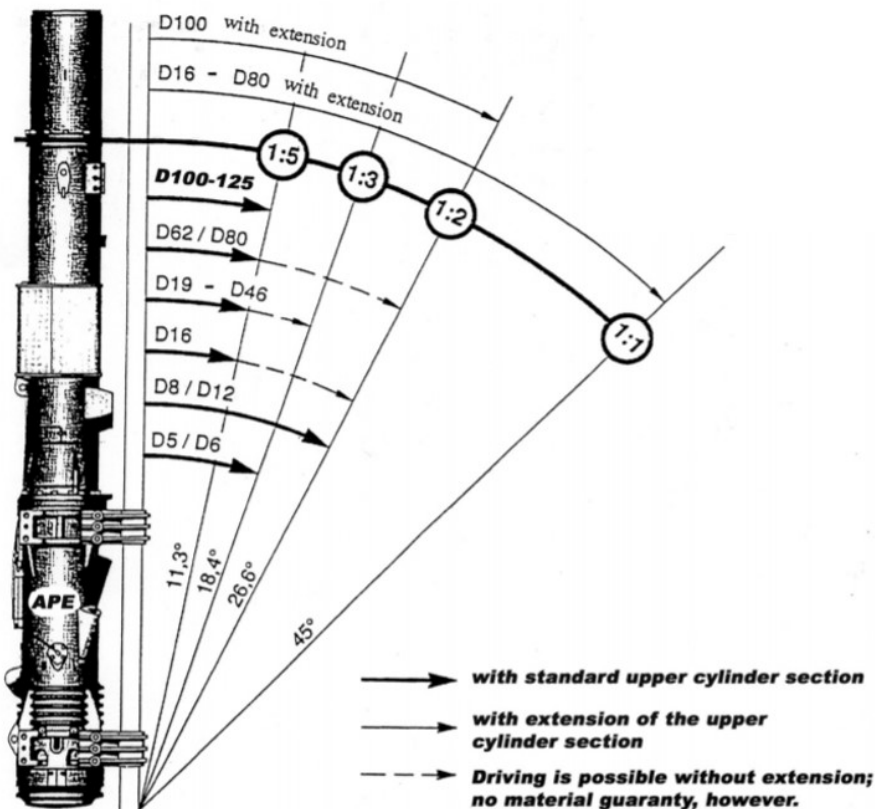


Figure G-16: Pile driving hammer cylinder extension requirements for various batter angles

Anchoring

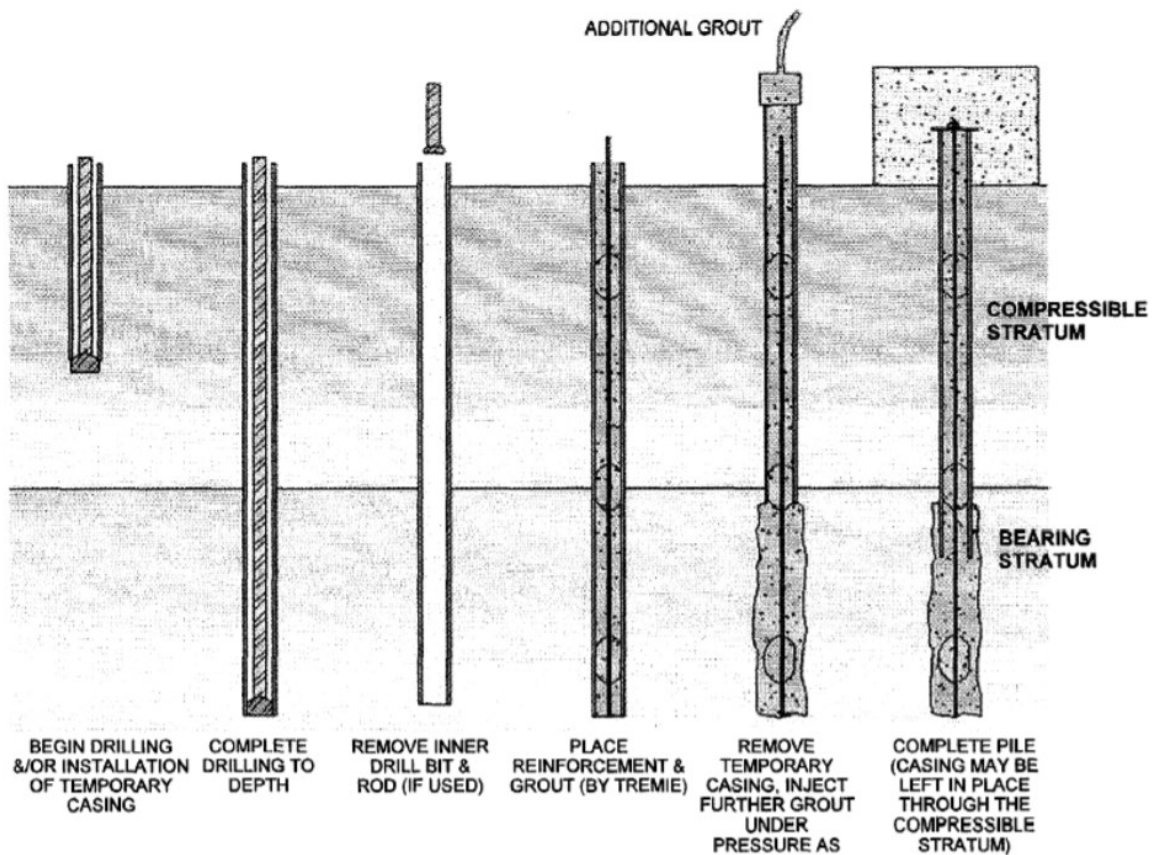


Figure G-17: Micropiling construction sequence (basis for rock anchoring method common in Chile). [source: Design and Construction of Micropiles, L. Shaw and F.C. Chung]

Corrosion

Several corrosion mechanisms exist on steel piles, but the most significant mechanism in Accelerated Low Water Corrosion (ALWC) is microbially induced corrosion, in which the actions of micro-organisms generate additional corrosion through an increase or decrease of dissolved oxygen in the seawater. As Figure G-18 shows, the rate of loss of steel is greatest in the low water zone.

Mitigation measures that may be applied, other than the 4mm of added steel thickness already implemented, include treatment with epoxy of the susceptible shaft part of the pile (below Mean Sea Level). However, particularly effective is sacrificial anode cathodic protection, where a zinc or aluminium anode is welded onto each steel pile (PDCA, 2001).

For the jetty to be constructed in Dichato, the most suitable option is sacrificial anode cathodic protection, since applying a protective coating would require regular maintenance, which is often not carried out sufficiently in Chilean port works. The other form of cathodic protection, Impressed Current Cathodic Protection, is uneconomical for small jetties. The sacrificial anodes usually have a protective limit of 5-7m of pile length and a lifetime of 10 years (PDCA, 2001).

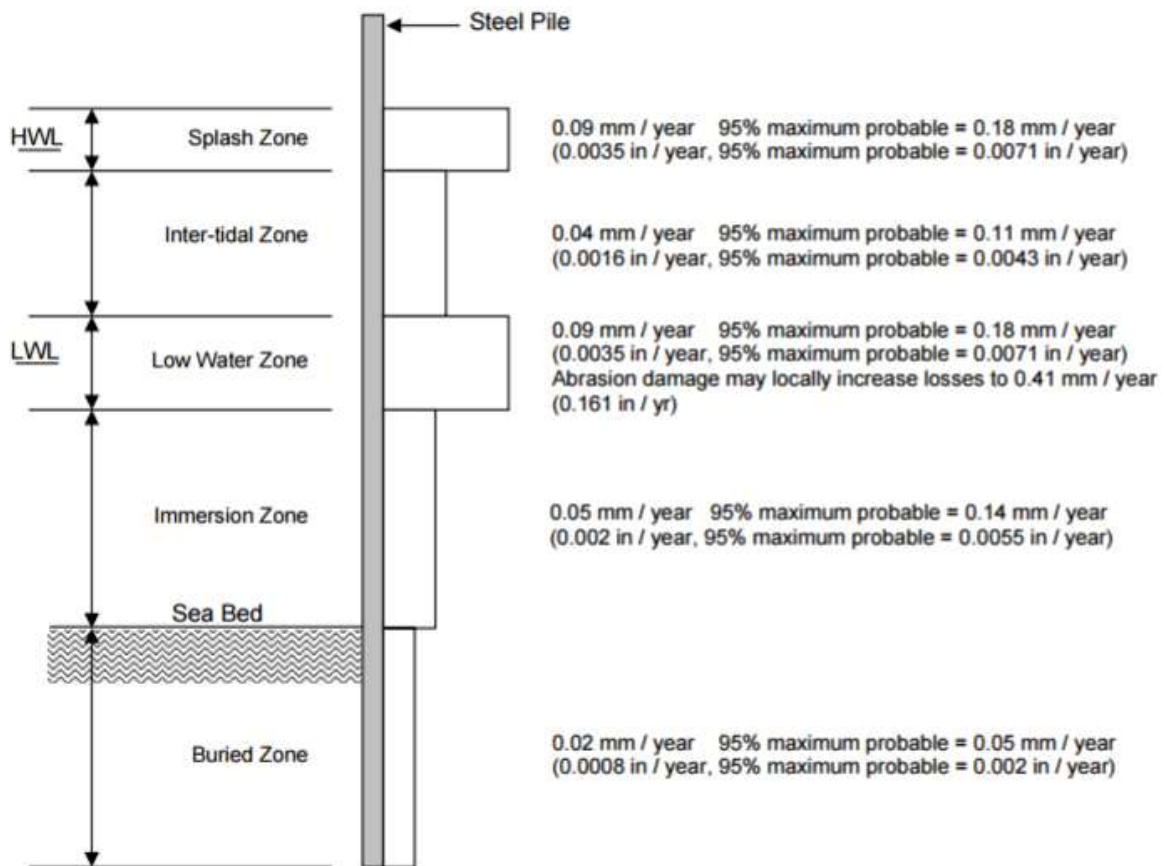


Figure G-18: Loss of thickness for steel piles in seawater (after Morley and Brace, 1963)

G.6.2 FAILURE MECHANISMS

Besides uplift and buckling, the foundation piles of the jetty may be subjected to the following two general failure mechanisms: 1) (differential) settlement and 2) liquefaction-induced failures.

Deformation and settlement

The settlement of point bearing piles S_0 consists of the elastic compression of the pile S_e and the deformation of the subsurface below the point S_s , according to

$$S_0 = S_e + S_s = \frac{PL}{A_p E_p} + \frac{Pd}{A_p E_s} \quad (15)$$

With P = pile load; L = length of pile; d = diameter of pile; A_p = cross-sectional area of the pile; E_p = Young's Modulus of the pile; and E_s = Young's Modulus of the soil layer below the pile point. Table * gives the values taken for each parameter, for the most heavily loaded and the least heavily loaded vertical piles in load condition CB21. The settlement of the inclined piles is considered of lesser importance since battered piles generally show superior settlement behaviour.

Table G-9: Ultimate pile settlements for vertical piles

		Smallest vertical pile load	Largest vertical pile load
P	kN	34.6 (pile C19)	192.0 (pile C49)
L	m	6.0	
d	m	0.262	
A_p	m ²	3.883e-3	
E_p	kN/m ²	2.1e8	
E_s	kN/m ²	1.0e6	
S_0	m	0.0026	0.014

Liquefaction and lateral spreading

Horizontal loading due to lateral spreading may cause bending or buckling of the steel pipes, see Figure G-19 and Figure G-20. This is the case even for extremely gentle slopes of a mere 2° or 3° to the horizontal (Haigh, 2000). Similar failure modes may develop for pile groups, resulting in possible rotation of the pile cap which may cause significant distress to the superstructure, especially if the piles are not well rock-socketed into the bedrock, i.e. no plastic hinges develop at the pile tips. For raked piles, however, liquefaction induced damage is substantially reduced due to the ability of inclined piles to resist lateral loads. However, buckling in the positive (compression) pile must still be taken into account in the pile design.

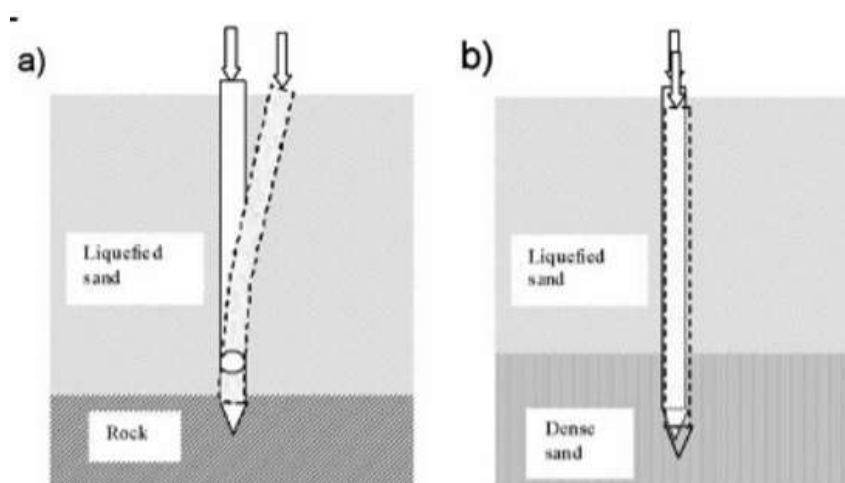


Figure G-19: Modes of collapse for single piles in liquefiable soil (a) buckling instability (b) bearing failure

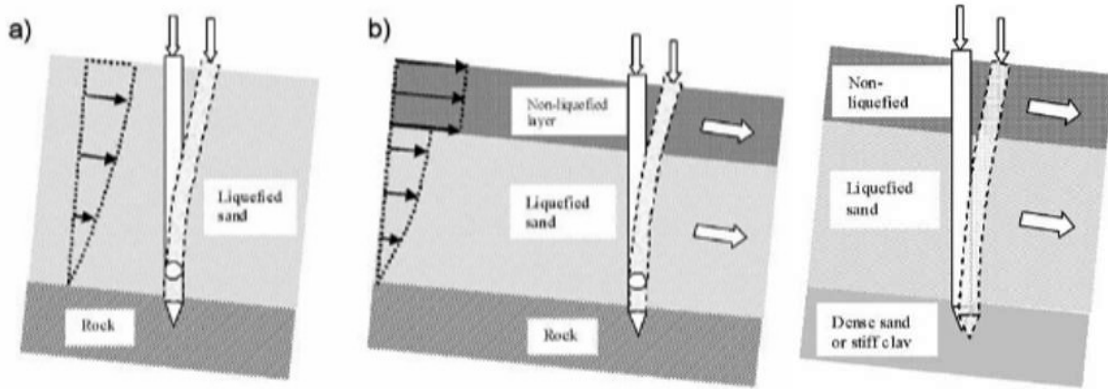


Figure G-20: Failure of piles under combined lateral and axial loads in laterally spreading soil (a) liquefiable sand only with buckling (b) with non-liquefied crustal layer with flexural bending (c) with dense sand bottom stratum with combined bending and settlement failure.

The liquefaction potential, or LP , of a soil is defined as the ratio between the Cyclic Resistance Ratio CRR (the capacity of the soil to resist liquefaction) and the Cyclic Stress Ratio CSR (the seismic demand on a soil layer)

$$LP = \frac{CRR}{CSR} \quad (16)$$

First, the seismic demand is computed using the following formula

$$CSR = (\tau_{av}/\sigma'_{vo}) = 0.65 \left(\frac{a_{max}}{g} \right) \left(\frac{\sigma_{vo}(z)}{\sigma'_{vo}(z)} \right) r_d(z) \quad (17)$$

Where a_{max} = peak horizontal acceleration at the ground surface generated by the earthquake, at $0.4g$ in this region in Chile; g = acceleration of gravity; σ_{vo} and σ'_{vo} are the total and effective overburden stresses, respectively; and r_d = stress reduction coefficient, at $1.0 - 0.00765z$ for $z \leq 9.15$ m.

Next, the CRR is computed based on correlations with a corrected SPT blow count $(N_1)_{60}$. The correction factors account for hammer energy, borehole diameter, rod length, sampler lining and reference overburden stress. See Appendix * for the determination of these factors. The CRR value is determined using the clean-sand base curve by Youd and Idriss (2001), which is a conservative assumption regarding the fine content of the soils. This curve is based on an earthquake magnitude of around 7.5. A formula approximating the clean-sand curve is

$$CRR_{7.5} = \frac{1}{34 - (N_1)_{60}} + \frac{(N_1)_{60}}{135} + \frac{50}{[10 \cdot (N_1)_{60} + 45]^2} - \frac{1}{200} \quad (18)$$

SPT BLOW COUNTS				CORRECTED SPT BLOW COUNT					
Depth below MSL, m	SPT N start jetty	SPT N end jetty	SPT N when excavated	Start jetty		End jetty		When excavated	
				Depth, m	N160	Depth, m	N160	Depth, m	N160
0	0	0	0	0	0	0	0	0	0
1	5	0	0	1	8.5	1	0	1	0
2	7	10	0	2	11.9	2	17	2	0
3	40	40	40	3	68	3	68	3	68
4	70	70	70	4	105.529	4	101.0363	4	101.0363
5	70	70	70	5	94.38798	5	90.36961	5	90.36961
6	70	70	70	6	82.49579	6	82.49579	6	82.49579
7	70	70	70	7	76.37626	7	76.37626	7	76.37626
8	70	70	70	8	71.44345	8	71.44345	8	71.44345

MATERIAL PROPERTIES

	abbreviation	y_sat	y_unsat	% fines	alpha	beta
sand	SM		17	7	45	5 1.2
silt	ML		20	10	80	5 1.2
sandstone	R		22	12	0	

TOTAL & EFFECTIVE STRESSES

Depth, m	Start jetty		End jetty		When excavated	
	sig0/sig'0	sig0/sig'0	sig0/sig'0	sig0/sig'0	sig0/sig'0	sig0/sig'0
0		0		0		0
1	2.428571429			0		0
2	2.428571429	2.111111111				0
3	2	2.222222222				1.909090909
4	1.75	1.909090909				1.833333333
5	1.75	1.833333333				1.833333333
6	1.833333333	1.833333333				1.833333333
7	1.833333333	1.833333333				1.833333333
8	1.833333333	1.833333333				1.833333333

LIQUEFACTION POTENTIAL

Start jetty				End jetty			
Depth, m	CSR	CRR	LP	Depth, m	CSR	CRR	LP
0		0		0		0	
1	0.626598143	0.100137229	0.159810925	1	0	0	0
2	0.621767714	0.130256029	0.209493073	2	0.540491	0.180831	0.334568
3	0.508066		1	3	0.564518	1	1.2
4	0.441077		1	4	0.481175	1	1.2
5	0.43759625		1	5	0.458434	1	1.2
6	0.454787667		1	6	0.454788	1	1.2
7	0.451141167		1	7	0.451141	1	1.2
8	0.447494667		1	8	0.447495	1	1.2

When excavated			
Depth, m	CSR	CRR	LP
0		0	
1		0	
2		0	
3	0.484972091		1
4	0.462080667		1
5	0.458434167		1
6	0.454787667		1
7	0.451141167		1
8	0.447494667		1

Figure G-21: Liquefaction data for jetty foundation design

Scour

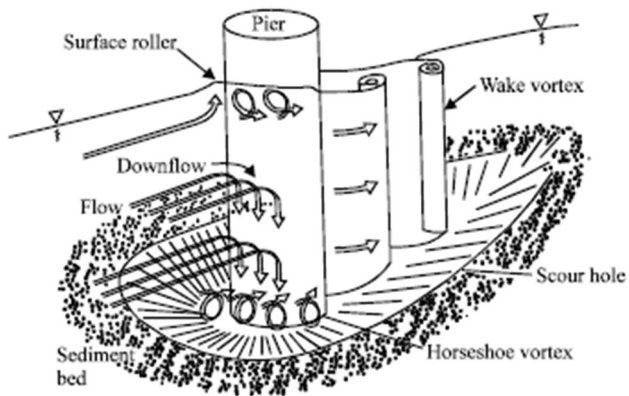


Figure G-22: Scour around a cylinder
(from Bresurers/Raudkivi, 1991)

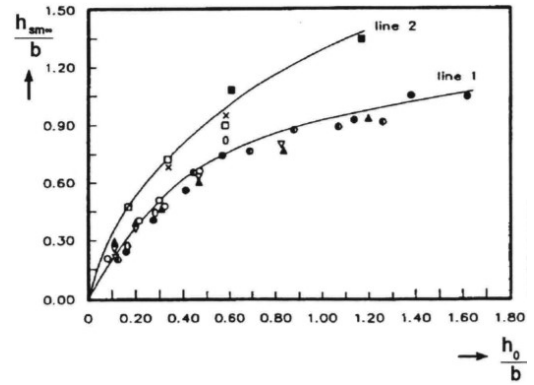


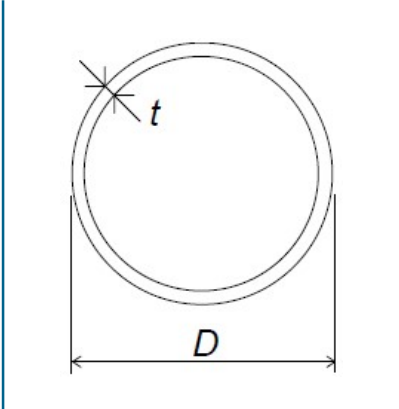
Figure G-23: Relative scour depth as a function of water depth and pile diameter

G.7 STRUCTURAL CHECKS

G.7.1 STRAIGHT STEEL PILES: FIRST APPROACH

The steel piles are designed and checked in accordance with the ANSI/AISC 360-10 (American Institute of Steel Construction, 2010). In Chile, the most frequently applied method to calculate steel member is the ASD (Allowable Stress Design) method, which uses material factors to calculate design resistances. These material factors have already been taken into consideration in the load combinations. For the first iteration, we have chosen the round steel profile with outer diameter of 262 mm and a wall thickness of 6 mm.

Table G-10: Pile $\phi 262/6$



Property	Magnitude	Unity
D	262	mm
t	6	mm
Weight	37.88	kgf/m
D_{INT}	250	mm
A	4,825	mm ²
I	40,000,000	mm ⁴
J	79,100,000	mm ⁴
S	302,000	mm ³
Z	393,000	mm ³
r	91	mm

The properties of the type of steel A36 that is chosen, is presented in Table G-11

Table G-11: Steel type A36

Property	Magnitude	Unity	Magnitude	Unity
E	2,038,902.00	kgf/cm ²	200,000	N/mm ²
G	784,193.08	kgf/cm ²	79,300	N/mm ²
F_y	2,531.05	kgf/cm ²	250	N/mm ²
F_u	4,080.00	kgf/cm ²	400	N/mm ²

G.7.1.1 Classification section elements

Though the manual calculation will not be presented in the report in its entirety, the manual calculation of the slenderness is presented below. This is one of the first calculation steps necessary to carry out the checks, presented in chapter B of ANSI/AISC 360-10 (American Institute of Steel Construction, 2010).

The sectional elements of the element subject to bending can be classified into Compact, Non-Compact and Slender using the following classification limits:

$$"C" < \lambda_p < "NC" < \lambda_r < "S"$$

For round hollow steel sections, the relevant ratio can be calculated as follows:

$$\frac{D}{t} = \frac{262}{6} = 43.67$$

The values for λ_p and λ_r for the section are defined as follows:

$$\lambda_p = 0.07 \frac{E}{F_y} = 0.07 \times \frac{2,038,902.00}{2,531.05} = 56.5$$

$$\lambda_r = 0.31 \frac{E}{F_y} = 0.31 \times \frac{2,038,902.00}{2,531.05} = 249.7$$

As the ratio is below the λ_p -value, the section in compression is classified as “C”, compact.

For an element subject to compression, there is a similar limit:

$$"C"/"NC" < \lambda_r < "S"$$

The value for λ_r for the section in this case is defined as:

$$\lambda_r = 0.11 \frac{E}{F_y} = 0.11 \times \frac{2,038,902.00}{2,531.05} = 88.6$$

As the ratio is below the λ_r it can also be classified as non-slender or “C”/“NC” in case of compression.

G.7.1.2 Unity checks

According to the software ETABS, the governing straight pile is situated at grid point G3. The associated load combination is CS2/4 which resulted into forces as described in Table G-12.

Table G-12: Governing forces -straight piles first approach (all units in kgf, cm)

Load Combination	Axial P	Shear V _x	Shear V _y	Torsion T	Moment M _x	Moment M _y
CS2/4	-5,509.96	7,306.86	112.48	7,209.543	8,263.947	485,611.9

The governing unity check as calculated in Excel turns out to be the check for the interaction of bending, torsion, shear and axial loads. This was to be expected, as the pile is subject to all of these forces, as opposed to the beam, which was mostly subject to bending and some shear. For the manual calculation steps, refer to chapter E (Design of members for compression), chapter F (Design of members for flexure), chapter G (Design of members for shear) and chapter H (Design of members for combined forces and torsion) of the ANSI/AISC 360-10 (American Institute of Steel Construction, 2010).

Table G-13: Unity check straight pile first approach

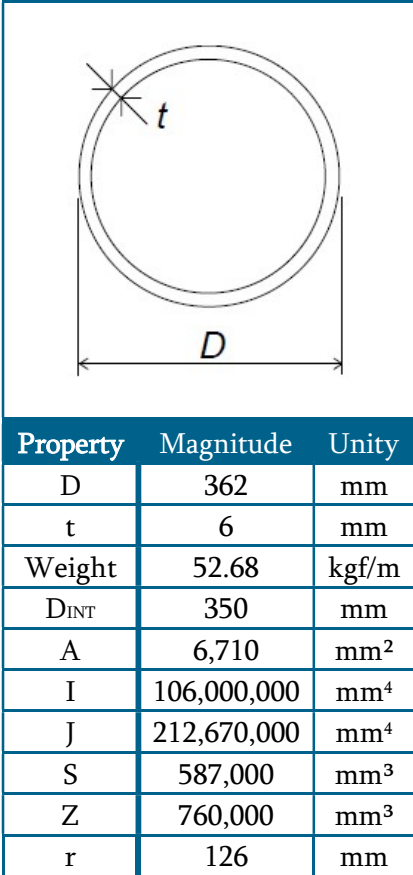
Flexión - Torsión - Corte -Axial			
ASD		LRFD	
Interacción	1,46	No Cumple	Interacción 0,00 OK

Although this pile did give good results for the foundation check, with a structural unity check of 1.46, the chosen pile section is not satisfactory and needs to be redesigned.

G.7.2 STRAIGHT STEEL PILES: FINAL DESIGN

As the unity check was much too high, we now choose a larger section as presented in Table G-14.

Table G-14: Pile Ø362/6



The properties of the type of steel A36 that is chosen, is presented in Table G-15.

Table G-15: Steel type A36

Property	Magnitude	Unity	Magnitude	Unity
E	2,038,902.00	kgf/cm ²	200,000	N/mm ²
G	784,193.08	kgf/cm ²	79,300	N/mm ²
F _y	2,531.05	kgf/cm ²	250	N/mm ²
F _u	4,080.00	kgf/cm ²	400	N/mm ²

G.7.2.1 Classification section elements

Though the manual calculation will not be presented in the report in its entirety, the manual calculation of the slenderness is presented below. This is one of the first calculation steps necessary to carry out the checks, presented in chapter B of ANSI/AISC 360-10 (American Institute of Steel Construction, 2010).

The sectional elements of the element subject to bending can be classified into Compact, Non-Compact and Slender using the following classification limits:

$$"C" < \lambda_p < "NC" < \lambda_r < "S"$$

For round hollow steel sections, the relevant ratio can be calculated as follows:

$$\frac{D}{t} = \frac{362}{6} = 60.33$$

The values for λ_p and λ_r for the section are defined as follows:

$$\lambda_p = 0.07 \frac{E}{F_y} = 0.07 \times \frac{2,038,902.00}{2,531.05} = 56.5$$

$$\lambda_r = 0.31 \frac{E}{F_y} = 0.31 \times \frac{2,038,902.00}{2,531.05} = 249.7$$

As the ratio is below the λ_p -value, the section in compression is classified as "NC", non-compact.

For an element subject to compression, there is a similar limit:

$$"C"/"NC" < \lambda_r < "S"$$

The value for λ_r for the section in this case is defined as:

$$\lambda_r = 0.11 \frac{E}{F_y} = 0.11 \times \frac{2,038,902.00}{2,531.05} = 88.6$$

As the ratio is below the λ_r it can also be classified as non-slender or "C"/"NC" in case of compression.

G.7.2.2 Unity checks

According to the software ETABS, the governing straight pile is situated at grid point G3. The associated load combination is CS2/4 which resulted into forces as described in Table G-16.

Table G-16: Governing forces – straight piles final design (all units in kgf, cm)

Load Combination	Axial P	Shear V _x	Shear V _y	Torsion T	Moment M _x	Moment M _y
CS2/4	-5,530.98	7,352.46	107.32	4,360.13	2,468.992	492,264.064

As with the previous design, the governing unity check as calculated in Excel turns out to be the check for the interaction of bending, torsion, shear and axial loads. This was to be expected, as the pile is subject to all of these forces, as opposed to the beam, which was mostly subject to bending and some shear. For the manual calculation steps, refer to Appendix E (Design of members for compression), Appendix F (Design of members for flexure), Appendix G (Design of members for shear) and Appendix H (Design of members for combined forces and torsion) of the ANSI/AISC 360-10 (American Institute of Steel Construction, 2010).

Table G-17: Unity check straight piles final design

Flexión - Torsión - Corte -Axial			
ASD		LRFD	
Interacción	0,68 OK	Interacción	0,00 OK

With a unity check of 0.68, the newly chosen pile has satisfactory results.

Note that in order to protect the steel piles from corrosion and to ensure that they will live up to the necessary standards in the future as well, we will add an additional 4 mm to its thickness as recommended by Dr. Dechent. The calculation is based on the worst-case scenario, where 4 mm thickness is corroded completely and only 6 mm remains.

G.7.3 INCLINED STEEL PILES: FIRST APPROACH

The steel piles are designed and checked in accordance with the ANSI/AISC 360-10 (American Institute of Steel Construction, 2010). In Chile, the most frequently applied method to calculate steel member is the ASD (Allowable Stress Design) method, which uses material factors to calculate design resistances.

As a pile of diameter 262 mm and a thickness 6 already failed for this design during its foundation check, a round steel profile with outer diameter of 362 mm and a wall thickness of 6 mm has been chosen, the same as we chose for the first iteration of the straight piles. For all its properties, refer to Chapter 6.2.6.4.

G.7.3.1 Classification section elements

These piles can be considered as “NC” (non-compact) when it comes to bending checks and as “C”/“NC” (non-slender) when it comes to compression.

G.7.3.2 Unity checks

According to the software ETABS, the governing straight pile is situated at grid point G3. The associated load combination is CS3/5 which resulted into forces as described Table G-18.

Table G-18: Governing forces -inclined piles first approach (all units in kgf cm)

Load Combination	Axial P	Shear V _x	Shear V _y	Torsion T	Moment M _x	Moment M _y
CS3/5	-52,576.87	252.71	1,081.27	7,568.66	247,809.6	35,929.48

As for the case with straight piles, the highest outcome to the unity checks as calculated in Excel turns out to be for the check for the interaction of bending, torsion, shear and axial loads. For the manual calculation steps, refer to chapter E (Design of members for compression), chapter F (Design of members for flexure), chapter G (Design of members for shear) and chapter H (Design of members for combined forces and torsion) of the ANSI/AISC 360-10 (American Institute of Steel Construction, 2010).

Table G-19: Unity check inclined piles first approach

Flexión - Torsión - Corte -Axial			
ASD		LRFD	
Interacción	0,78 OK	Interacción	0,00 OK

With a unity check of 0.78, the chosen pile section is satisfactory and does not need to be redesigned. However, during the final iteration, it should be checked again as the loads shall be slightly different.

G.7.4 INCLINED STEEL PILES: FINAL DESIGN

The design of the inclined piles has not undergone any changes, as the unity checks were already in order. However, as other parts of the design have been redesigned, the piles should be checked again to make sure they still live up to the demands.

G.7.4.1 Unity checks

According to the software ETABS, the governing straight pile is situated at grid point G3. The associated load combination is CS3/5 which resulted into forces as described in Table G-20.

Table G-20: Governing forces -straight piles final design (all units in kgf, cm)

Load Combination	Axial P	Shear V _x	Shear V _y	Torsion T	Moment M _x	Moment M _y
CS3/5	-46,197.33	101.89	897.59	4,332.413	205,724.7	13,629.92

Similar to the previous check, the highest outcome to the unity checks as calculated in Excel turns out to be for the check for the interaction of bending, torsion, shear and axial loads. For the manual calculation steps, refer to the other Appendices.

Table G-21: Unity check inclined piles final design

Flexión - Torsión - Corte -Axial			
ASD		LRFD	
Interacción	0,65 OK	Interacción	0,00 OK

With a unity check of 0.65, the chosen pile section lives up to the demands.

Note that, also for the inclined piles, in order to protect the steel piles from corrosion and to ensure that they will live up to the necessary standards in the future as well, we will add an additional 4 mm to its thickness as recommended by Dr. Dechent. The calculation is based on the worst-case scenario, where 4 mm thickness is corroded completely and only 6 mm remains.

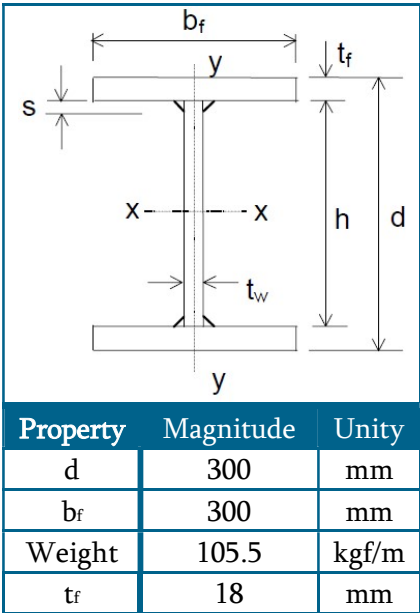
G.7.5 STEEL BEAMS: FIRST APPROACH

The steel H-beams underneath the concrete deck are designed and checked in accordance with the ANSI/AISC 360-10 (American Institute of Steel Construction, 2010). In Chile, the most frequently applied method to calculate steel member is the ASD (Allowable Stress Design) method, which uses material factors to calculate design resistances, Ω .

G.7.5.1 Properties

The occurring loads and the governing load combination is calculated by ETABS. For the first check iteration, we will use beams as dimensioned by the rules of thumb, H300x300x105.5. The beam’s properties are presented in Table G-22. For a more rapid calculation of the unity checks, we were provided with Excel sheets by the Universidad de Concepción.

Table G-22: Beam 300x300x105.5



t_w	10	mm
h	264	mm
h_0	282	mm
A	13,440	mm ²
I_x	230,000,000	mm ⁴
I_y	81,000,000	mm ⁴
J	1,260,000	mm ⁴
C_w	1.610×10^{12}	mm ⁶
S_x	1,536,000	mm ³
Z_x	1,697,000	mm ³
r_y	77.6	mm

The properties of the type of steel A36 that is chosen, is presented in Table G-23.

Table G-23: Steel type A36

Property	Magnitude	Unity	Magnitude	Unity
E	2,038,902.00	kgf/cm ²	200,000	N/mm ²
G	784,193.08	kgf/cm ²	79,300	N/mm ²
F_y	2,531.05	kgf/cm ²	250	N/mm ²
F_u	4,080.00	kgf/cm ²	400	N/mm ²

G.7.5.2 Classification section elements

The slenderness of the elements of the H-section needs to be calculated separately. For elements subject to bending the following limits apply, as presented by chapter B of ANSI/AISC 360-10 (American Institute of Steel Construction, 2010): if the width-to-thickness ratio is below the value λ_p , it is considered a compact (C) element; if it lies between λ_p and λ_r , it is considered a non-compact (NC) element; if the value is greater than λ_r , it is considered a slender (S) element. In summary:

$$"C" < \lambda_p < "NC" < \lambda_r < "S"$$

The flanges have a width-to-thickness ratio of:

$$\frac{\left(\frac{(b_f - t_w)}{2}\right)}{t_f} = \frac{145}{18} = 8.05$$

The values for λ_p and λ_r for the flanges are defined as follows:

$$\lambda_p = 0.38 \sqrt{\frac{E}{F_y}} = 0.38 \sqrt{\frac{2,038,902.00}{2,531.05}} = 10.79$$

$$\lambda_r = 0.95 \sqrt{\frac{k_c E}{F_L}} = 0.95 \sqrt{\frac{0.76 \times 2,038,902.00}{0.7 \times 2,531.05}} = 28.10$$

Where:

$$k_c = \frac{4}{\sqrt{\frac{h}{t_w}}} = \frac{4}{\sqrt{\frac{264}{10}}} = 0.778 \text{ with lower and upper limit } k_{c,min} = 0.35 < k_c < k_{c,max} = 0.76, \text{ thus}$$

$$k_c = 0.76.$$

And:

$$F_L = 0.7F_y.$$

As the width-to-thickness ratio is below the λ_p -value, the flanges are classified as “C”, compact.

The web has a width-to-thickness ratio of:

$$\frac{h}{t_w} = \frac{264}{10} = 26.4$$

The values for λ_p and λ_r for the flanges are defined as follows:

$$\lambda_p = 3.76 \sqrt{\frac{E}{F_y}} = 3.76 \sqrt{\frac{2,038,902.00}{2,531.05}} = 106.72$$

$$\lambda_r = 5.70 \sqrt{\frac{E}{F_y}} = 5.70 \sqrt{\frac{2,038,902.00}{2,531.05}} = 161.78$$

As the width-to-thickness ratio is below the λ_p -value, the web is classified as “C”, compact.

G.7.5.3 Unity checks

According to ETABS, the governing beam is the beam which is located at grid line 2. The governing load combination is CS2/1, which results into forces described in Table G-24.

Table G-24: Forces – Steel beam first approach (all units in kgf, cm)

Load combination	Axial P	Shear V _x	Shear V _y	Torsion T	Moment M _x	Moment M _y
CS2/1	0	0	1495.81	21.088	285,683.236	0

The outcome in the Excel sheet shows bending is the governing property that needs to be checked, which was to be expected from the input provided by ETABS in Table G-25.

For calculation of the bending resistance in ASD, the following partial factor needs to be taken into account for the design strength, according to the code:

$$\Omega_b = 1.67$$

For I-beams with both a compact web and compact flanges, the code prescribes two limit states for which the beam needs to be checked: (1) yielding and (2) lateral-torsional buckling. The lowest bending strength of the two needs to be used for the unity check. The calculations can be found in chapter F2 of the ANSI/AISC 360-10 (American Institute of Steel Construction, 2010).

Table G-25: Unity check steel beam first approach

FLEXIÓN						
Ω_b	1,67					
ϕ_b	0,90					
Lb	500,00 cm					
Cb	1,68					
CASO:	F2					
Eje Fuerte	Mnx		4295293,09 kgf-cm			
Eje Débil	Mny		2066855,43 kgf-cm			
		ASD		LRFD		
Eje Fuerte	M_n / Ω_b	2572031,79 kgf-cm		$\phi_b M_n$	3865763,78 kgf-cm	
Relación		0,11 OK			0,11 OK	
Eje Débil	M_n / Ω_b	1237637,98 kgf-cm		$\phi_b M_n$	1860169,89 kgf-cm	
Relación		0,00 OK			0,00 OK	

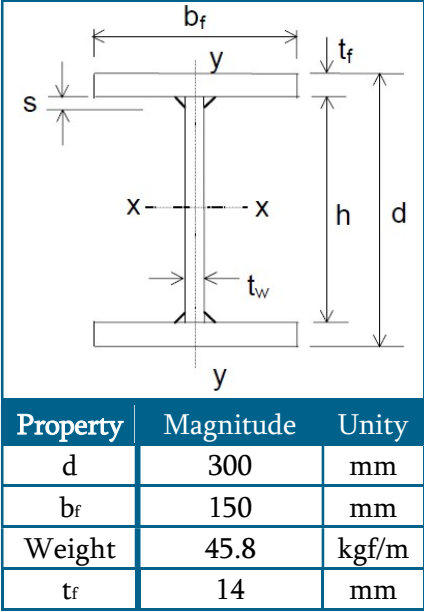
As Table G-25 shows, imported from Excel, the Unity Check for this beam under bending equals to 0.11, which is satisfactory, even a bit low.

G.7.6 STEEL BEAMS: FINAL DESIGN

G.7.6.1 Properties

As the first iteration, had quite a low outcome for its governing unity check, we choose a smaller beam profile, H300x150x45.8. The beam's properties are presented in Table G-26.

Table G-26: Beam 300x150x45.8



t_w	6	mm
h	272	mm
h_0	258	mm
A	5,832	mm ²
I_x	96,000,000	mm ⁴
I_y	7,880,000	mm ⁴
J	295,000	mm ⁴
C_w	0.1610×10^{12}	mm ⁶
S_x	640,000	mm ³
Z_x	712,000	mm ³
r_y	36.8	mm

The properties of the type of steel A36 that is chosen, is presented in Table G-27.

Table G-27: Steel type A36

Property	Magnitude	Unity	Magnitude	Unity
E	2,038,902.00	kgf/cm ²	200,000	N/mm ²
G	784,193.08	kgf/cm ²	79,300	N/mm ²
F_y	2,531.05	kgf/cm ²	250	N/mm ²
F_u	4,080.00	kgf/cm ²	400	N/mm ²

G.7.6.2 Classification section elements

The sectional elements of the beam can be classified into Compact, Non-Compact and Slender using the following classification limits according to chapter B of ANSI/AISC 360-10 (American Institute of Steel Construction, 2010):

$$"C" < \lambda_p < "NC" < \lambda_r < "S"$$

The flanges have a width-to-thickness ratio of:

$$\frac{\left(\frac{b_f - t_w}{2}\right)}{t_f} = \frac{72}{14} = 5.14$$

The values for λ_p and λ_r for the flanges are defined as follows:

$$\lambda_p = 0.38 \sqrt{\frac{E}{F_y}} = 0.38 \sqrt{\frac{2,038,902.00}{2,531.05}} = 10.79$$

$$\lambda_r = 0.95 \sqrt{\frac{k_c E}{F_L}} = 0.95 \sqrt{\frac{0.594 \times 2,038,902.00}{0.7 \times 2,531.05}} = 24.8$$

Where:

$k_c = \frac{4}{\sqrt{\frac{h}{t_w}}} = \frac{4}{\sqrt{\frac{272}{6}}} = 0.594$ with lower and upper limit $k_{c,min} = 0.35 < k_c < k_{c,max} = 0.76$, thus $k_c = 0.594$.

And:

$$F_L = 0.7F_y.$$

As the width-to-thickness ratio is below the λ_p -value, the flanges are classified as “C”, compact.

The web has a width-to-thickness ratio of:

$$\frac{h}{t_w} = \frac{272}{6} = 45.33$$

The values for λ_p and λ_r for the flanges are defined as follows:

$$\lambda_p = 3.76 \sqrt{\frac{E}{F_y}} = 3.76 \sqrt{\frac{2,038,902.00}{2,531.05}} = 106.72$$

$$\lambda_r = 5.70 \sqrt{\frac{E}{F_y}} = 5.70 \sqrt{\frac{2,038,902.00}{2,531.05}} = 161.78$$

As the width-to-thickness ratio is below the λ_p -value, the web is classified as “C”, compact.

G.7.6.3 Unity checks

For the final design all loads have been re-evaluated. According to ETABS, the governing beam is the beam which is located at grid line 2. The governing load combination is CS2/1, which results into forces described in Table G-28.

Table G-28: Governing forces – Steel beam final design (all units in kgf, cm)

Load combination	Axial P	Shear V _x	Shear V _y	Torsion T	Moment M _x	Moment M _y
CS2/1	0	0	881.63	12.808	155.567,961	0

The Excel-sheet shows the governing check is the bending check. For the step-by-step manual calculation, refer to chapter F of ANSI/AISC 360-10 (American Institute of Steel Construction, 2010). For bending calculation in ASD, the following partial factor needs to be taken into account for the design strength, according to the code:

$$\Omega_b = 1.67$$

The beam is loaded by a bending moment $M_y = 155,567.961$ kgf-cm about its major axis. Also this new beam needs to be checked for: (1) yielding and (2) lateral-torsional buckling. The lowest bending strength of the two is used for the unity check. The outcomes from the Excel sheet are presented in Table G-29.

Table G-29: Unity check steel beam final design

FLEXIÓN						
Ω_b	1,67	Esbelteces	λ_p	Límites		
ϕ_b	0,90			λ_r	Tipo	
Lb	500,00 cm			Ala Superior	5,36	10,79
Cb	1,64	Alma	45,33	106,72	161,78	C
CASO:	F2	Ala inferior	5,36	10,79	24,84	C
Eje Fuerte	Mnx	1801034,43 kgf-cm				
Eje Débil	Mny	404836,39 kgf-cm				
		ASD		LRFD		
Eje Fuerte	M_n / Ω_b	1078463,73 kgf-cm	$\phi_b M_n$	1620930,99 kgf-cm		
Relación		0,14 OK		0,14 OK		
Eje Débil	M_n / Ω_b	242417,00 kgf-cm	$\phi_b M_n$	364352,75 kgf-cm		
Relación		0,00 OK		0,00 OK		

The unity check shows a value of 0.14, which is OK.

G.7.7 CONCRETE DECK

The design of the concrete deck will be calculated according to the standard ACI-318-08 (ACI Committee 318, 2008). In Chile, concrete is generally designed using the LRFD (Load Resistance Factor Design) method, which uses partial factors (ϕ) to calculate design loads. The concrete width that will be considered for this calculation is 100 cm (1 m), which is the standard Chilean approach.

Table G-30: Input properties of concrete

Property	Magnitude	Unity
Compressive strength, F'_c	250	kgf/cm ²
Width, B	100	cm
Height, H	25	cm
Height cover on reinforcement	6	cm
Effective height, d	19	cm

Table G-31: Input properties of steel reinforcement

Property	Magnitude	Unity
Yield strength, F_y	4200	kgf/cm ²

Table G-32: Partial load factor

Property	Magnitude	Unity
Partial load factor, ϕ	0.9	[-]

From the chosen concrete, the factor β_1 for Whitney's equivalent stress block can be derived. In order to simplify the actual stress diagram in the compressive zone of the concrete to a linear block, the compressive strength of the concrete needs to be multiplied by this factor β_1 . Also, a shape factor a needs to be applied, which determined the height of the block compared to the actual compression height c . Both factors are shown in Table G-33. The stress configuration in the concrete deck is visualized in Figure G-24.

Table G-33: Factor for Whitney's equivalent stress block

Property	Magnitude	Unity
Whitney's factor, β_1	0.85	[-]
Shape factor, a	0.85	[-]

Following the Chilean approach, the preferred height of the compressive zone can be calculated as follows:

$$c = 0.286 \times d = 5.434 \text{ cm}$$

In which the value 0.286 is based on the limiting values for the strains of steel (7.5‰) and concrete (3‰), as follows:

$$\frac{\varepsilon_c}{c} = \frac{\varepsilon_s}{d - c}$$

Rearranged, this becomes:

$$\frac{\varepsilon_c}{\varepsilon_s + \varepsilon_c} d = c$$

Filling in the values 7.5‰ for ε_s and 3‰ for ε_c , you get:

$$0.286d = c$$

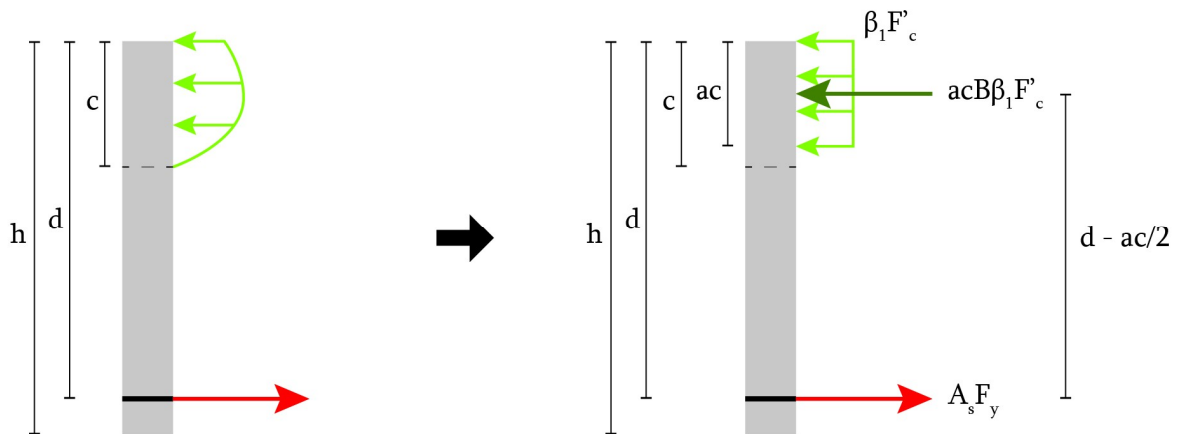


Figure G-24: Stress configuration concrete deck

For calculating the maximal occurring moments, the model from ETABS is imported to the software SAFE (SAFE, 2016). The deck setup in SAFE is presented in Figure G-25.

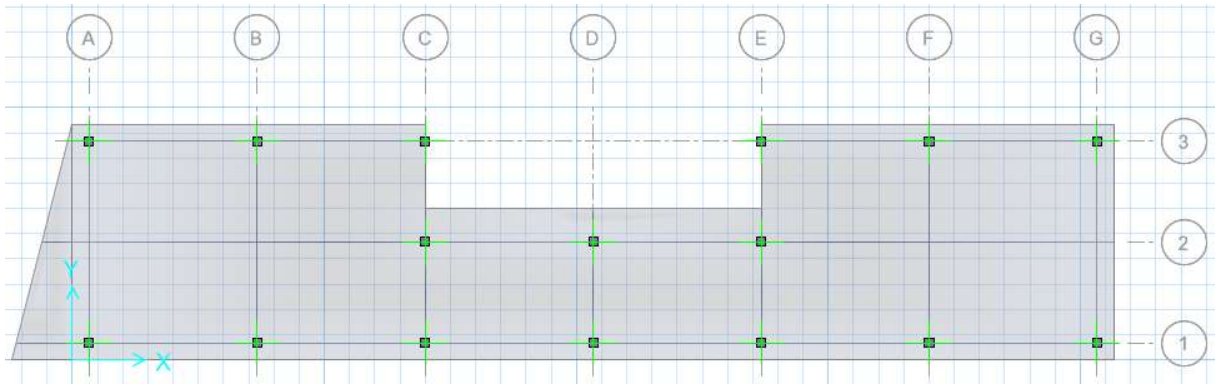


Figure G-25: Concrete deck in SAFE

SAFE calculates the internal moment distribution over both the length and the width of the deck, taking into account all load combinations applied on the ETABS model. The graphic outcomes are presented from Figure G-27 to Figure G-31.

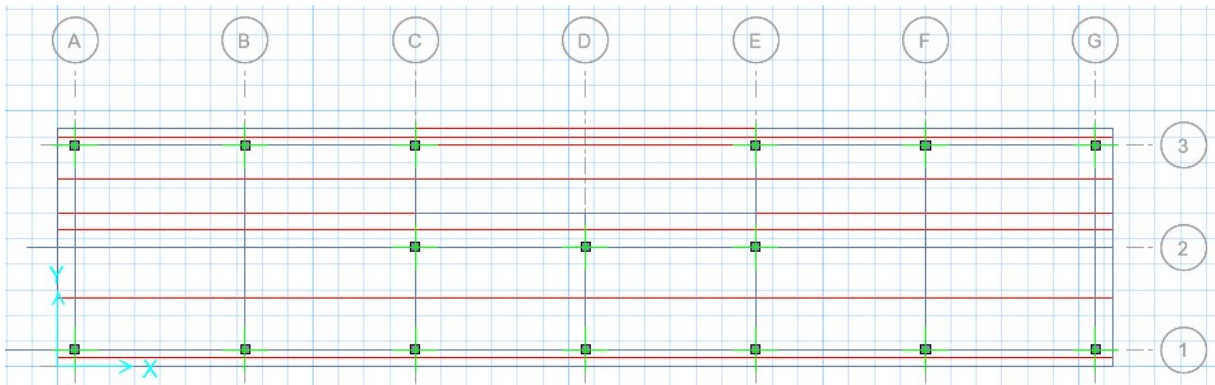


Figure G-26: Sections over length of deck

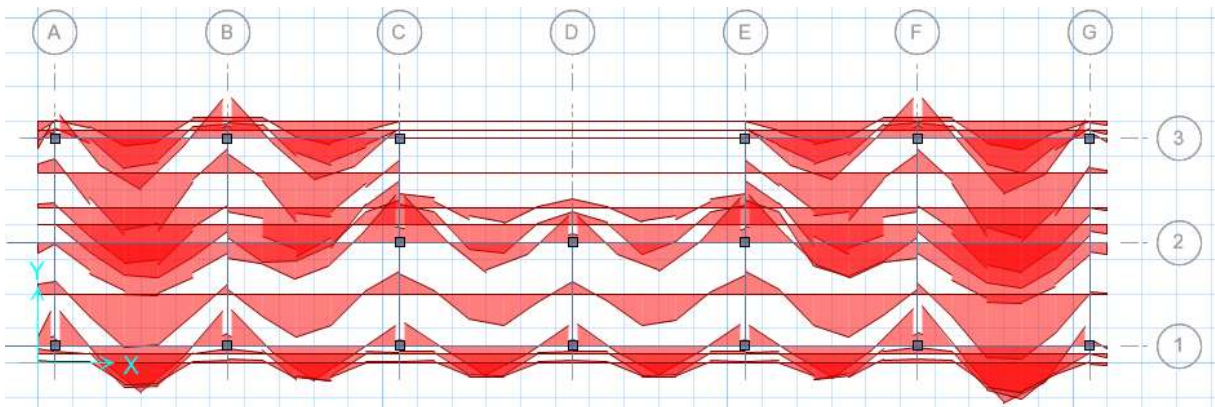


Figure G-27: Maximum of occurring positive moments ($M_{max,1} = 197\,902.04\text{ kgf-cm}$)

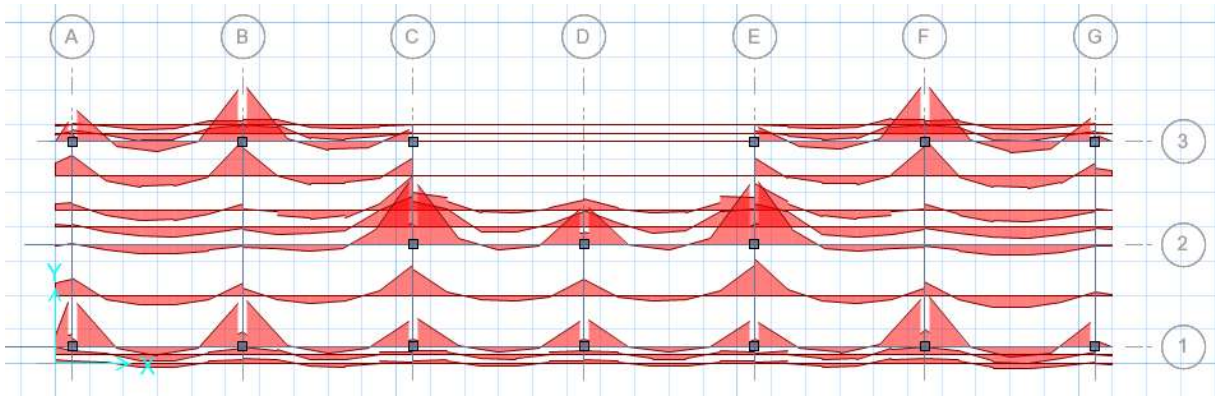


Figure G-28: Minimum of occurring negative moments ($M_{min,1} = -366,847.37 \text{ kgf-cm}$)

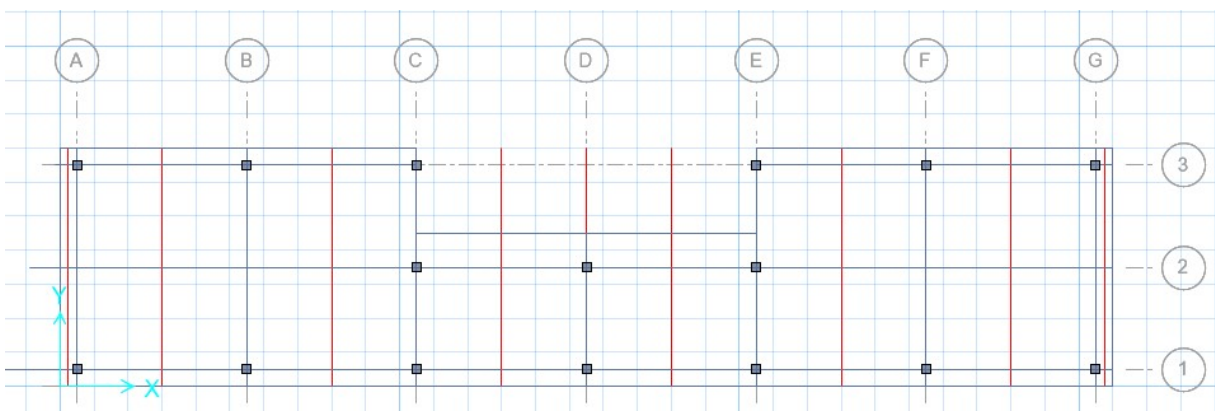


Figure G-29: Sections over width of the deck

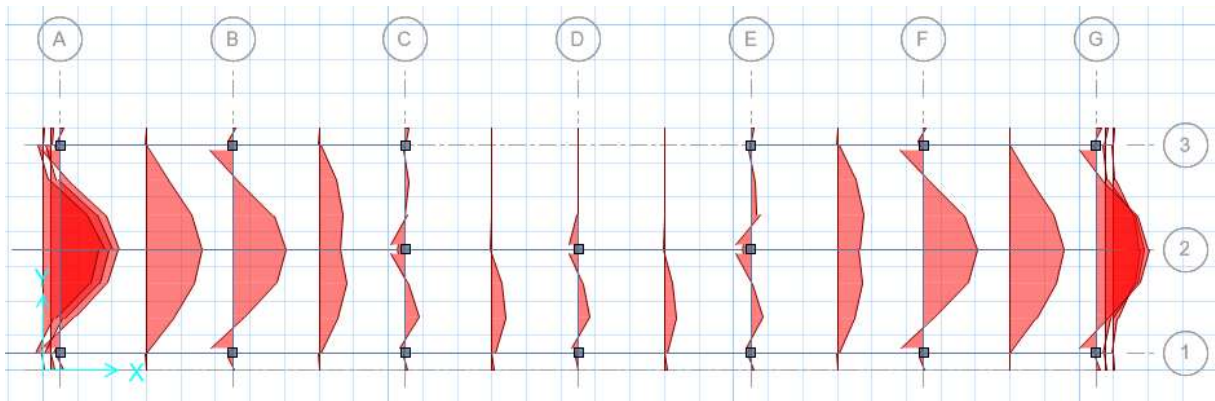


Figure G-30: Maximum of occurring positive moments ($M_{max,2} = 363,359.69 \text{ kgf-cm}$)

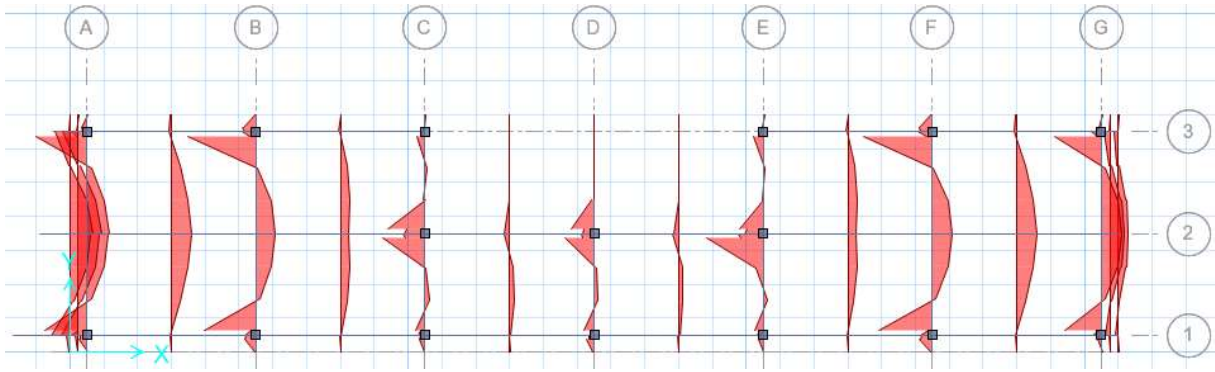


Figure G-31: Minimum of occurring negative moments ($M_{min,2} = - 409,251.74 \text{ kgf-cm}$)

A summary of the highest occurring moments is presented in Table G-34.

Table G-34: Largest occurring moments

Property	Magnitude	Unity
Maximum moment length, $M_{max,1}$	197 902.04	kgf-cm
Minimum moment length, $M_{min,1}$	(-) 366,847.37	kgf-cm
Maximum moment width, $M_{max,2}$	363,359.69	kgf-cm
Minimum moment width, $M_{min,2}$	(-) 409,251.74	kgf-cm
Maximum absolute moment, M_{max}	409,251.74	kgf-cm

Using the maximum absolute moment that occurs, the design moment can be calculated using the partial factor ϕ .

$$M_n = \frac{M_{max}}{\phi} = \frac{409,251.74}{0.9} = 454,724.16 \text{ kgf-cm}$$

In order to ensure horizontal equilibrium in the concrete section, the resulting force in the concrete compressive zone has to be equal to the force occurring in the steel, thus:

$$A_s F_y = ac B \beta_1 F'_c$$

The occurring moment can now be described as the result of two equal forces $A_s F_y$, with their internal lever arm of $(d - ac/2)$, thus:

$$M = A_s F_y \left(d - \frac{ac}{2} \right)$$

Rewriting this value using the design moment, gives a minimum value for A_s .

$$A_{s,min} = \frac{M_n}{F_y \left(d - \frac{ac}{2} \right)} = \frac{454,724.16}{\left(19 - \frac{0.85 \times 5.434}{2} \right)} = 6.49 \text{ cm}^2$$

Note that though the chosen reinforcement are should the amount of reinforcement should not exceed this value excessively, as the steel should yield before crushing of the concrete occurs in the compressive zone. A Chilean rule of thumb for this shows the following value:

$$A_{s,max} = \frac{F'_c \times \beta_1}{4 \times F_y} \times (B \times h) = \frac{250 \times 0.85}{4 \times 4200} \times (100 \times 25) = 31.6 \text{ cm}^2$$

The resulting reinforcement design is presented in Table G-35.

Table G-35: Properties concrete deck and reinforcement

Property	Magnitude	Unity
Concrete cover	6	cm
Diameter of bar	1.0	cm
Number of bars	9	[-]
Reinforcement area (per 100 cm width)	7.07	cm ²
C.t.c. distance	11.1	cm

For practical reasons, the reinforcement will be designed the same in both directions, both at the bottom and at the top of the concrete deck. The final design is presented in Figure G-32.

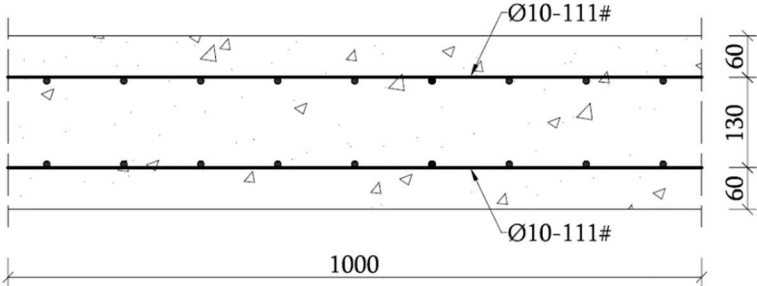


Figure G-32: Design concrete deck and reinforcement (units in mm)

H DESIGN: BREAKWATER

H.1 DETERMINATION DESIGN STORM

To get to wave heights for the Servicability Limit State and the Ultimate Limit State (SLS and the ULS), use has to be made of some statistics. Wave statistics for 23 years are obtained from WaveClimate.com (BMT Argoss, 2016). In this data, measured every 3 hours (with a total of 67208 measurements); wave height, wave direction, wave period and also wind data are included. For the purpose of a design storm, the period and wave heights are of importance.

All the wave data is plotted into a table in bins. The bins are divided in wave height (steps of 0,2m) and wave direction (steps of 22,5 degrees). The bins of the wave height are of the biggest importance and are used in the next steps. The directional bins are plotted to determine the main directions of the highest waves. The result is Table H-1.

The waves however have two important main directions. An analysis to the wind- and swell waves has to be performed. This will be executed in the next paragraph, H.1.1.

Table H-1: Main direction waves

lower	lower upper	348,75	11,25	33,75	56,25	78,75	101,25	123,75	146,25	168,75	191,25	213,75	236,25	258,75	281,25	303,75	326,25	348,75	ClassObs
0,2	0,4	0	0	0	0	0	0	0	0	0	0	0	0	0	0	0	0	0	0
0,4	0,6	0	0	0	0	0	0	0	0	0	0	2	10	0	0	0	0	0	12
0,6	0,8	0	0	0	0	0	0	0	0	0	2	23	19	4	1	0	0	0	49
0,8	1	0	0	0	0	0	0	0	0	0	5	104	100	30	0	2	0	0	241
1	1,2	0	0	0	0	0	0	0	0	0	2	24	272	247	65	11	1	1	623
1,2	1,4	0	0	0	0	0	0	0	2	4	75	706	540	122	24	3	1	1	1477
1,4	1,6	0	0	0	0	0	0	2	2	2	108	1300	866	217	27	4	2	2	2530
1,6	1,8	0	0	0	0	0	0	4	1	1	163	2038	1091	316	44	18	0	0	3676
1,8	2	1	1	0	0	0	0	5	2	1	310	2565	1313	306	81	28	11	1	4624
2	2,2	3	0	0	0	0	0	0	1	4	455	3247	1503	308	87	27	11	11	5646
2,2	2,4	1	0	0	0	0	0	0	0	3	540	3643	1352	311	97	49	34	34	6030
2,4	2,6	4	0	0	0	0	0	0	0	4	563	3777	1297	299	112	59	31	31	6146
2,6	2,8	4	1	0	0	0	0	0	0	0	645	3686	1137	264	114	50	23	23	5924
2,8	3	6	0	0	0	0	0	0	0	0	705	3374	1044	277	103	55	37	37	5601
3	3,2	14	1	0	0	0	0	0	0	0	679	2871	913	282	120	64	27	27	4971
3,2	3,4	5	0	0	0	0	0	0	0	0	639	2461	776	244	122	57	34	34	4338
3,4	3,6	4	1	0	0	0	0	0	0	0	592	1911	595	221	101	55	30	30	3510
3,6	3,8	7	0	0	0	0	0	0	0	0	515	1512	480	154	77	55	28	28	2828
3,8	4	9	0	0	0	0	0	0	0	0	383	1185	351	133	72	48	21	21	2202
4	4,2	5	0	0	0	0	0	0	0	0	282	817	278	124	47	48	20	20	1621
4,2	4,4	3	1	0	0	0	0	0	0	0	194	652	211	90	58	45	18	18	1272
4,4	4,6	0	0	0	0	0	0	0	0	0	131	457	171	79	42	39	16	16	935
4,6	4,8	1	0	0	0	0	0	0	0	0	93	352	154	69	31	26	16	16	742
4,8	5	2	0	0	0	0	0	0	0	0	41	270	150	64	29	28	12	12	596
5	5,2	1	0	0	0	0	0	0	0	0	26	159	107	56	32	21	5	5	407
5,2	5,4	4	0	0	0	0	0	0	0	0	25	97	90	50	23	18	7	7	314
5,4	5,6	6	0	0	0	0	0	0	0	0	5	88	73	36	15	10	2	2	235
5,6	5,8	2	0	0	0	0	0	0	0	0	4	53	58	25	9	4	10	10	165
5,8	6	2	0	0	0	0	0	0	0	0	1	37	39	18	5	12	4	4	118
6	6,2	0	0	0	0	0	0	0	0	0	0	25	40	15	3	9	10	10	102
6,2	6,4	0	0	0	0	0	0	0	0	0	0	13	23	8	2	10	6	6	62
6,4	6,6	1	0	0	0	0	0	0	0	0	0	11	14	6	3	2	0	0	37
6,6	6,8	0	0	0	0	0	0	0	0	0	0	14	27	4	2	3	4	4	54
6,8	7	1	0	0	0	0	0	0	0	0	0	9	26	3	3	2	0	0	44
7	7,2	1	0	0	0	0	0	0	0	0	0	0	12	1	2	0	0	0	18
7,2	7,4	1	0	0	0	0	0	0	0	0	0	5	9	1	3	0	0	0	17
7,4	7,6	1	0	0	0	0	0	0	0	0	0	1	11	0	0	0	0	0	13
7,6	7,8	1	0	0	0	0	0	0	0	0	0	2	7	0	0	0	0	0	10
7,8	8	3	0	0	0	0	0	0	0	0	0	3	3	0	0	0	0	0	9
8	8,2	0	0	0	0	0	0	0	0	0	0	0	3	0	0	0	0	0	3
8,2	8,4	0	0	0	0	0	0	0	0	0	0	0	2	0	0	0	0	0	2
8,4	8,6	0	0	0	0	0	0	0	0	0	0	0	2	0	0	0	0	0	2
8,6	8,8	0	0	0	0	0	0	0	0	0	0	0	1	0	0	0	0	0	1
8,8	9	0	0	0	0	0	0	0	0	0	0	0	1	0	0	0	0	0	1
9	9,2	0	0	0	0	0	0	0	0	0	0	0	0	0	0	0	0	0	0
total		93	5	0	0	0	0	11	8	21	7205	37742	15146	4202	1500	852	423		67208

H.1.1 WAVE DIRECTION ANALYSIS

The wave climate is dominated by waves from two directions. The prevailing waves are from the SW, originating around the ‘roaring forties’, This is the storm wave belt blowing from west to east around 40 degrees south in latitude, north of Antarctica. The waves from the north are mainly occurring in winter when the wind changes direction to a northerly wind. These waves are described as wind waves with shorter wave periods than the south-western Swell waves.

To be able to get to certain design wave heights, the wave data (BMT Argoss, 2016) have to be separated in the two important directions. The two tables, Table H-2 and Table H-3, are separated as wind and swell waves, which is a possibility at waveclimate.com. Table H-2 describes wind waves. The highest wind waves are coming from the north-western to northern directions. The highest swell waves of Table H-3 are coming from the South-western directions. Taking this knowledge into account a Peak-over-threshold analysis can be executed for both conditions. This analysis will be performed the same way as in the first iteration step in Appendix F.

Table H-2: Wind wave height versus direction, plotted in bins

Occurrence of height of wind sea (m) in rows versus direction of wind sea in columns		101.25	123.75	146.25	168.75	191.25	213.75	236.25	258.75	281.25	303.75	326.25	total					
lower	upper	112.5	33.75	56.25	78.75	101.25	123.75	146.25	168.75	191.25	213.75	236.25	258.75	281.25	303.75	326.25	total	
0.0	0.2	279	141	110	76	52	36	93	194	811	2474	2544	2121	1883	1128	764	433	13119
0.2	0.4	127	61	47	34	21	13	45	83	392	1239	1299	1075	873	532	371	228	6440
0.4	0.6	96	43	38	14	10	17	20	67	423	1385	1300	873	676	470	340	195	5967
0.6	0.8	79	34	15	12	7	6	15	47	368	1389	1235	705	474	399	284	167	5230
0.8	1.0	77	22	7	12	6	5	13	22	282	1537	1316	523	335	310	229	133	4828
1.0	1.2	64	17	3	8	5	5	9	16	187	1633	1275	353	263	266	230	154	4458
1.2	1.4	36	9	2	4	4	1	4	7	141	1540	1262	235	186	205	183	127	3946
1.4	1.6	42	5	1	0	7	0	3	8	87	1603	1064	133	155	197	169	124	3598
1.6	1.8	30	6	2	1	0	3	2	2	72	1489	882	93	132	166	156	79	3115
1.8	2.0	21	3	0	0	0	0	2	1	58	1555	762	39	109	149	142	76	2917
2.0	2.2	25	0	0	0	0	0	0	2	36	1364	611	38	85	116	137	79	2493
2.2	2.4	17	3	0	0	0	0	1	30	1210	510	36	95	122	102	61	2188	
2.4	2.6	13	2	0	0	0	0	0	14	1046	451	32	69	107	97	51	1882	
2.6	2.8	15	0	0	0	0	0	0	10	898	336	11	51	105	86	46	1558	
2.8	3.0	10	0	0	0	0	0	0	2	698	280	16	43	66	66	54	1235	
3.0	3.2	14	1	0	0	0	0	0	2	582	187	11	32	76	80	62	1047	
3.2	3.4	8	1	0	0	0	0	0	2	491	151	12	41	56	60	41	863	
3.4	3.6	7	0	0	0	0	0	0	3	330	92	9	24	42	50	28	585	
3.6	3.8	9	0	0	0	0	0	0	0	265	67	6	21	44	41	29	482	
3.8	4.0	4	0	0	0	0	0	0	0	185	45	3	14	29	48	17	345	
4.0	4.2	3	0	0	0	0	0	0	0	126	29	4	11	30	40	17	261	
4.2	4.4	2	0	0	0	0	0	0	0	82	13	2	11	24	28	15	177	
4.4	4.6	1	0	0	0	0	0	0	0	38	4	2	9	22	25	15	116	
4.6	4.8	0	0	0	0	0	0	0	0	25	3	0	8	12	24	9	81	
4.8	5.0	2	0	0	0	0	0	0	0	14	0	2	1	7	17	15	58	
5.0	5.2	1	0	0	0	0	0	0	0	6	1	1	4	10	15	7	45	
5.2	5.4	5	0	0	0	0	0	0	0	6	0	1	4	8	9	5	24	
5.4	5.6	6	0	0	0	0	0	0	0	1	0	2	1	4	5	2	28	
5.6	5.8	1	0	0	0	0	0	0	0	0	0	0	0	1	6	7	15	
5.8	6.0	1	0	0	0	0	0	0	0	0	0	1	0	1	5	5	13	
6.0	6.2	0	0	0	0	0	0	0	0	0	0	1	0	1	3	3	8	
6.2	6.4	2	0	0	0	0	0	0	0	0	0	0	0	4	3	3	9	
6.4	6.6	1	0	0	0	0	0	0	0	0	0	0	0	0	2	0	3	
6.6	6.8	0	0	0	0	0	0	0	0	0	0	0	0	0	1	0	2	
6.8	7.0	1	0	0	0	0	0	0	0	0	0	0	0	0	0	0	1	
7.0	7.2	1	0	0	0	0	0	0	0	0	0	0	0	0	0	0	1	
7.2	7.4	0	0	0	0	0	0	0	0	0	0	0	0	0	0	0	0	
7.4	7.6	2	0	0	0	0	0	0	0	0	0	0	0	0	0	0	2	
7.6	7.8	1	0	0	0	0	0	0	0	0	0	0	0	0	0	0	1	
7.8	8.0	0	0	0	0	0	0	0	0	0	0	0	0	0	0	0	0	
total		1003	349	225	161	112	86	207	450	2920	22911	14719	6340	5608	4701	3818	2298	67208

Table H-5: Swell wave height versus peak period, plotted in bins

Occurrence of height of swell (m) in rows versus peak period of swell (s) in columns		2	3	4	5	6	7	8	9	10	11	12	13	14	15	16	17	18	19	20	21	22	23	24	total
lower	upper	3	4	5	6	7	8	9	10	11	12	13	14	15	16	17	18	19	20	21	22	23	24	total	
0.0	0.2	0	1	8	17	20	6	2	0	0	3	8	32	70	0	115	182	0	177	0	91	0	33	0	763
0.2	0.4	0	2	7	22	24	10	2	0	2	14	56	76	7	0	117	107	0	51	0	9	0	1	0	500
0.4	0.6	0	0	9	23	20	6	6	8	14	31	61	111	169	0	162	67	0	23	0	5	0	1	0	718
0.6	0.8	0	0	2	23	36	6	8	22	54	94	127	195	221	0	140	69	0	23	0	7	0	1	0	1028
0.8	1.0	0	0	0	9	38	10	23	43	141	212	259	241	274	0	221	102	0	32	0	8	0	4	0	1011
1.0	1.2	0	0	0	6	31	19	36	80	274	409	487	437	357	0	211	99	0	38	0	11	0	0	0	2497
1.2	1.4	0	0	0	4	18	30	47	102	392	799	764	647	432	0	246	126	0	30	0	5	0	1	0	3643
1.4	1.6	0	0	0	1	31	26	53	163	521	1008	1060	791	545	0	271	155	0	39	0	10	0	1	0	4683
1.6	1.8	0	0	0	1	34	28	50	163	513	1274	1417	907	668	0	405	188	0	46	0	18	0	0	0	6772
1.8	2.0	0	0	0	0	30	29	52	125	438	1267	1678	1144	645	0	387	164	0	49	0	16	0	0	0	6024
2.0	2.2	0	0	0	0	16	33	50	119	362	1280	1860	1280	648	0	394	172	0	51	0	8	0	0	0	6272
2.2	2.4	0	0	0	0	6	30	51	90	297	941	1730	1418	652	0	346	159	0	35	0	7	0	0	0	7262
2.4	2.6	0	0	0	0	9	17	38	71	176	755	1612	1517	668	0	301	119	0	27	0	0	0	0	0	5207
2.6	2.8	0	0	0	0	1	14	34	61	156	514	1228	1538	699	0	254	98	0	22	0	0	0	0	0	4613
2.8	3.0	0	0	0	0	2	8	26	50	114	397	1033	1392	628	0	230	92	0	11	0	1	0	0	0	3985
3.0	3.2	0	0	0	0	1	5	20	41	114	250	721	1039	638	0	187	46	0	13	0	0	0	0	0	3095
3.2	3.4	0	0	0	0	0	3	16	26	60	208	488	876	628	0	181	40	0	5	0	0	0	0	0	3207
3.4	3.6	0	0	0	0	0	1	9	25	30	134	356	670	499	0	146	42	0	9	0	0	0	0	0	1923
3.6	3.8	0	0	0	0	0	2	7	15	27	90	246	468	463	0	138	29	0	6	0	1	0	0	0	1492
3.8	4.0	0	0	0	0	0	2	9	31	63	167	349	385	301	0	159	35	0	7	0	1	0	0	0	1208
4.0	4.2	0	0	0	0	0	1	6	21	48	124	246	300	210	0	99	27	0	7	0	0	0	0	0	852
4.2	4.4	0	0	0	0	0	0	1	4	14	39	88	176	211	0	98	19	0	5	0	1	0	0	0	656
4.4	4.6	0	0	0	0	0	0	1	6	8	24	83	126	161	0	105	25	0	2	0	0	0	0	0	541
4.6	4.8	0	0	0	0	0	0	0	4	3	20	42	126	120	0	80	23	0	2	0	0	0	0	0	423
4.8	5.0	0	0	0	0	0	0	0	2	2	16	39	93	89	0	63	17	0	6	0	0	0	0	0	322
5.0	5.2	0	0	0	0	0	0	0	1	6	34	78	60	60	0	42	11	0	1	0	0	0	0	0	233
5.2	5.4	0	0	0	0	0	0	0	0	3	23	54	50	50	0	40	12	0	0	0	0	0	0	0	182
5.4	5.6	0	0	0	0	0	0	0	0	2	12	30	35	35	0	27	10	0	0	0	0	0	0	0	118
5.6	5.8	0	0	0	0	0	0	0	0	3	12	16	31	31	0	23	7	0	0	0	0	0	0	0	92
5.8	6.0	0	0	0	0	0	0	0	0	1	11	23	21	21	0	11	6	0	1	0	0	0	0	0	74
6.0	6.2	0	0	0	0	0	0	0	0	1	5	7	13	13	0	26	8	0	1	0	0	0	0	0	61
6.2	6.4	0	0	0	0	0	0	0	0	1	1	5	12	12	0	11	6	0	0	0	0	0	0	0	36
6.4	6.6	0	0	0	0	0	0	0	0	0	3	12	16	16	0	7	2	0	0	0	0	0	0	0	22
6.6	6.8	0	0	0	0	0	0	0	0	0	0	3	14	14	0	11	3	0	1	0	0	0	0	0	32
6.8	7.0	0	0	0	0	0	0	0	0	0	0	6	6	6	0	13	6	0	0	0	0	0	0	0	31
7.0	7.2	0	0	0	0	0	0	0	0	0	0	1	3	3	0	1	0	0	0	0	0	0	0	0	12
7.2	7.4	0	0	0	0	0	0	0	0	0	0	0	0	0	0	2	3	0	0	0	0	0	0	0	11
7.4	7.6	0	0	0	0	0	0	0	0	0	0	0	4	4	0	2	2	0	1	0	0	0	0	0	9
7.6	7.8	0	0	0	0	0	0	0	0	0	0	0	3	3	0	1	3	0	1	0	0	0	0	0	8
7.8	8.0	0	0	0	0	0	0	0	0	0	0	0	0	0	0	2	2	0	0	0	0	0	0	0	4
8.0	8.2	0	0	0	0	0	0	0	0	0	0	0	0	0	0	2	1	0	0	0	0	0	0	0	3
8.2	8.4	0	0	0	0	0	0	0	0	0	0	0	0	0	0	0	2	0	0	0	0	0	0	0	2
8.4	8.6	0	0	0	0	0	0	0	0	0	0	0	0	0	0	0	1	0	0	0	0	0	0	0	1
8.6	8.8	0	0	0	0	0	0	0	0	0	0	0	0	0	0	0	1	0	0	0	0	0	0	0	1
8.8	9.0	0	0	0	0	0	0	0	0	0	0	0	0	0	0	0	1	0	0	0	0	0	0	0	1
9.0	9.2	0	0	0	0	0	0	0	0	0	0	0	0	0	0	0	0	0	0	0	0	0	0	0	0
total		0	3	26	108	317	283	534	1237	3777	9884	18884	16381	10521	0	5777	2292	0	724	0	197	0	46	0	67208

H.1.3 SLS/ULS

The Servicability Limit State and the Ultimate Limit State are dependent on two different events. For the SLS, the downtime of the jetty is set on 5% per year, which is decided in the program of requirements. This downtime results in an acceptable non service of 18 days a year.

The (ULS) storm wave height is a value based on a probability of failure and the lifetime of the structure. In this case the lifetime is set on 25 years and the probability of failure under normal storm conditions (no tsunami conditions) is 10%. This is a rather average value in the range of 5%-20% (Verhagen, d'Angremond, & van Roode, 2009). These values refer to a design storm of about once every 250 years, (237 to be more exact), using the formulas underneath. The ULS storm wave height is meant to design the sizes of the armour stones and equals 10m +MSL. This wave height is obtained via a Weibull transgression, as more in detail discussed in appendix H.1.4.

$$p = 1 - e^{-ft}$$

$$f_{designstorm} = -\frac{1}{t} \ln(1 - p)$$

f = Average frequency of the event per year

p = Probability of failure during lifetime

t = Lifetim period

Table H-6: Return periods ULS and SLS

	Return period
ULS	1/250 years
SLS	18/1 year

H.1.4 PEAK OVER THRESHOLD PER WAVE DIRECTION

Table H-2 and Table H-3 are transferred to a table where the lower wave values are taken out (Peak over Threshold). This is of importance to limit the importance of the smaller waves to the design storm, as more detailed described in the first determination of a design storm in Appendix F.3. The results are given below; a description is given underneath the tables.

Table H-7: NW wind waves, PoT-analysis

1													
Analysis wave direction													
lower	upper	326,25	ClassObs	CumObs	P	Q	LN(Q)	ln(H)	Qs	LN(Qs)	Gumbel	Weibull	
2,8	3	348,75	37	37	0,120	0,880	0,128	1,099	11,826	2,470	-0,753	0,190	
3	3,2		27	64	0,207	0,793	0,232	1,163	10,652	2,366	-0,454	0,308	
3,2	3,4		34	98	0,317	0,683	0,381	1,224	9,174	2,216	-0,138	0,460	
3,4	3,6		30	128	0,414	0,586	0,535	1,281	7,870	2,063	0,126	0,604	
3,6	3,8		28	156	0,505	0,495	0,703	1,335	6,652	1,895	0,381	0,753	
3,8	4		21	177	0,573	0,427	0,851	1,386	5,739	1,747	0,585	0,878	
4	4,2		20	197	0,638	0,362	1,015	1,435	4,870	1,583	0,798	1,012	
4,2	4,4		18	215	0,696	0,304	1,190	1,482	4,087	1,408	1,014	1,151	
4,4	4,6		16	231	0,748	0,252	1,377	1,526	3,391	1,221	1,235	1,294	
4,6	4,8		16	247	0,799	0,201	1,606	1,569	2,696	0,992	1,496	1,465	
4,8	5		12	259	0,838	0,162	1,821	1,609	2,174	0,777	1,734	1,622	
5	5,2		5	264	0,854	0,146	1,927	1,649	1,957	0,671	1,849	1,697	
5,2	5,4		7	271	0,877	0,123	2,096	1,686	1,652	0,502	2,031	1,816	
5,4	5,6		2	273	0,883	0,117	2,150	1,723	1,565	0,448	2,089	1,854	
5,6	5,8		10	283	0,916	0,084	2,475	1,758	1,130	0,123	2,432	2,077	
5,8	6		4	287	0,929	0,071	2,642	1,792	0,957	-0,044	2,606	2,189	
6	6,2		10	297	0,961	0,039	3,248	1,825	0,522	-0,651	3,229	2,586	
6,2	6,4		6	303	0,981	0,019	3,942	1,856	0,261	-1,344	3,932	3,023	
6,4	6,6		0	303	0,981	0,019	3,942	1,887	0,261	-1,344	3,932	3,023	
6,6	6,8		4	307	0,994	0,006	5,040	1,917	0,087	-2,442	5,037	3,685	
6,8	7		0	307	0,994	0,006	5,040	1,946	0,087	-2,442	5,037	3,685	
7	7,2		2	309	1,000	0,000		1,974	0,000				
7,2	7,4		0	309	1,000	0,000		2,001	0,000				
7,4	7,6		0	309	1,000	0,000		2,028	0,000				
7,6	7,8		0	309	1,000	0,000		2,054	0,000				
7,8	8		0	309	1,000	0,000		2,079	0,000				
8	8,2		0	309	1,000	0,000		2,104	0,000				
8,2	8,4		0	309	1,000	0,000		2,128	0,000				
8,4	8,6		0	309	1,000	0,000		2,152	0,000				
8,6	8,8		0	309	1,000	0,000		2,175	0,000				
8,8	9		0	309	1,000	0,000		2,197	0,000				
9	9,2		0	309	1,000	0,000		2,219	0,000				
total			309										
		N23	309										
		Ns	13,43										
							Gumbel	Weibull					
							alfa	1,24	1,24				
							beta	1,39	0,86				
							gamma	5,11	2,64				

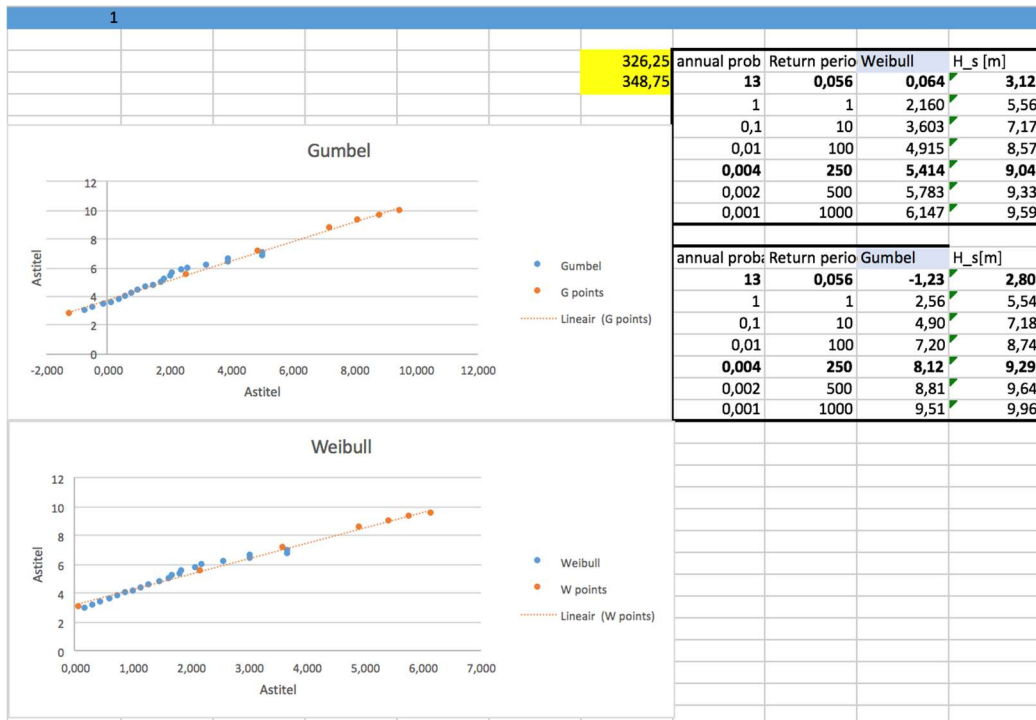


Figure H-1: NW wind waves, Gumbel and Weibull results and return period wave conditions

Table H-8: SW swell waves, PoT-analysis

lower	upper	ClassObs	CumObs	P	Q	LN(Q)	ln(H)	Qs	LN(Qs)	Gumbel	Weibull
2,8	3	1044	1044	0,040	0,960	0,040	1,099	12,903	2,557	-1,172	0,075
3	3,2	913	1957	0,074	0,926	0,077	1,163	12,438	2,521	-0,956	0,127
3,2	3,4	776	2733	0,104	0,896	0,109	1,224	12,042	2,488	-0,818	0,168
3,4	3,6	595	3328	0,126	0,874	0,135	1,281	11,739	2,463	-0,727	0,199
3,6	3,8	480	3808	0,144	0,856	0,156	1,335	11,494	2,442	-0,660	0,223
3,8	4	351	4159	0,158	0,842	0,172	1,386	11,315	2,426	-0,613	0,241
4	4,2	278	4437	0,168	0,832	0,184	1,435	11,174	2,414	-0,578	0,256
4,2	4,4	211	4648	0,176	0,824	0,194	1,482	11,066	2,404	-0,551	0,266
4,4	4,6	171	4819	0,167	0,833	0,183	1,526	10,983	3,612	-0,582	0,254
4,6	4,8	154	4973	0,318	0,682	0,382	1,569	30,348	3,413	-0,137	0,460
4,8	5	150	5123	0,464	0,536	0,624	1,609	23,826	3,171	0,265	0,684
5	5,2	107	5230	0,569	0,431	0,841	1,649	19,174	2,954	0,573	0,870
5,2	5,4	90	5320	0,657	0,343	1,070	1,686	15,261	2,725	0,867	1,056
5,4	5,6	73	5393	0,728	0,272	1,303	1,723	12,087	2,492	1,149	1,238
5,6	5,8	58	5451	0,785	0,215	1,537	1,758	9,565	2,258	1,418	1,414
5,8	6	39	5490	0,823	0,177	1,732	1,792	7,870	2,063	1,636	1,557
6	6,2	40	5530	0,862	0,138	1,982	1,825	6,130	1,813	1,908	1,736
6,2	6,4	23	5553	0,885	0,115	2,160	1,856	5,130	1,635	2,099	1,861
6,4	6,6	14	5567	0,898	0,102	2,286	1,887	4,522	1,509	2,233	1,948
6,6	6,8	27	5594	0,925	0,075	2,587	1,917	3,348	1,208	2,548	2,152
6,8	7	26	5620	0,950	0,050	2,999	1,946	2,217	0,796	2,973	2,424
7	7,2	12	5632	0,962	0,038	3,267	1,974	1,696	0,528	3,248	2,598
7,2	7,4	9	5641	0,971	0,029	3,529	2,001	1,304	0,266	3,514	2,765
7,4	7,6	11	5652	0,981	0,019	3,986	2,028	0,826	-0,191	3,977	3,050
7,6	7,8	7	5659	0,988	0,012	4,446	2,054	0,522	-0,651	4,440	3,331
7,8	8	3	5662	0,991	0,009	4,733	2,079	0,391	-0,938	4,729	3,503
8	8,2	3	5665	0,994	0,006	5,139	2,104	0,261	-1,344	5,136	3,743
8,2	8,4	2	5667	0,996	0,004	5,544	2,128	0,174	-1,749	5,542	3,980
8,4	8,6	2	5669	0,998	0,002	6,237	2,152	0,087	-2,442	6,236	4,377
8,6	8,8	1	5670	0,999	0,001	6,930	2,175	0,043	-3,135	6,930	4,765
8,8	9	1	5671	1,000	0,000						
9	9,2	0	5671	1,000	0,000						
total		5671									
N23		1023									
Ns		44,48									
alfa							Gumbel	Weibull			
beta							1,24	1,24			
gamma							1,64	1,01			
							8,21	4,50			



Figure H-2: SW swell waves, Gumbel and Weibull results and return period ave conditions

The first two figures; Table H-7 and Figure H-1, describe the NW wind waves in a small directional spreading (22.5 degrees). The same analysis is done for a wider spreading of 67.5 degrees. This analysis is not documented here, just the results in the summary at the end of this appendix. The threshold value is chosen at such a value, that the waveheight is at least 2.8m and the maximum Ns ('storms' per year after PoT) is 50. The analysis is similar to the first determination of the design storm in Appendix F.

H.1.5 OFFSHORE DESIGN CONDITIONS

In summary, the values of the wave heights are placed below, in Table H-9. Because of the good fit of both Gumbel and Weibull, an average is taken of both. The peak periods are displayed with them. The for scenarios are all investigated with Delft3D on their consequences. The values seem to describe the wave climate very well. In the investigation of the huge storm in August 2015, the highest waves (from the north-west) where measured at 10.23m (Winckler, 2016), which is very similar to 10.25m (1/250 years) in our analysis and suits as a very good design value.

Table H-9: Offshore wave heights, outcome for a narrow (NW and SW) and broad (NW-N and S-W) angle

		Average Gumbel-Weibull			
		SLS	TP SLS	ULS	TP ULS
Small	NW	2,96	7,5	9,16	12
Large	NW-N	4,11	9	10,25	13,3
Small	SW	5,39	13,5	10,58	17,5
Large	S-W	5,80	13,5	10,26	17,5

H.2 WAVE MODELLING

To make an appropriate design of the breakwater, it is essential to make an extensive study into the onshore wave climate at the particular location of the breakwater. It is necessary to make use of 3D wave modelling because of the difficult bathymetry in the Coliumo bay. SWANOne, used in the first iteration step, does not give enough insight into the behaviour of the wave propagation into the bay.

Therefore, in the preliminary design of the breakwater, use is made of the Deltares software DELFT3D-WAVE to translate offshore wave conditions to onshore.

H.2.1 DELFT3D-WAVE

The wave module of Delft3D makes use of the SWAN(Simulating WAVes Nearshore) Model. SWAN computes wave propagation, wave generation by wind, non-linear wave-wave interactions and dissipation, for a given bottom topography, wind field, water level and current field in waters of deep, intermediate and finite depth. In the following part a brief explanation of the model is given. All information is gained from the SWAN home-page (SWAN, 2017).

H.2.1.1 Governing equations

The basic equation of SWAN is the spectral action balance equation. It is formulated in Cartesian Co-ordinates and optionally in spherical co-ordinates to accommodate small- and large-scale. The action balance equation in Cartesian co-ordinates is formulated as follows:

$$\frac{\partial N(\sigma, \theta; x, y, t)}{\partial t} + \frac{\partial c_{g,x}(\sigma, \theta; x, y, t)}{\partial x} + \frac{\partial c_{g,y}(\sigma, \theta; x, y, t)}{\partial y} + \frac{\partial c_{\theta}(\sigma, \theta; x, y, t)}{\partial \theta} + \frac{\partial c_{\sigma}(\sigma, \theta; x, y, t)}{\partial \sigma} = \frac{S(\sigma, \theta; x, y, t)}{\sigma}$$

Which reduces to the energy balance equation in the absence of an ambient current:

$$\frac{\partial E(\omega, \theta; x, y, t)}{\partial t} + \frac{\partial c_{g,x}E(\omega, \theta; x, y, t)}{\partial x} + \frac{\partial c_{g,y}E(\omega, \theta; x, y, t)}{\partial y} + \frac{\partial c_{\theta}E(\omega, \theta; x, y, t)}{\partial \theta} = S(\omega, \theta; x, y, t)$$

The energy input driven by wind is determined based on wind speed at 10 m elevation. Dissipation is represented in SWAN by white-capping, bottom friction depth-induced breaking, partial absorption by structures and energy blocking by obstacles. The wave-wave interactions are also taken into account. SWAN is a so called third-generation wave model. This means that the model operates the most advanced computation of the quadruplet wave-wave interaction. The wave-wave interaction is explicitly calculated with the DIA of Hasselmann (Hasselmann, Hasselmann, Allender, & Barnett, 1985). This also applies for triad wave-wave interactions. These are calculated with the lumped-triad approximation of (Eldeberky, 1996).

H.2.1.2 Numerical scheme

SWAN makes use of geographic up-wind Schemes. The propagation of wave energy in geographic space is determined by calculating the wave energy in geographic grid points. The wave energy in grid point is determined by the state at the up-wave geographic grid points. Due to refraction, diffraction and nonlinear wave-wave interactions energy transfer in different directions occurs. To calculate this interaction, the so called Gauss-Seidel iteration process is carried out for each time step.

The Gauss-Seidel iteration process is done as follows. For each iteration, sweeping through grid rows and columns in geographical domain wave energy calculations are carried out, starting from each of the four corners of the computational grid. After four sweeps, wave energy has been propagated over the entire geographical domain. During each sweep, only the unknown values are updated. For instance, the first sweep starts at the lower left-hand corner and all grid points

After each propagation update at geographic grid point, an update in the spectral space is made. Since, the wave energy at a single spatial location depends on the upwind grid points only.

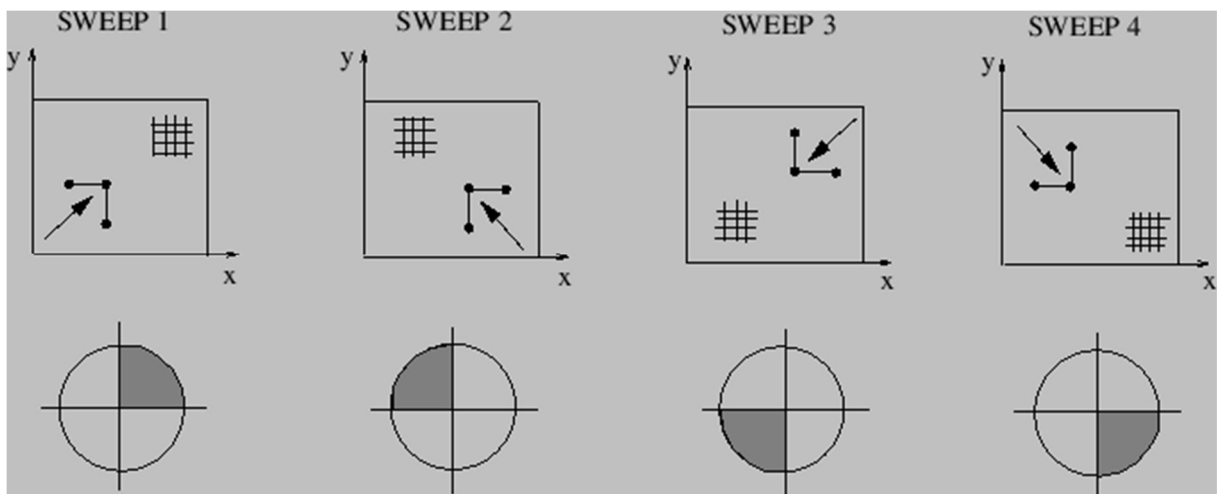


Figure H-3: The iterative solution procedure for wave energy propagation in geographical space for each of four sweeps

There are three numerical calculation schemes available to calculate the wave energy propagation in geographic space. To name the first-order BSBT scheme (Backward Space, Backward Time), The second-order Selling and Leendertse scheme and the second-order SORDUP scheme. The BSBT scheme is formulated as follows:

$$\begin{aligned} & \left[\frac{N^{i_t} - N^{i_t-1}}{\Delta t} \right]_{i_x, i_y, i_\sigma, i_\theta}^n + \left[\frac{(c_{g,x}N)_{i_x} - c_{g,x}N_{i_x-1}}{\Delta x} \right]_{i_y, i_\sigma, i_\theta}^{i_t, n} + \left[\frac{(c_{g,y}N)_{i_y} - c_{g,y}N_{i_y-1}}{\Delta y} \right]_{i_x, i_\sigma, i_\theta}^{i_t, n} \\ & + \left[\frac{(1-v)(c_\sigma N)_{i_{\sigma+1}} + 2v(c_\sigma N)_{i_\sigma} - (1+v)(c_\sigma N)_{i_{\sigma-1}}}{2\Delta\sigma} \right]_{i_x, i_y, i_\theta}^{i_t, n} \\ & + \left[\frac{(1-\eta)(c_\theta N)_{i_{\theta+1}} + 2\eta(c_\theta N)_{i_\theta} - (1+\eta)(c_\theta N)_{i_{\theta-1}}}{2\Delta\theta} \right]_{i_x, i_y, i_\sigma}^{i_t, n} = \left[\frac{S}{\sigma} \right]_{i_x, i_y, i_\sigma, i_\theta}^{i_t, n*} \end{aligned}$$

H.2.2 MODEL INPUT

DELFT3D makes use of several input files. The most important input is the bathymetry data. The data of the bathymetry of the area was provided by Dr. R. Aránguiz and M. eng. M. Villagrán. The bathymetry data is depicted in Figure H-4.

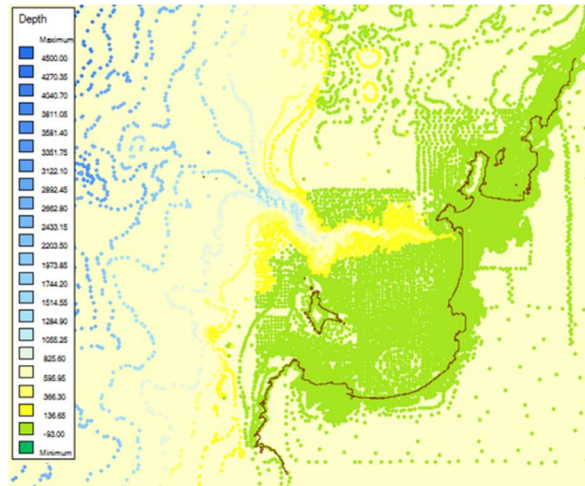


Figure H-4: Bathymetry data of BioBío region

To be able to use bathymetry data in DELFT3D, this data needs to have the right format. The bathymetry data of the entire BioBio area is transferred to the right extensions, an .xyz (bathymetry) and .ldb (landboundary) file in GlobalMapper. With RGFGRID, grids are made for the whole area of BioBio and for the Coliumo bay in more detail. The grids, together with the bathymetry (.xyz) and landboundary (.ldb) are input for the QUICKIN program which creates depth (.dep) files for the two grids. The approach of DELFT3D is summarized in the flowchart in Figure H-5.

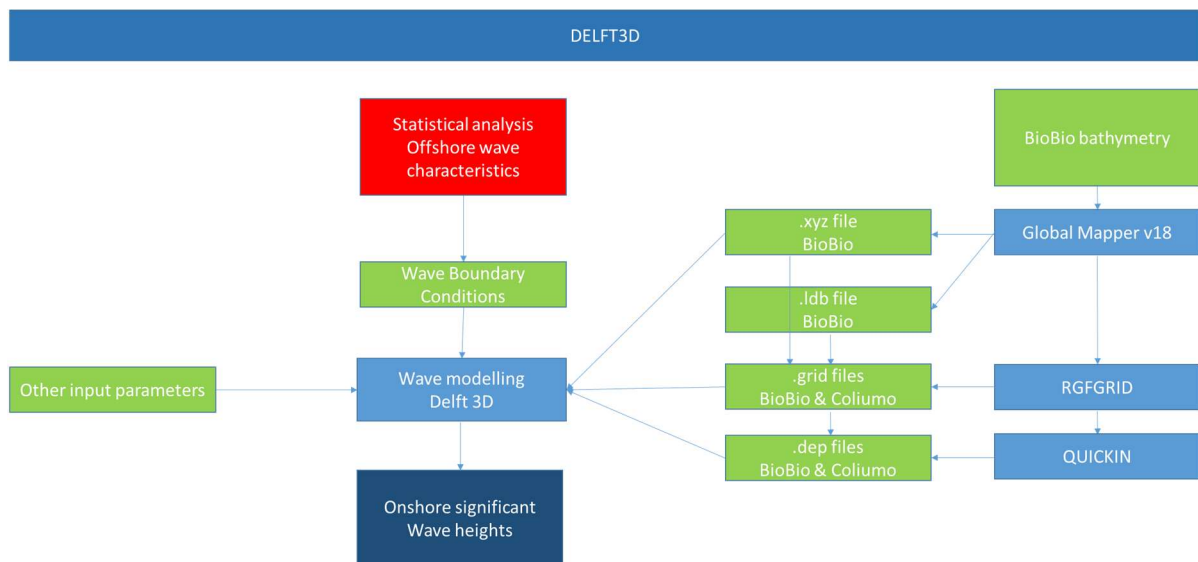


Figure H-5: Flowchart of method

The calculations of the wave propagation are performed in two different grids. The big BioBio grid and the Coliumo Bay grid. The Coliumo bay grid is nested in the BioBio grid.

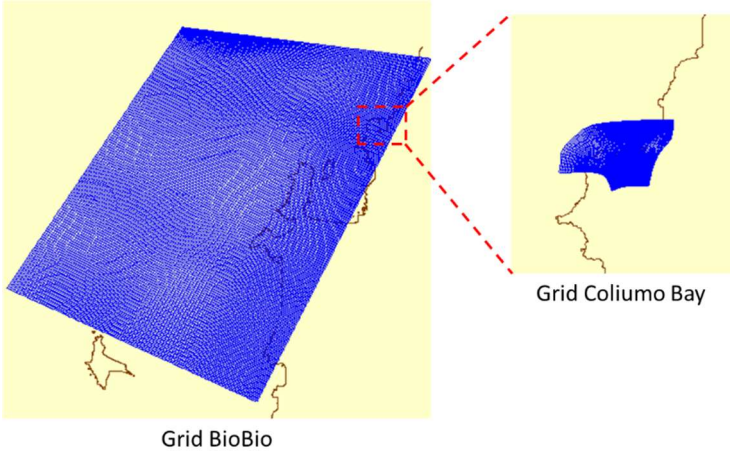


Figure H-6: Grids

As mentioned in Appendix H.1: *Determination design storm* only 4 scenarios are elaborated. There is chosen to use the parameterisation option within DELFT3D to define the wave characteristics. DELFT3D converts these data to a Jonswap spectrum with a peak enhancement factor $\gamma=3$ and an f-5 spectral tail. In consultation with Dr. R. Aránguiz, the peak enhancement factor is changed to $\gamma=6$ in order to describe the wave conditions at the Pacific Ocean in the right way. The following offshore wave and accompanying wind characteristics are implemented in the model study.

Table H-10: Boundary conditions

	Wave characteristics						Wind	
	Hs (m)	Tp (s)	direction(°)	spreading(°)	Boundarries		U (m/s)	direction(°)
NW-N								
SLS	4,11	9	337,5	33,75	N	W	10	338
ULS	10,25	13,3	337,5	33,75	N	W	30	338
SW								
SLS	5,39	13,5	247,5	11,25	S	W	9	200
ULS	10,58	17,5	247,5	11,25	S	W	22	200

The values of the incident wave conditions are specified as shown in Figure H-7. Along the boundaries the wave conditions are assumed to be constant.

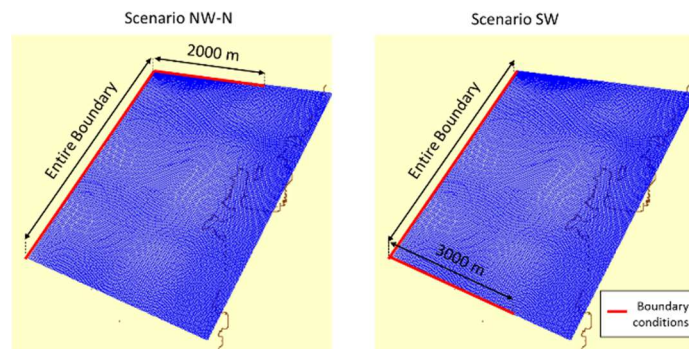


Figure H-7: Location of boundary conditions

Later on the governing ULS and SLS onshore wave conditions will be determined, out of these 4 scenarios.

To Clarify the influence of the tide, the calculations are executed for the following water levels:

Lowest all time: -0.95 m.

Mean sea level: 0 m.

Highest all time: +1.11 m.

Within the Delft3D-WAVE module it is possible to couple the model with current information. In this case there is chosen to only use a stand-alone Wave calculation. This chose is made because of lack of reliable information about the current characteristics. For depth-induced breaking, non-linear triad interactions and bottom friction the default settings are used. In this case it is not possible to calculate the diffraction. The process diffraction can only be solved accurately when a detailed grid is applied. The grid needs to fulfil the following requirement: $dx \leq \frac{1}{10} L$ (Ilic, 1994)

In case of much coarser grids, the SWAN computation can become unstable and results are not reliable, in this case the software shows an error warning.

H.2.3 RESULTS DELFT3D

The DELFT3D model generates outcomes for the grids as well as for predefined locations. In this case the location of the breakwater. The results of all different scenarios, as described in the determination of the design storm, presented in the upcoming figures and table. All results are during high water, HAT: +1.11 m.

Figure H-8 and Figure H-9 show the wave heights of the different scenarios are shown in the different grids and zoomed in to the location of the breakwater at Calleta Villarica. For both the ULS and SLS the NW-N scenario appears to be Governing. This can be explained by the northern facing of Coliumo Bay. When looking at the figures it is important to keep in mind that the colour scales are different in the different zooms.

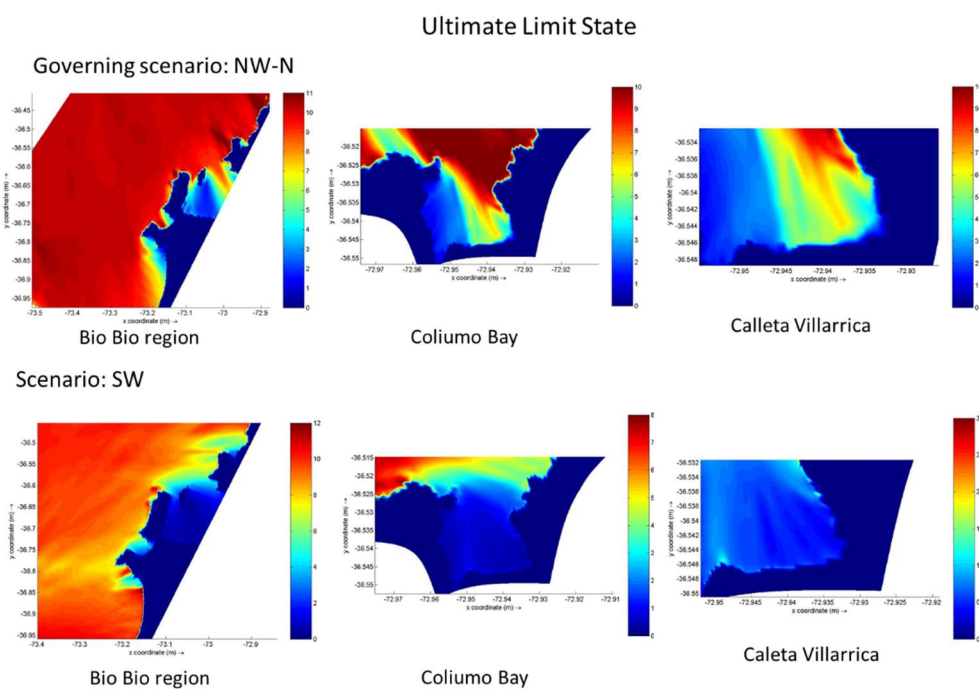


Figure H-8: Results for ULS

Serviceability Limit State

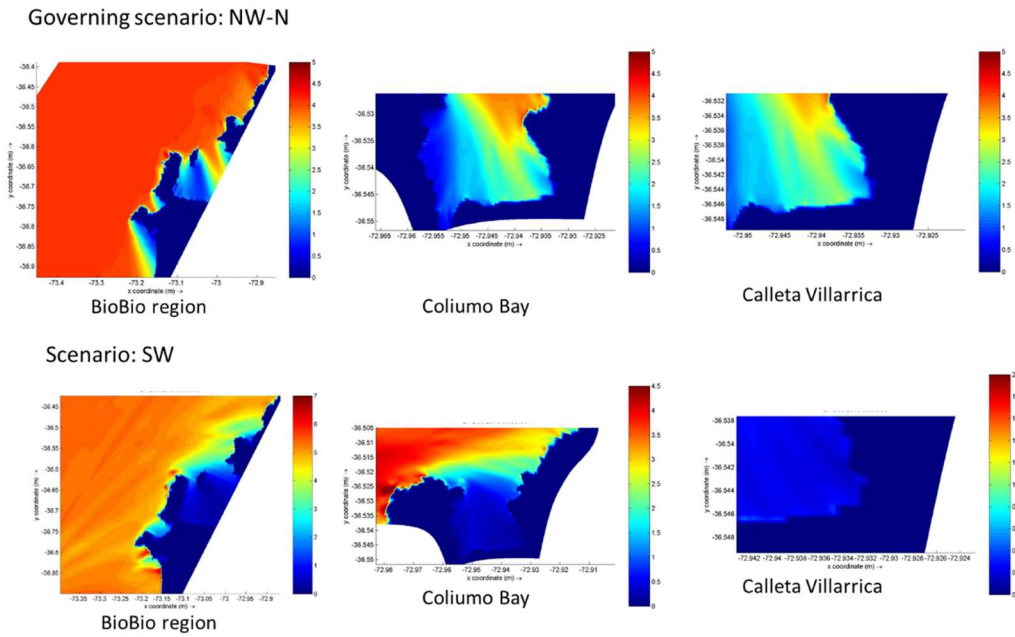


Figure H-9: Results for SLS

The values wave climate at the specific location of the breakwater are summarized in Table H-11. As mentioned before the NW-N is the governing scenario. The values of NW-N ULS and NW-N_SLS will be used as design values for the breakwater.

Table H-11: Output DELFT3D for different scenarios at breakwater location

	Depth	Hsig	Dir	RTpeak	Tm01
	[m]	[m]	[degr]	[sec]	[sec]
NW-N_ULS					
llw	2,70	3,54	292,44	13,75	10,98
mssl	3,65	4,07	296,30	13,75	10,87
hhw	4,76	4,49	300,09	13,75	10,74
SW_ULS					
llw	2,19	0,67	310,95	20,00	15,31
mssl	3,14	0,85	311,69	17,65	16,00
hhw	4,25	0,84	304,65	17,65	16,33
NW-N_SLS					
mssl	3,54	1,56	304,81	9,46	6,46
hsl	4,67	1,71	308,29	9,46	6,45
SW_SLS					
mssl	3,15	0,17	297,51	13,75	12,27
hhl	4,25	0,17	300,38	13,75	12,33

H.3 BREAKWAT3.0

The mooring facility of the EMBD will be protected from the incoming waves by a breakwater. This is necessary to create a safe climate to ensure that the facility can fulfil the required mooring functions. There is chosen to make use of a low crested conventional rubble mound breakwater to meet the requirements of maximum wave transmission through the breakwater.

The design is limited to a preliminary design of the solution as mentioned in chapter 1. The final detailed design going beyond the scope of this report. Therefore, is chosen to make use of the Deltares software BREAKWAT version 3.1.

BREAKWAT is a design tool for several types of coastal structures under wave loading. The software is suitable to design the conventional rubble mound breakwater that will protect the mooring facility of the EMBD. The predictions of BREAKWAT are based on small-scale physical model tests, so the tool may not be used in the final design stage. The detailed design should be verified based on dedicated physical model tests for the particular wave conditions and structure geometry of the structure to be built. However, BREAKWAT can be used up to the conceptual design of coastal structures and appropriate to make the preliminary design of the breakwater. In the following part a brief explanation of the design tool is given. All information is gained from the BREAKWAT home-page (BREAKWAT, 2017).

H.3.1 GOVERNING EQUATIONS

BREAKWAT is a gathering of equations to describe wave loading of coastal structures. In this case, basically two equation are used. One to determine the wave transmission through the structure and another to determine the stone size.

If waves overtop a structure, the waves plunge into the water again. If the overtopping is severe enough this causes new waves behind the breakwater. In case of a permeable structure waves with long periods can lead to transmission of wave energy through the breakwater. To compute the wave transmission BREAKWAT makes use of the formula by De Jong and d'Angremond (De Jong, 1996). The formula reads as follows:

$$C_t = a - [0.4(R_c / H_s)]$$

where

$$a = (B / H_s)^{-0.31} [1 - \exp(-0.5\xi_{0p}^2)] A_{dir}$$

$$\xi_{0p} = 1.0 / [(\cot \alpha_s) \sqrt{2\pi H_s / (gT_p^2)}]$$

With the following parameters and limits:

Parameters:

C_t	transmission coefficient	(-)
H_s	Incident significant wave height	(m)
T_p	Peak wave period	(s)
B	Crest width	(m)
R_c	Crest freeboard above still water level	(m)
$\cot(\alpha_s)$	Slope angle of the structure	(-)
A_{str}	Coefficient dependin on the structure type	(-)

Limits:

0.075	≤	C_t	≤	0.8
0.01 m	<	H_s	<	20 m
0.5 s	<	T_p	<	30 s
1.1	<	$\cot(\alpha_s)$	<	7.0
0.5	<	ζ_{0p}	<	10.0
0.005	≤	$2\pi H_s / g T_p^2$	≤	0.07

The transmitted wave height can be calculated as follows: $H_{st} = C_t * H_s$

To ensure stability of the breakwater under wave loading the stone size is determined by using the Van der Meer rock stability formula.

For plunging waves:

$$\frac{H_s}{\Delta D_{n50}} = \left(\frac{H_{2\%}}{H_s} \right)^{-1} 8.68 P^{0.18} \left(\frac{bS}{\sqrt{N}} \right)^{0.2} \zeta_m^{-0.5} \quad \text{if} \quad \zeta_m < \zeta_{mc}$$

For surging waves:

$$\frac{H_s}{\Delta D_{n50}} = \left(\frac{H_{2\%}}{H_s} \right)^{-1} 1.4 P^{-0.13} \left(\frac{bS}{\sqrt{N}} \right)^{0.2} \sqrt{\cot \alpha_s} \zeta_m^P \quad \text{if} \quad \zeta_m > \zeta_{mc}$$

With the following parameters and limits:

Parameters:

M_{50}	Armour unit mass	(kg)
H_s	Incident significant wave height	(m)
T_m	Mean wave period	(s)
S	Dimensionless damage level	(-)
ρ_a	Armour density	(kg/m ³)
ρ_w	Water density	(kg/m ³)
N	Number of incoming waves	(-)
P	Notional permeability	(-)
$H_{2\%}/H_s^*$	Wave height ratio	(kg/m ³)
A_e	Erosion area	(m ²)

Limits:

0.1	≤	P	≤	0.6
0.01 m	<	H_s	<	20 m
0.5 s	<	T_p	<	30 s
1.1	<	$\cot(\alpha_s)$	<	7.0
0.005	≤	$2\pi H_s / g T_p^2$	≤	0.06
0	<	N	<	7500
1.10	<	$H_{2\%}/H_s$	<	1.40
2000	<	ρ_a	<	3100 kg/m ³

With the dimensionless damage level:

$$S = \frac{A_e}{D_{n50}^2}$$

H_s , S or M_{50} can be selected as input or output parameter. In this case is chosen to select M_{50} and the associated D_{n50} as output parameter.

H.3.2 MODEL INPUT

The crest height is calculated with the governing SLS wave conditions and a maximum transmitted wave height of 0.3m. The slope of the structure is taken at 1:2 and the structure type coefficient is 0,64 for a rubble mound breakwater (Verhagen, d'Angremond, & van Roode, 2009). Assumed is an angle of the incoming waves at 0 degrees. The input is summarised in Table H-12.

Table H-12: Input parameters for crest height

Parameter	Value	Unit
H_{st}	0.3	(m)
H_s	1.71	(m)
T_p	9.5	(s)
B	3	(m)
$Cot(\alpha)$	2.0	(-)
A_{str}	0.64	(-)

The size of the stones is based on the ULS wave conditions. There is chosen to allow a damage level between 3 and 5. Using this values, the ULS wave conditions will cause intermediate damage and repair is needed (Verhagen, d'Angremond, & van Roode, 2009). To calculate the stone dimensions, a iterative process is used. The stone size is used as design parameter, and is chosen in such way that the required Damage level is achieved. The wave height ratio $H_{2\%}/H_s$ is taken at 1.4 (Holthuijsen, 2007). The notional permeability coefficients for a breakwater without filter and core is 0,6 (Verhagen, d'Angremond, & van Roode, 2009).The input is summarised in Table H-13.

Table H-13: Input parameters for stone dimensions

Parameter	Value	Unit
H_s	4.5	(m)
$H_{2\%}/H_s$	1.40	(-)
T_m	10.7	(s)
P	0.60	(-)
$Cot(\alpha)$	2.0	(-)
N	3000	(-)
M_{50}	10000	(kg)
ρ_w	1025	(kg/m ³)
ρ_a	2650	(kg/m ³)

H.3.3 RESULTS BREAKWAT

The calculations with BREAKWAT 3.1 give a crest height is 1.45m above the highest sea level, which means the crest height is at a height of **2,56m above MSL**. To ensure rock stability up to a damage level of 3.4 during ULS conditions, **W50 of 10.000 kg** with an associated **Dn50 of 1.56m** are necessary. The outcomes are listed in Table H-14.

Table H-14: Dimensions of the breakwater

Parameter	Value	Unit
Crest Height	1.45	(m)
C_t	0.16	(-)
H_{st}	0.29	(m)
D_{n50}	1.59	(-)
S	3.36	(-)

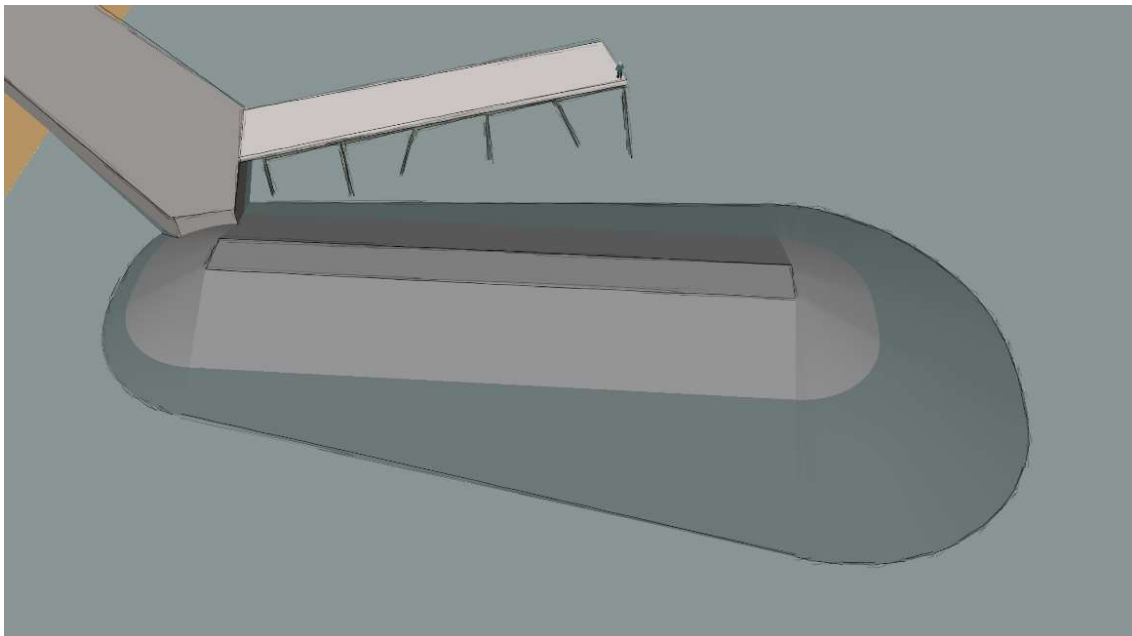


Figure H-10: 3D visualisation of the breakwater in front of the jetty. The waves are perpendicular on the breakwater, originating from the bottom of the figure.

H.4 PLAXIS 2D

PLAXIS 2D is a two-dimensional finite element program, developed for the analysis of deformation, stability and groundwater flow in geotechnical engineering (Brinkgreve, 2016). A vast range of soil models may be used to model the subsurface, including Mohr-Coulomb, a robust and simple non-linear model based on soil parameters known in most practical situations; as well as more advanced models to accurately capture non-linear behaviour such as the Hardening Soil or the Soft Soil Creep models. Furthermore, PLAXIS 2D can incorporate staged construction, consolidation and safety analyses.

H.4.1 CALCULATION MODES

PLAXIS 2D is used to model the settlements of the breakwater under its own weight. Furthermore, the impact of waves on the breakwater cross-section may be investigated using a flow function.

To analyse the influence of the subsoil conditions on the settlement of the breakwater two situations are investigated: 1) where a soft sandy layer overlies the sandstone 2) where the sandy layer has been dredged and the breakwater rests directly on the sandstone. A safety analysis is conducted for each subsurface scenario. A strength reduction method results in a factor of safety for failure, where the deformation output illustrates the mode of failure in terms of slip surface. Finally, in order to model the wave load on the breakwater, the groundwater head is assigned a harmonic flow function with a certain amplitude and period corresponding to the design wave properties used in the breakwater design.

H.4.2 IMPLEMENTATION OF BREAKWATER

The implementation of the breakwater in PLAXIS 2D is elaborated step-by-step:

1. A new project is created in plane strain (the breakwater measures 30 m in length) and boundaries X_{min} , X_{max} , Y_{min} and Y_{max} of 0.0m, 40.0m, -15.0m and 2.2m, respectively, to ensure the boundary conditions do not affect computation results.
2. The subsurface conditions are defined, as well the armourstone for the breakwater. Three materials are created, all employing a drained Mohr-Coulomb model, as this model reflects non-linear behaviour whilst at the same time being limited in the required number of soil parameters. Table H-15 gives the defined materials and their properties.
3. The rock $_ll$ considered consists of granite, since the breakwater is a coastal structure [A. Waltham, 2009]. Information about the stiffness parameters of rock fill is limited. The values for plastic and cyclic loading largely depend on the crushing potential of the grains. Quartz sand and excellent quality rock hardly crushes in the range of effective stresses relevant for hydraulic engineering structures, like breakwaters. In this case, excellent rock is assumed to be used for the breakwater. If this will actually be used, it is highly dependent on the availability and/or economic factors. The best way to $_nd$ good estimates of the parameters of the rock $_ll$ is to perform large scale oedometer tests and shear tests. When excellent rock quality is assumed, the values of the stiffness parameters are in the same range as quartz sand [CUR & CETMEF, 2007]. Also, it is assumed that the quarried rock $_ll$ consists of round particles and is more or less uniformly graded.

4. The build-up of the subsurface and breakwater geometry are inputted. In the first test scenario, the subsurface consists of a 2m layer of silty sand underlain by the sandstone. In the second test scenario, the top layer is dredged and the breakwater rests directly on the sandstone. Since the breakwater cross-section is symmetrical about the y-axis, only half of the model is given to save computation time. The modelled cross-section is taken near the end of the breakwater, where the water depth is highest, at 5.0m, since here the breakwater is at its largest and imposes most weight on the subsurface. Figure H-11 **Error! Reference source not found.** shows the trapezoidal geometry of the breakwater cross-section, measuring 3m in width at the crest, with a 1:2 slope. The crest height is MSL +2.2m, with a submerged height of 5.0m.
5. A fine finite element mesh is generated. Ideally the sensitivity of the output to the mesh size is investigated prior to obtain an optimum in terms of computation efficiency.
6. In terms of flow conditions, the hydraulic head is set at Mean Sea Level MSL (0.0m). The flow boundary conditions are open for open X_{min} , X_{max} and Y_{max} and closed for Y_{min} .
7. A calculation of the initial phase is made using a Gravity Loading calculation type for each of the two subsurface scenarios. Additionally, the factor of safety for each is computed using a safety calculation.
8. A harmonic wave is implemented using a *transient groundwater flow* setting and a harmonic flow function on the right-side hydraulic boundaries with a wave amplitude of 0.95m and a period of 14.5s (the design wave height and peak period used in the preliminary breakwater design).

Table H-15: Material input parameters for PLAXIS2D model of breakwater

Parameter	Unit	Breakwater: Armourstone	Subsurface: Silty sand	Subsurface: Sandstone
Model	-	Mohr-Coulomb	Mohr-Coulomb	Mohr-Coulomb
Drainage type	-	Drained	Drained	Drained
γ_{unsat}	kN/m ³	16	20	21
γ_{sat}	kN/m ³	20	20	21
E'	kN/m ²	1.0e5	1.0e4	1.0e6
ν'	-	0.3	0.3	0
c'_{ref}	kN/m ²	0	0	1e6
φ'	°	50	30	38
ψ	°	15	2	0
k_x	m/s	1.0	1.0e-6	1.0e-7
k_y	m/s	1.0	1.0e-6	1.0e-7

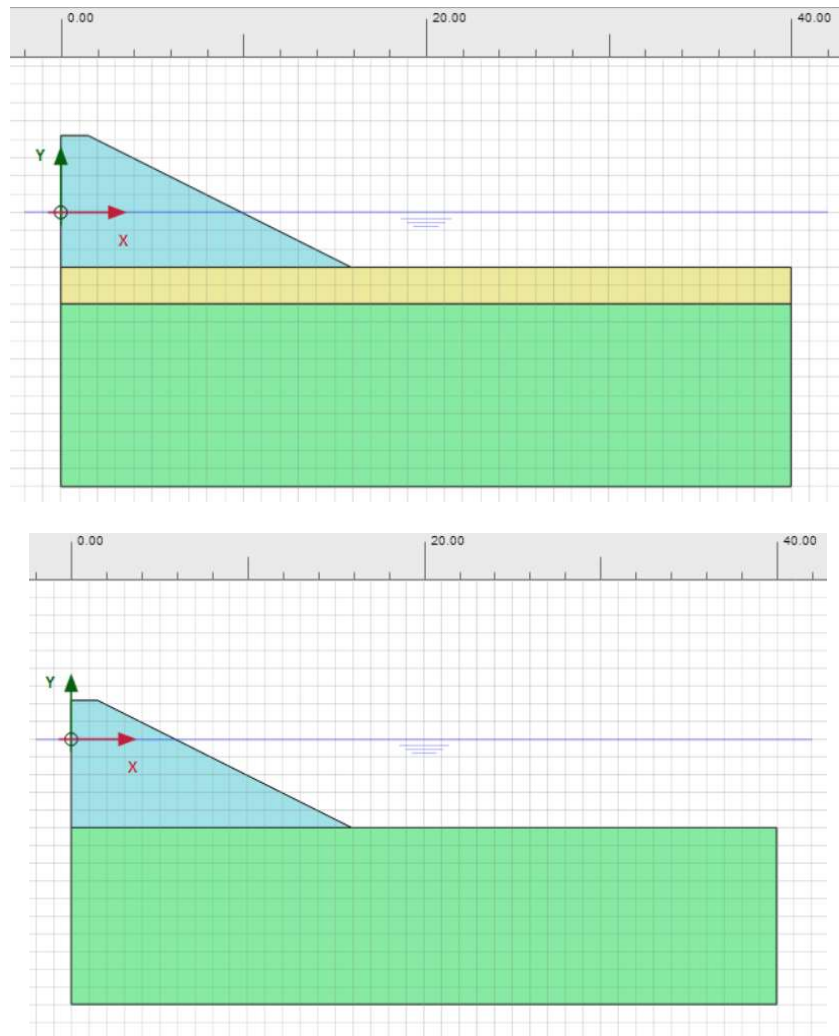


Figure H-11: Breakwater geometry for subsurface scenarios 1 (top) and 2 (bottom)

H.4.3 RESULTS

H.4.3.1 Settlement under own weight

Figure H-12 and Figure H-13 illustrate the settlement of the breakwater and the subsurface under the initial gravity loading. The maximum deformation for the situation with a thin sand layer (scenario 1) is 33 mm. For scenario 2, in which the sand layer has been removed, the maximum settlement becomes just 8 mm. The difference in settlement is therefore of a factor 4 in magnitude. However, overall, the settlements are small due to the relatively high stiffness of the breakwater and underlying strata.

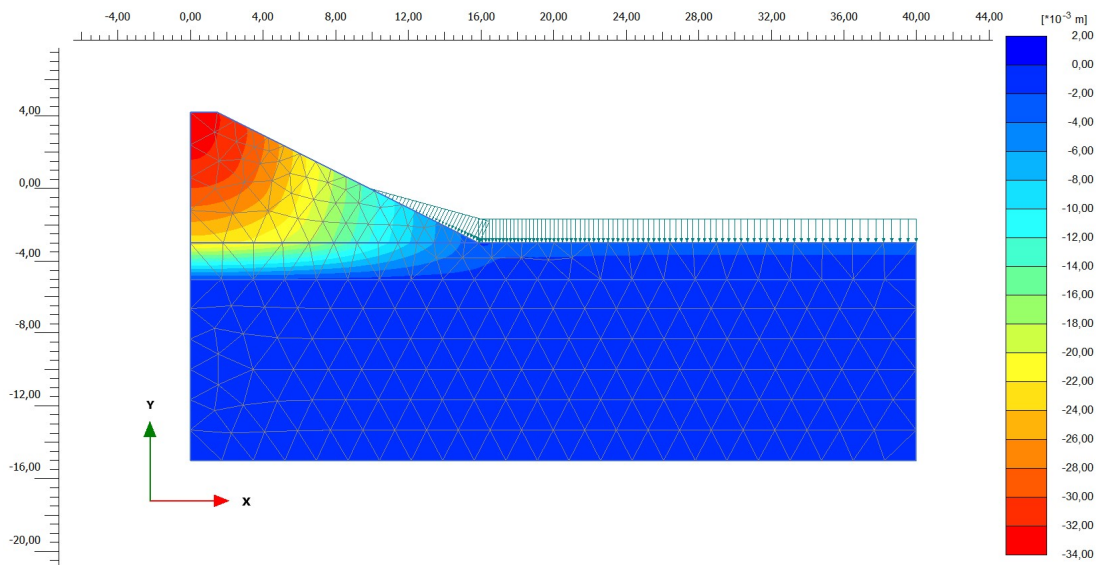


Figure H-12: Total vertical displacement u_y for breakwater in subsurface scenario 1 (with sand layer)

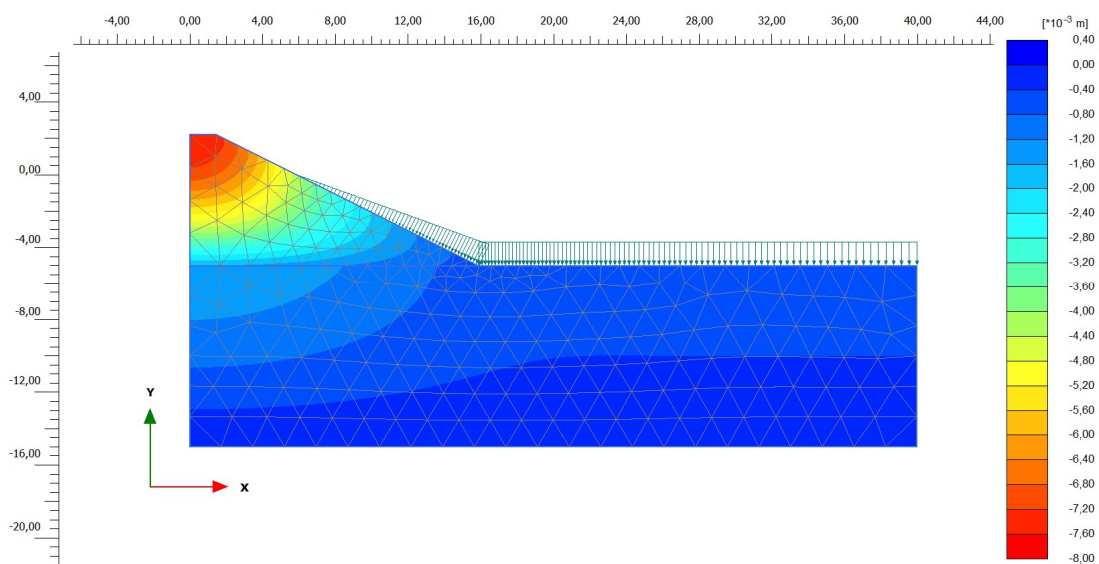


Figure H-13: Total vertical displacement u_y for breakwater in subsurface scenario 2 (without sand layer)

H.4.3.2 Factor of safety for global stability under MSL conditions

The global stability of the breakwater slope is analysed using a strength reduction method, in which the resulting safety factor refers to maximum shear strength available over the shear strength needed for equilibrium. Additional displacements are generated during a *Safety* calculation which have no physical meaning, but the incremental displacements give a good idea of the likely failure mechanism. For each of the subsurface scenarios this is shown in Figure H-14 and Figure H-15.

The computed global factors of safety are 1.66 and 2.23 for with and without a sand layer, respectively. This means that under normal mean sea level (static) conditions, disregarding wave or

current action, the breakwater is stable. Figure H-16 shows the global factor of safety ΣM_{sf} versus the total displacement $|u|$ at a point at the toe. The point at which the curve reaches a plateau of a more or less constant ΣM_{sf} value, may be interpreted as the global factor of safety.

Especially if the sand layer were to be removed, the failure mechanism shows a very shallow slip surface as it cannot penetrate through the sandstone. The failure mechanism for scenario 1, with sand layer, shows a circular slip failure surface as commonly encountered.

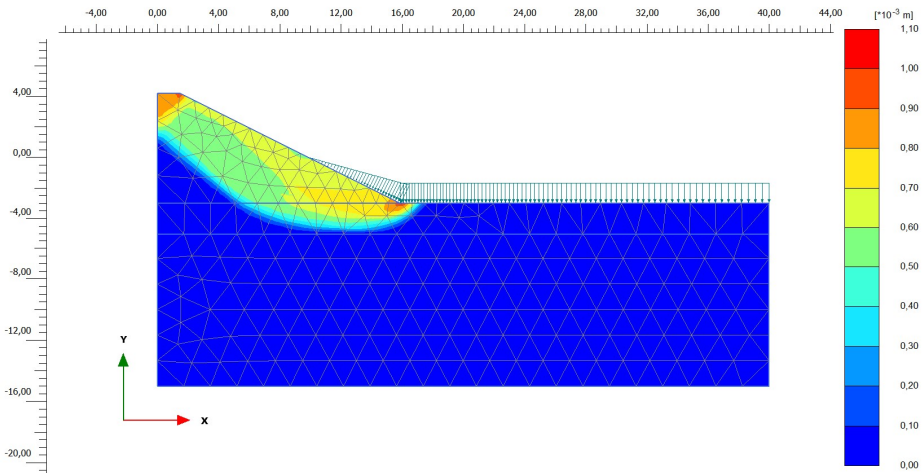


Figure H-14: Failure mechanism for subsurface scenario 1 (with sand layer)

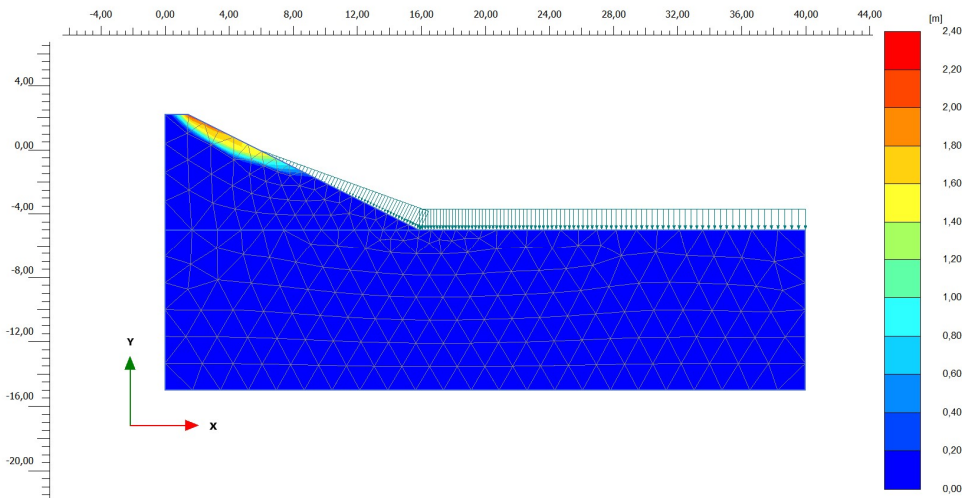


Figure H-15: Failure mechanism for subsurface scenario 2 (without sand layer)

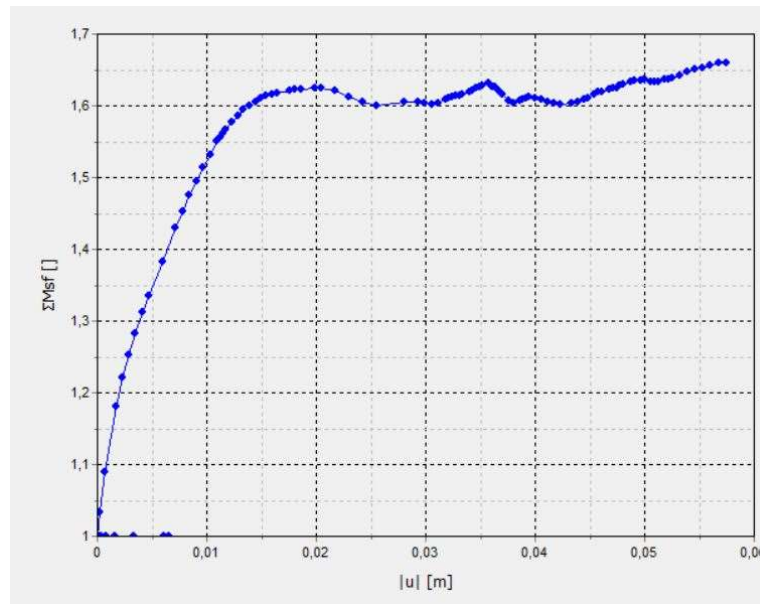


Figure H-16: Determination of factor of safety at the breakwater toe for subsurface scenario 1

H.4.3.3 Stability under harmonic wave load

The deformations induced under ‘flow only’ conditions (i.e. no gravity loading) are negligible and the factor of safety against instability remains around 2.2 and 1.7 respectively for the subsurface scenarios with or without sand.

Figure H-17 and Figure H-18 show the variation in groundwater head and pore pressure for soil scenario 1 (with a sand layer), both for points at the breakwater toe and the crest. Figure H-19 and Figure H-20 show the same but for soil scenario 2 (without sand). One can see that the variation in the toe is rather regular and the generated pore pressures are generally 4 times higher at the toe than at the crest of the breakwater. Overall, the sandy layer in soil scenario 1 dampens the pore pressure build up in the breakwater as it is more porous than the sandstone.

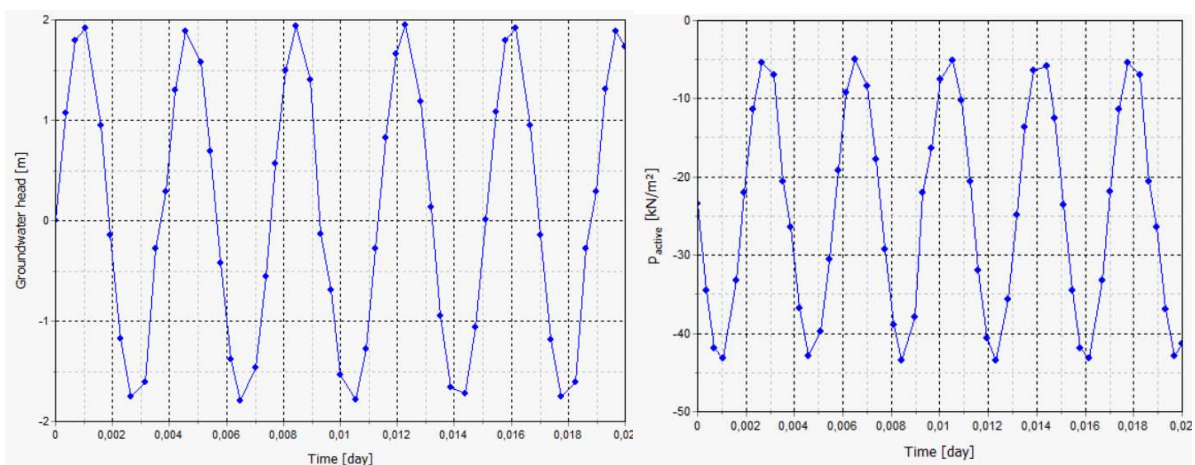


Figure H-17: Pressure head (left) and active pore pressure (right) variation with time for harmonic wave hydraulic conditions, for a point at the breakwater toe, soil scenario 1

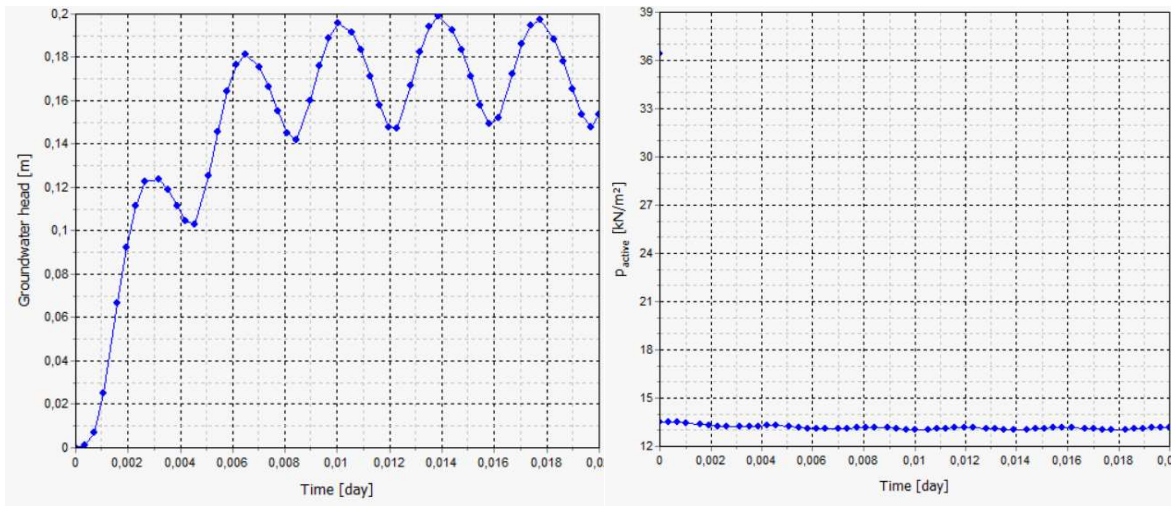


Figure H-18: Pressure head (left) and active pore pressure (right) variation with time for harmonic wave hydraulic conditions, for a point at the breakwater crest, soil scenario 1

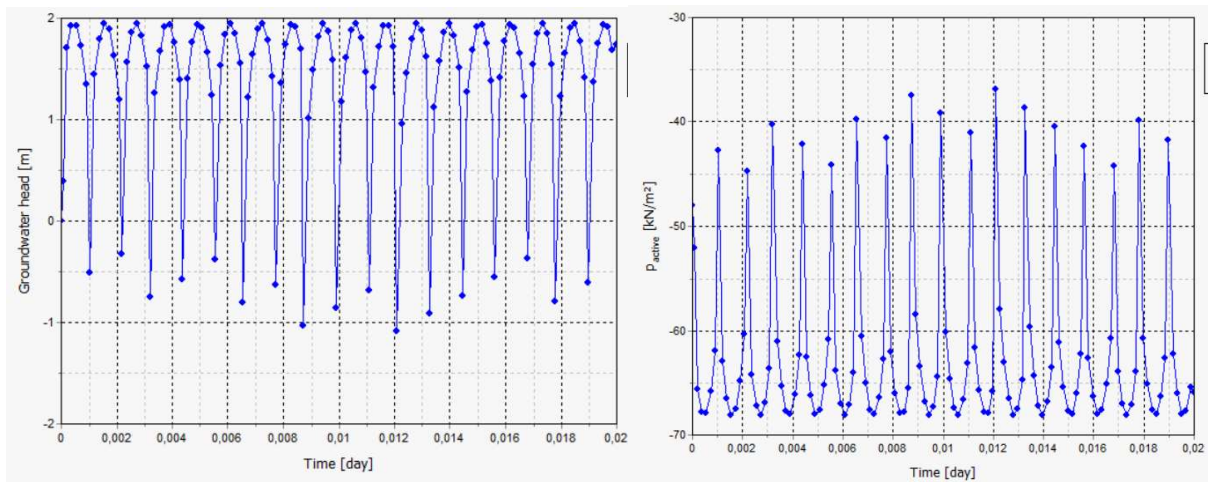


Figure H-19: Pressure head (left) and active pore pressure (right) variation with time for harmonic wave hydraulic conditions, for a point at the breakwater toe, soil scenario 2

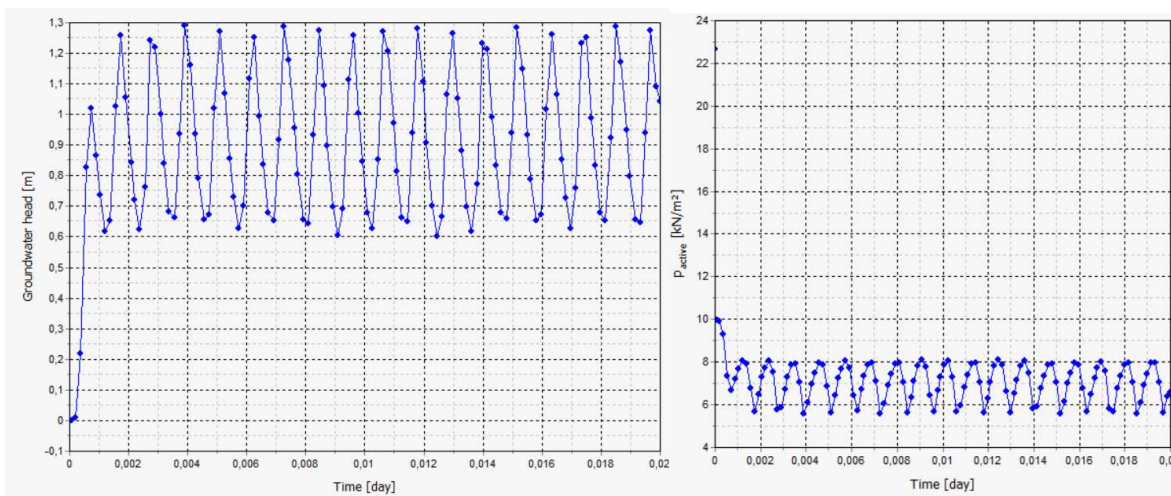


Figure H-20: Pressure head (left) and active pore pressure (right) variation with time for harmonic wave hydraulic conditions, for a point at the breakwater crest, soil scenario 2

H.4.4 CONCLUSIONS ON PLAXIS 2D MODELLING

Overall, the breakwater settlement is minimal under gravity loading, and ranges between 10 and 30 mm depending on whether the sand layer is removed or not. The sand layer allows for more deformation and the global stability of this configuration is a factor 1.3 less safe than if the layer were to be removed. However, both configurations have acceptable factors of safety against global failure.

The soil model for the breakwater is a very rough approximation of the true form of the pile of 0.70m diameter rocks. Hydraulic conductivity is difficult to estimate as well. PLAXIS is very sensitive to parameter input, especially to the friction angle in the case of the breakwater model. Numerical modelling in PLAXIS may be better suited to an earth or rock-filled core-type breakwater.

I. DESIGN: PAVEMENT

A design is made for a low-volume traffic road according to the Chilean guideline *Guía de Diseño Estructural de Pavimentos para Caminos de Bajo Volumen de Tránsito* (2002). Currently, the design of a low-volume road must comply with the minimum geometric design standards (longitudinal and in cross-section), signalling requirements and a minimum level of structural durability. Low-volume traffic roads are designed with a lifetime of 5 to 10 years for less than 150,000 equivalent axles. The design is governed by the maximum stresses rather than fatigue behaviour, induced by a truck with a single double-wheeled axle of 11 tonnes.

The Chilean pavement guideline delineates four types of pavement structures for light roads: 1) granular structure with surface protection in the form of an asphaltic seal or superficial treatment 2) granular structure with asphaltic protection 3) stabilised base asphalt structure with surface protection and 4) granular structure with stabilized cement subbase and asphaltic surface protection. For low-volume traffic roads only the first option is considered economical. The structure of this type of pavement is shown in Figure I-1. The design specifications and considerations are

- The protective surface layer may consist of a Simple or Double Surface Treatment (TSS or TSD), or a sealing cap, amongst others. The surface treatment must restore the texture and weatherproofing of the surface, but does not contribute to ride or structural capacity improvement.
- A granular base of 100% CBR⁵ must be considered, and a subbase of 40-50% CBR.
- For subgrade soil conditions with low capacity a floor or an embankment of CBR 20% must be constructed first.
- The design must be carried out for dry, normal and saturated conditions.
- The bottom layers must be designed to achieve a greater life span, as top layers are more easily repaired.
- The structure must be designed for an overloaded truck with 50% reliability.
- The serviceability limit state for a low-volume road refers to the level of wearing of the top layer of the pavement structure. It is defined by the International Roughness Index, IRI. The initial design IRI is limited at 3m/km and the final design IRI is 8m/km.
- Optimal use ought to be made of locally available material.
- The surface treatment is not designed for fatigue, since this not governing for light traffic. The granular base and subbase *are* designed for fatigue using the formula

$$N = 10^{A \cdot F + B}$$

With

$$F = \frac{\sigma_3 \cdot \varphi + c_{term}}{\sigma_1 - \sigma_3}$$

⁵ California Bearing Ratio: a simple strength test that compares the bearing capacity of a material with that of a well-graded crushed stone. High quality crushed stone material has a CBR of 100%, whilst sandy material typically has value between 20%-40%.

Where N = allowable equivalent axles; A, B = factors depending on level of reliability; σ_1 = compressive stress in middle part of layer; σ_3 = tensile stress in middle part of layer; φ = internal friction angle; and c_{term} = cohesion term.

The following design steps are followed:

1. *Selection of range of traffic loads:* Light traffic (< 150.000 equivalent axles per year)
2. *Selection of bearing capacity range of subsoil:* The geophysical test conducted at the site (see Appendix *) indicates a top 3m of gravelly sand as subgrade soil, with an estimated CBR of between 10 and 30%. Thus, the sand provides sufficient bearing capacity for direct construction of the pavement, and may be classified as subgrade soil type S5.
3. *Selection of climate type:* This concerns temperature and hydraulic conditions. The governing hydraulic condition for granular base structures is the saturated case, as major failures may initiate when saturated conditions are coupled with overloaded trucks and quality variability. A drainage system must be designed considering the type of subgrade material; the base width; the transverse slope; the existence of the embankment; and the annual average precipitation. In the BioBío region, the climate type condition is generally of type (1), which means that the precipitation must be greater than 2000mm to meet the saturated conditions.
4. *Design chart for light traffic:* Chart number 2 for normal conditions, and chart number 3 for saturated conditions.

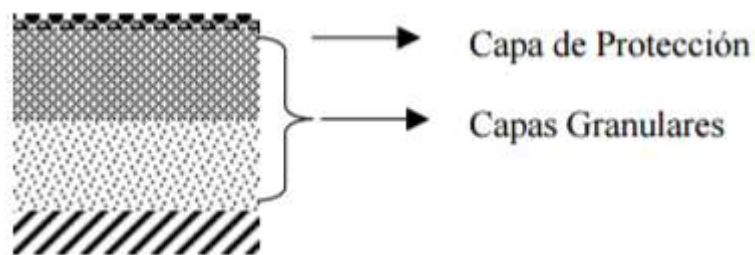


Figure I-1: Structure of granular pavement with surface protection layer

Ejes Equivalentes (x Sentido)	Tránsito T0 (Hasta 150.000 Ejes Equivalentes)	
	Opción de Diseño 1	Opción de Diseño 2
Suelo S1 (CBR < 3%)	/	/
Suelo S2 (3% < CBR < 6%)	18 16 (*)	16 16 (*)
Suelo S3 (7% < CBR < 10%)	18 18	16 20
Suelo S4 (11% < CBR < 14%)	18 14	16 16
Suelo S5 (15% < CBR < 19%)	26	16 12
Suelo S6 (CBR > 20%)	/	/

SIMBOLOGIA

- Capa de Protección
- Base Granular CBR 100%
- Subbase Granular CBR 50%
- Subbase Granular CBR 40%

Figure I-2: Design of pavement structure for light-traffic road in saturated conditions (Thenoux & al, 2002)

I STONE AND SAND ANALYSIS

I.1 DICHATO REVETMENT GRADING ANALYSIS

To obtain insight into the feasibility of the computed stone dimensions needed to construct the breakwater, a stone size analysis is conducted at Dichato at a section of existing shore protection along the bay. The revetment consists of granitic rock, see Figure I-2. A 3x3m² plot is chosen at random along the shore protection, and all stones that fall inside this area with at least 50% of their size are labelled in Figure I-1.

In a sample of natural quarry blocks there will be a range of block weights: grading. The particle weight distribution is often presented in a percentage lighter by weight cumulative curve, where M_{50} expresses the median block mass. Several methods exist to determine the M_{50} of a rock block sample. In most design formulas, not the weight but the nominal diameter D_{n50} is used (Schiereck, 2003). The relation between the two is as follows

$$D_{n50} = \sqrt[3]{\frac{M_{50}}{\rho_s}}$$

With ρ_s equal to the solid particle density. To relate the nominal diameter D_{n50} to the median grain size diameter D (from the square opening sieve size for grain distribution analysis), a shape factor F_s^* is used, which is generally taken as 0.84 for armour stone rocks (Laan, 1981). The conversion factor F_s relates the median nominal diameter and the median mass:

$$F_s = \frac{M_{50}}{(\rho_s D_{50}^3)} = (0.84)^3 \cong 0.60$$

Using this relation, weights emerge from the measured size data as given in Table I-1⁶. The resulting M_{50} is 1355 kg, with a grading width of 9.1. Using tables 3.4 *Armourstone grading width related to the uniformity* and 3.5 *Heavy, light and coarse European EN 13383 standard grading requirements* from the Rock Manual (Research, 2007), the revetment grading may be classified as ‘heavy’ and as having a ‘wide’ gradation. The gradation is too wide to be officially classified an EN standard heavy grade, but for rip-rap this is common, as it is generally bulk placed in revetments.

The results of the reference stone analysis indicate that the quarried granite is suitable as armourstone for the construction of the breakwater, as the required stones have a D_{n50} of 0.70m and a median weight M_{50} of 940 kg. However, the grading would be narrower for a breakwater application than for a revetment. Due to the lack of Chilean hydraulic structure design guidelines,

⁶ Using a solid particle density of 2600 kg/m³.

the recommended European EN 13383 grading requirement for a conservative design is highlighted in Table I-2.⁷

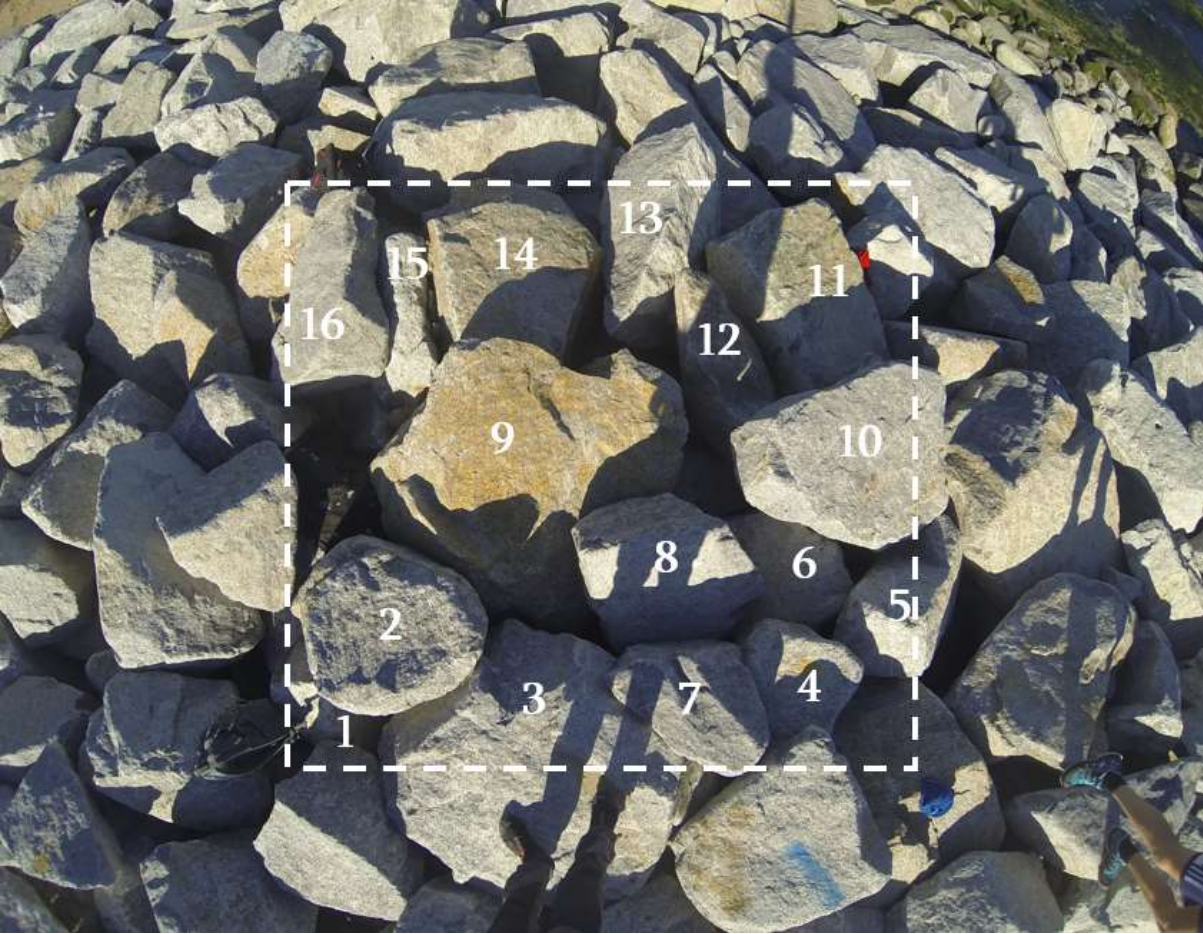


Figure I-1: Analysed stones from shore protection section in Dichato

⁷ Where ELL=Extreme Lower Limit, the mass below which no more than 5% passing by mass is permitted; NLL=Nominal Lower Limit (10%); NUL=Nominal Upper Limit (70%); and EUL=Extreme Upper Limit (97%). M_{em} refers to the effective mean mass, i.e. the average mass of a stone sample without fragments.



Figure I-2: Close-up of granitic armourstone used for shore protection rubble mount at Dichato

Table I-1: Stone dimension and mass analysis

Stone nr.	L (cm)	W (cm)	H (cm)	V (m ³)	M_nominal (kg)	M_sieve size (kg)
1	66	38	30	0.08	196	326
2	96	72	60	0.41	1078	1797
3	162	134	110	2.39	6208	10347
4	87	71	20	0.12	321	535
5	76	50	42	0.16	415	692
6	60	53	43	0.14	356	593
7	66	44	36	0.10	272	453
8	80	74	48	0.28	739	1231
9	155	155	62	1.49	3873	6455
10	125	88	31	0.34	887	1478
11	128	86	60	0.66	1717	2862
12	146	56	50	0.41	1063	1771
13	162	66	56	0.60	1557	2595
14	152	100	75	1.14	2964	4940
15	100	45	24	0.11	281	468
16	127	57	29	0.21	546	910
					M50	1355
					M85	4420.5
					M15	484.8
					M85/M15	9.1

Table I-2: Recommended EN 13383 standard heavy grading (shaded in blue)

Heavy	Class designation	ELL	NLL	NUL	EUL	M_{em}	
	Passing requirements kg	< 5% kg	< 10% kg	> 70% kg	> 97% kg	lower limit kg	upper limit kg
	10 000–15 000	6500	10 000	15 000	22 500	12 000	13 000
	6000–10 000	4000	6000	10 000	15 000	7500	8500
	3000–6000	2000	3000	6000	9000	4200	4800
	1000–3000	700	1000	3000	4500	1700	2100
	300–1000	200	300	1000	1500	540	690

I.2 DICHATO SAND GRADING ANALYSIS

Figure I-3 is an image of a sand sample at the beach of the Marine Biology Centre in Dichato, about 20m up shore from the shoreline. The particle size varies between 0.5mm and 2mm, classifying this sand as coarse to very coarse. At the shoreline, the sand is very coarse.



Figure I-3: Sand sample 20m onshore at Marine Biology Station, Dichato

J EXTREME IMPACT EVALUATION: TSUNAMI LOADS

J.1 COMPUTATION OF FORCES

To calculate the forces caused by a tsunami the method presented by the FEMA, P-55 Coastal Construction Manual (FEMA, 2011) is used. During a tsunami event the following forces can be distinguished:

Hydrostatic forces

The hydrostatic force is the force of the column of water encountering a component. The force acts as a triangular loading and perpendicular to the component. For the breakwater and jetty, the seawater is totally drawn back into the sea in between tsunami waves. When a wave comes in, the hydrostatic pressure is assumed to act as a column of water from one side of the component, as given in Figure J-1.

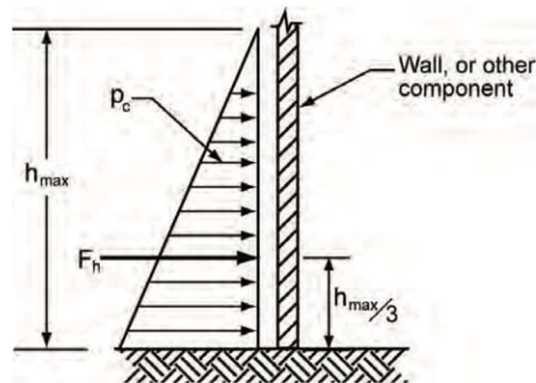


Figure J-1: Hydrostatic force [source: FEMA 2008, p646]

The hydrostatic force is calculated as follows:

$$F_h = \frac{1}{2} \rho_s g b h_{max}^2$$

In which h_{max} is the vertical length between the design run-up height and the base of the structure, b is the width of the element, or the width of the structure to be analysed.

Buoyant forces

The buoyant force equals the weight of the displaced water. The force acts vertically and in upward direction on the components. The formula to calculate the buoyant force:

$$F_b = \rho_s g V$$

In which V is the volume submerged. For the rubble mound breakwater, a pore volume of 40% is assumed. The volume of the beams of the jetty is assumed to be 10% of the volume of the deck.

Hydrodynamic forces

If water is flowing around components such as piles, the deck or stones, the water exerts forces, known as drag forces.

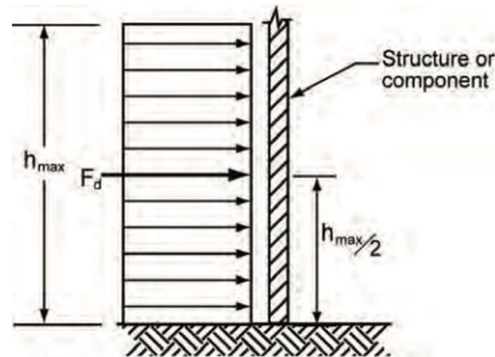


Figure J-2: Hydrodynamic force [source: FEMA 2008, p646]

$$F_d = \frac{1}{2} \rho_s C_d B (hu^2)_{max}$$

The C_d is a drag coefficient, which is assumed to be 2. An important parameter is $(hu^2)_{max}$, which represents a maximum momentum flux per unit mass during the tsunami (m^3/s^2).

Impulsive forces

The impulsive force is the force coming from the leading edge of the wave, hitting the structure at impact. The FEMA recommends for conservatism to take the impulsive forces as 1.5 times the hydrodynamic force, so:

$$F_s = 1.5 * F_d$$

Debris impact force

The debris impact force is the local force (acting on a single member) from waterborne debris hitting the structure during a tsunami. The biggest possible debris in the Coliumo bay are the fishing boats, measuring up to 20m. In this case, a 40ft (12,2m) shipping container is taken as the equivalent, because this is a recommended value, as stated in the FEMA P-646. For the container the m (mass= 30.000 kg) is assumed. To calculate the debris impact force, different approaches are possible.

$$F_i = m * \frac{|u_{max}|}{\Delta t}$$

The u_{max} is an absolute value, because also (especially) the retreating wave is of importance. The Δt is the time for the container to be decelerated. This is assumed to be 0.1s (Tugrul Tankut, 2009).

So far, the forces are to be calculated for the jetty as well as for the breakwater. The following forces only apply to the jetty:

Debris damming forces

When the debris, in this case a shipping container, is accumulated against the jetty, a damming effect occurs. This causes additional forces, acting like a hydrodynamic force. The formula to calculate is similar to the hydrodynamic force:

$$F_{dm} = \frac{1}{2} \rho_s C_d B_d (hu^2)_{max}$$

In this case the B_d is the width of the debris, 12.2m.

Hydrodynamic uplift forces

When the wave hits the jetty, an uplift of the structure is possible, due to the quickly rising water. The following formula describes the maximum uplift per square meter:

$$F_u = \frac{1}{2} \rho_s C_u A_f u_v^2$$

The u_v^2 is the water rise rate (vertical velocity), estimated as:

$$u_v = u \tan(\alpha)$$

in which the u is the horizontal flow velocity and α is the beach slope. The slope of the beach is estimated to be 1/50 and the maximum u horizontal is obtained from the NEOWAVE analysis.

Additional gravity loads

During a tsunami wave, it occurs that a column of water is pressing on the deck of the jetty.

$$f_r = \rho_s g h_r$$

The h_r is the maximum water height above the structure. In this case, the maximum run-up height minus the height of the deck above MSL.

J.2 NUMERICAL TSUNAMI SIMULATION

The forces caused by the tsunami are determined by making use of the numerical model study of the tsunami of 2010 (Aranguiz & Martinez, 2016). The model study is elaborated in NEOWAVE. NEOWAVE (Non-hydrostatic Evolution of Ocean WAVE) is a long wave model for tsunami numerical analysis according to Yamazaki et al 2010 (Yamazaki, 2010). The outcome of the model is obtained with help of professor Rafael Aránguiz from the UCSC (Universidad Católica de la Santísima Concepcion). Professor Aránguiz is one of the 5 (!) coastal engineers in Chile and is specialised in tsunamis.

In the numerical model study is the tsunami caused by the Maule earthquake in February 2010 simulated. The model is validated on data obtained from a Tide gauge on Dichato beachfront. The outcomes of the study are presented in Figure J-3. For the calculation of the tsunami forces datasets of 4 locations around the Marine Biology Center are extracted from the model. The exact locations are depicted in Figure J-4.

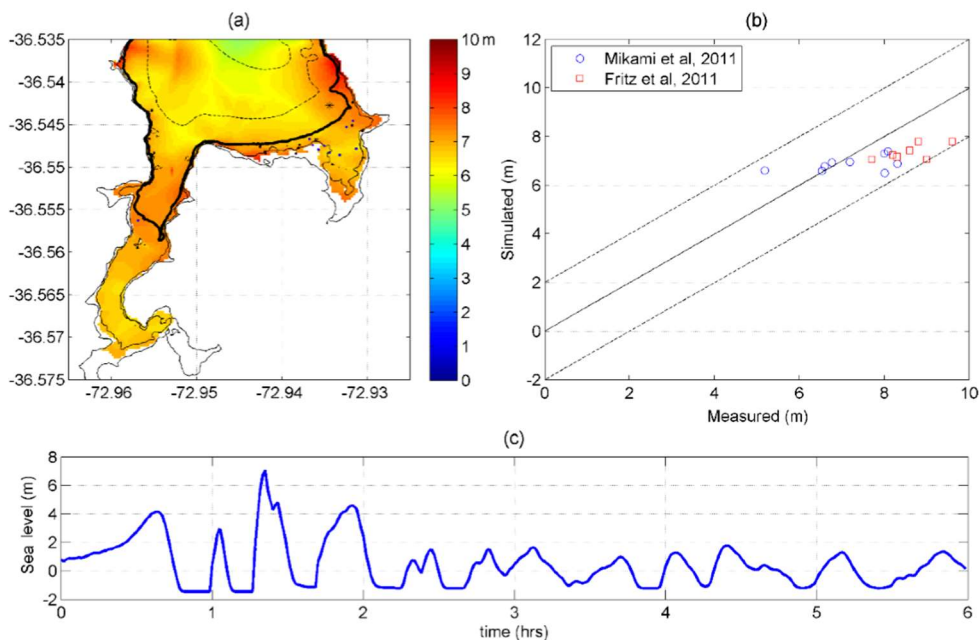


Figure J-3: (a) Inundation area obtained in the numerical simulation (b) Comparison of measured and simulated data (c) Tide gauge on Dichato beachfront



Figure J-4: Location of data sets

The data includes an x- and y-velocity and a water level, simulated as the tsunami of 2010. From the x- and y velocity, a nett velocity is obtained. With the use of MATLAB, the (hu^2) is calculated for every timestep of the simulated tsunami. In Figure J-5 the x-, y-, and nett velocity are given and the corresponding water level. What is important to notice is the long time frame of a tsunami and the third wave to be the largest (in this case).

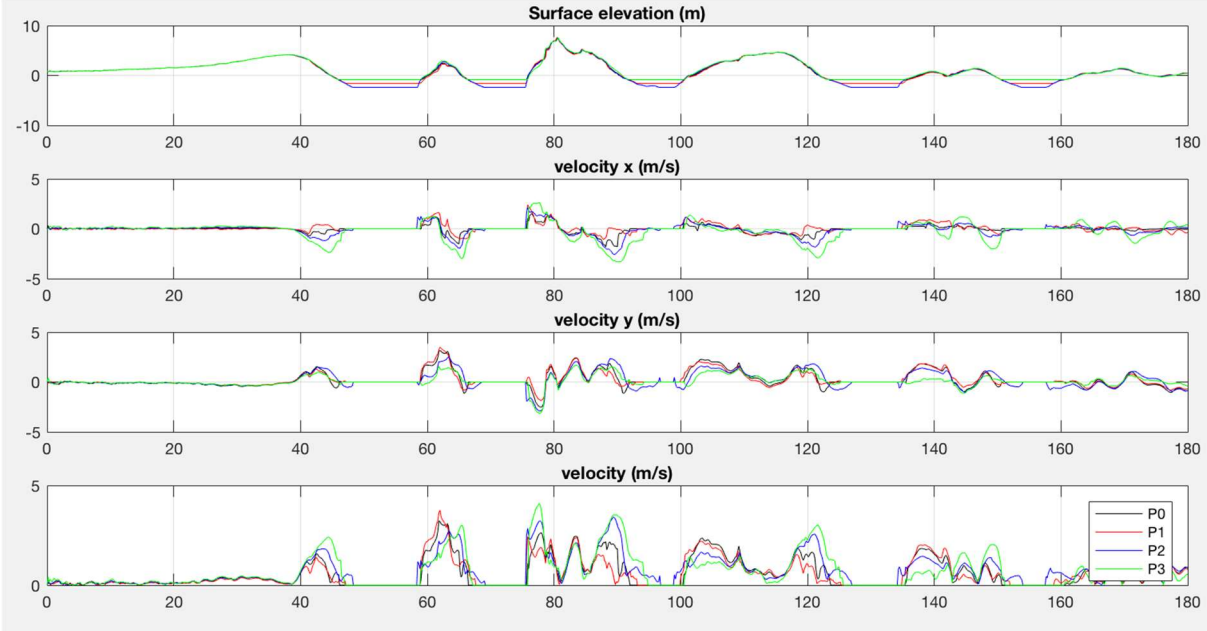


Figure J-5: Simulated water surface elevation, x-, y-, and net velocity during the 2010 tsunami

In Figure J-6 the calculated (hu^2) is given. The maximum for this case is at location 3: 34.22 (m³/s²). With this data the hydrodynamic forces can be calculated.

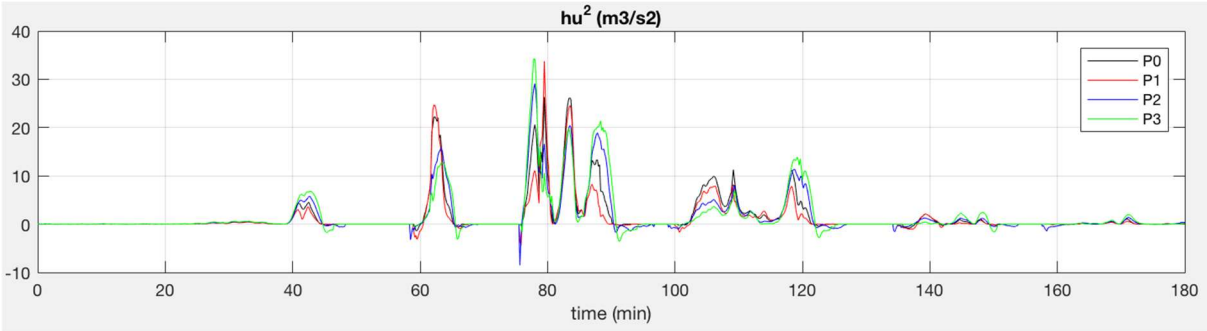


Figure J-6: hu² calculated via MATLAB, simulated for the 2010 tsunami in Coliumo bay

J.3 ASSUMPTIONS

The following assumptions have to be made for the calculation of tsunami forces.

Sea water density - ρ_w

The sea water density during a tsunami increases due to the mixture of sediment with seawater. Based on an assumption of a 10% volume concentration of sediment in seawater, the water density (ρ_w) increases to 1200 kg/m³.

Run-up height tsunami - R

The run-up heights of tsunamis are extremely variable along the coast, due to detailed local bathymetry and topography. In the calculation of tsunami forces, an additional 30% is added to the calculated run-up heights. The run-up height at the Marine Biology Center is calculated using a NEOWAVE model study. A predicted run-up height (R^*) of 8m is determined, giving an design run-up height (R) of $1.3 \cdot 8 = 10.4\text{m}$. (Martínez, Rojas, Villagra, Aranguiz, & Salazar-Carrillo, 2016) The results of the model are given in Figure J-7

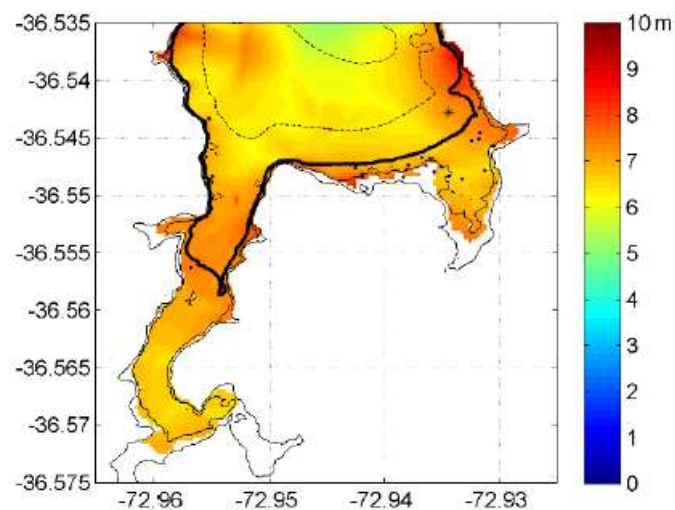


Figure J-7: Inundation area in Coliumo bay obtained with numerical simulation (Aranguiz & Martinez, 2016)

J.4 RESULTS

Combining the FEMA method with the outcomes of the Numerical tsunami simulation gives the following forces on the structure. For both the breakwater and the jetty the different forces are determined. Depending on the forces a distinction is made between the different parts of the jetty. The forces on the jetty are shown in Table J-1. The forces on the breakwater are shown in Table J-2.

Table J-1: Tsunami forces acting on the jetty

<u>Jetty</u>	<u>Piles</u>		<u>Deck</u>		<u>Total structure</u>	
	<i>value</i>	<i>unit</i>	<i>value</i>	<i>unit</i>	<i>value</i>	<i>unit</i>
Hydrostatic	14,47	kN/m length	23,84	kN/m width		
Hydronamic	14,87	kN/m length	22,59	kN/m width		
Impulsive	22,3	kN/m length	33,88	kN/m width		
Debris Impact					1230	kN
Buoyant					3,71	kN/m ²
Debris damming					492,76	kN
Uplift					0,3	kN/m ²
Additional gravity					61,8	kN/m ²

Table J-2: Tsunami forces acting on the breakwater

<u>Breakwater</u>		
<i>Force</i>	<i>value</i>	<i>unit</i>
Hydrostatic	15,1	kN/m width
Buoyant	42,4	kN/m width
Hydronamic	41,1	kN/m width
Impulsive	61,6	kN/m width
Debris Impact	1230	kN

J.5 LOAD COMBINATIONS

Not all tsunami loads will take place at the same time, consequently load combinations are composed. According to FEMA, P-55 Coastal Construction Manual (FEMA, 2011) tsunami load effects can be defined as displayed in Table J-3.

For the debris impact force, two worse case scenarios are taken into account. Firstly, the force is applied in the middle of the pile situated at grid point G1, called $F_{i,1}$. Secondly, the impact force is applied in the middle of the pile located at grid point D1, called $F_{i,2}$.

Also for the debris damming force, two scenarios are analysed. The first case describes the force acting on three piles located at grid point C1, D1, and E1. The second case describes the force acting on three piles situated at grid point E1, F1, and G1.

The hydrostatic forces only need to be considered in load combinations on individual components which does not belong to the scope of this project.

Table J-3: Tsunami load combinations

	F_h	F_b	F_d	F_s	$F_{i,1}$	$F_{i,2}$	$F_{dm,1}$	$F_{dm,2}$	F_u	F_r
$T_{s,1}$										
$T_{s,2}$										
$T_{s,3}$										
$T_{s,4}$										
$T_{s,5}$										
$T_{s,6}$										

The tsunami load effects (T) should be included in the following Strength Design Load Combinations:

$$\text{Load Combination 1: } 1.2 D + 1.0 T_s + 1.0 L_{REF} + 0.25L$$

$$\text{Load Combination 2: } 0.9 D + 1.0 T_s$$

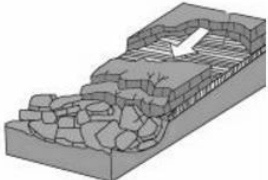


Where D is the dead load of the structure and L includes the live load on the structure. L_{REF} is the live load in the refuge area which is not of importance for this design and can be set to zero.

K EXTREME IMPACT EVALUATION: GEOHAZARDS

K.1 SLOPE FAILURE

K.1.1 BACKGROUND INFORMATION

Slope failures and landslides are defined by the Chilean Ministeria de Minería as any gravity driven downhill movement of a mass of rock, debris or soil. Slope failures have different contributing geologic, morphologic, physical and anthropological factors (Cruden and Varnes 1996). Some of the more common triggers of slope failures in the Chilean coastal area include seismic deformation and intense precipitation. Slope failures are classified per type of movement and the material involved, and may be discontinuity orientation dependent or independent, involving sliding and toppling, and mass failure, respectively (Hack et al. 2003). The most common types of failure in the Concepción, Talcahuano and Hualpén area are:

Discontinuity dependency	Slope failure mode	Description	Schematization
Orientation dependent (local failure)	Rock and soil sliding	Downhill movement of rock or soil mass along one or more discontinuities. In study area, often caused by strong seismic activity and heavy rains.	
Orientation independent (mass failure)	Rock fall	Blocks of rock detach rapidly from a slope surface and fall freely.	
	Debris flow	Mass failure with fluid-like behaviour. Rapid to very rapid flow of saturated, non-plastic debris, confined to one or more flow channels.	

K.1.2 SLOPE FAILURES IN CONCEPCIÓN AREA

Figure K-1 shows a landslide hazard map of the urban areas to the west of the Bay of Concepción, with Dichato lying slightly off the map to the North-East. Considering the similarities in geology within the area, this map can be used as a reference for landslide hazards around Columio Bay and in Dichato. The methodology for creating the landslide hazard map of Figure K-1 involved a heuristic approach with a combination of qualitative and semi-quantitative methods. An overlay was made of thematic maps of the main contributing factors to instability: geology, slope of terrain, and observed past slope failures.



Figure K-1: Landslide hazard map of west of Concepcion Bay, indicating slopes with high risk of landsliding, rockfall or debris flow in red or pink

The most common type of slope failures observed in the study area are rotational slides in regolith or soil formed from the chemical weathering of igneous and sedimentary rocks. Steep slopes or ones altered for construction are most vulnerable, and are mostly activated in times of seismic activity or heavy precipitation. Translational rock slides are observed in metamorphic rock along the main foliation direction or along contact surfaces with dykes and intrusions. Debris flows are common in areas with weathered granite. Rockfall phenomena occur mainly in the marine abrasion zone of the coastal cliffs, with lesser effect on the urban areas. Several of these phenomena may apply to Dichato, since the slopes are generally steep ($>25^\circ$, see Figure K-4) and there are granodioritic intrusions along the coastal slopes.

K.1.3 SLOPE INSTABILITY ASSESSMENT AT MARINE BIOLOGY STATION

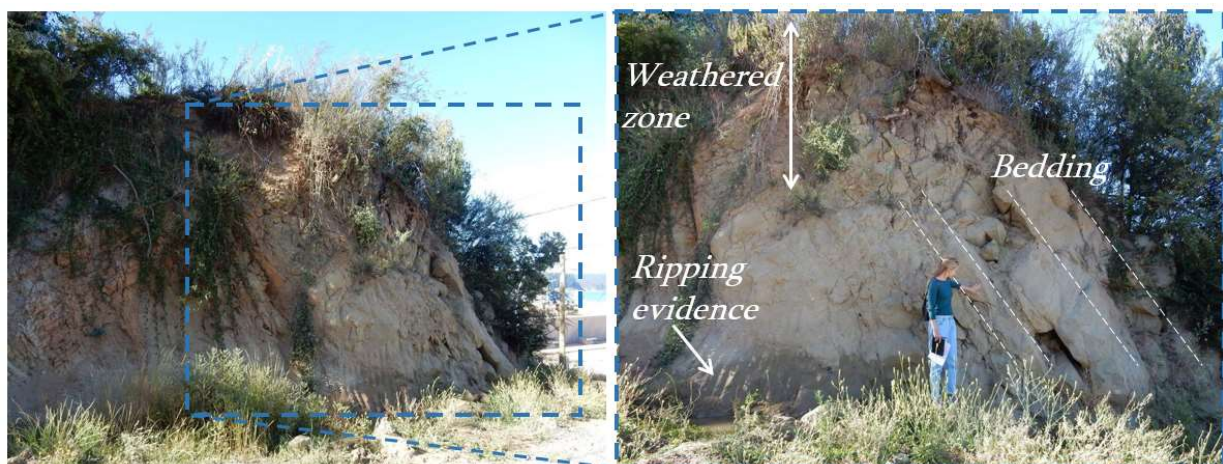


Figure K-2: Analysed slope across road from EMBD



Figure K-3: Close-up of slope material showing opened up joints (left) and medium-grained texture of rock (right)

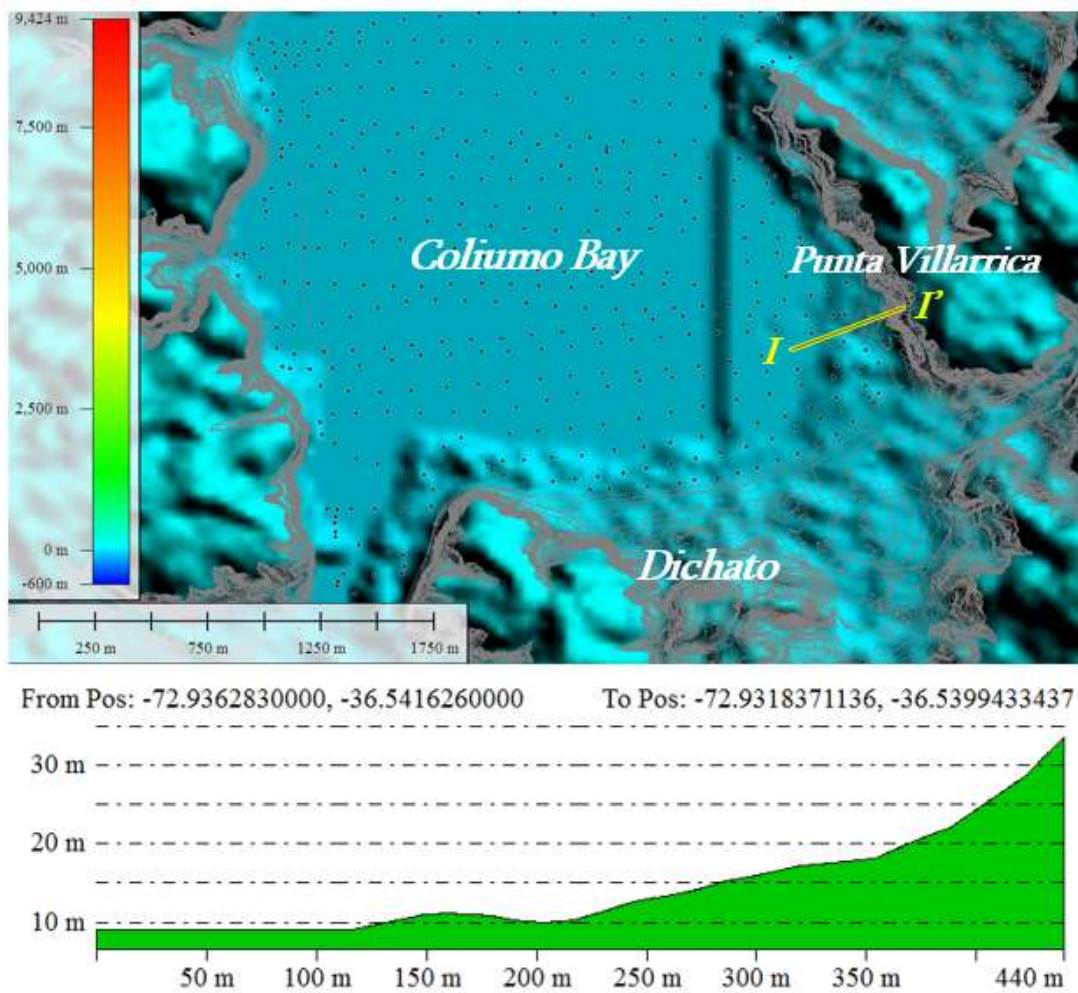
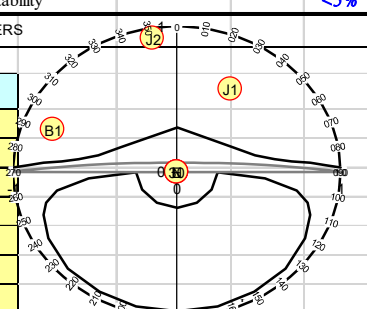


Figure K-4: Bathymetry and onshore topography for profile I-I' at Punta Villarrica (location of slope). 0 m level refers to Mean Sea Level, MSL.

K.1.4 SSPC FORM FOR MARINE BIOLOGY STATION SLOPE

ITC /TUD ENGINEERING GEOLOGY			exposure characterization				SSPC. SYSTEM	
LOGGED BY: <i>P. Lamens</i>			DATE: <i>23/12/2016</i>	TIME (hr): <i>09:15</i>		exposure no: <i>445-uu</i>	<i>1</i>	
WEATHER CONDITIONS			LOCATION				map no: <i>445-uu</i>	
Sun: (cloudy/fair/bright) <i>bright</i>			Map coordinates:				northing: <i>739.940</i>	
Rain: dry / drizzle/ slight/heavy <i>dry</i>							eastings: <i>983.640</i>	
METHOD OF EXCAVATION (ME)			DIMENSIONS/ ACCESSIBILITY					
insert value			Size total exposure: (m) l: <i>20</i> h: <i>5</i> d: <i>10</i>					
natural/hand-made: <i>1.00</i>			mapped on this form (m) l: <i>10</i> h: <i>5</i> d: <i>5</i>					
pneumatic hammer excavation: <i>0.76</i>			Accessibility: <i>poor/fair/good</i> <i>good</i>					
pre-splitting/smooth wall blasting: <i>0.99</i>			Sketch: 					
conventional blasting with result:								
good: <i>0.77</i>								
open discontinuities: <i>0.75</i>								
dislodged blocks: <i>0.72</i>								
fractured intact rock: <i>0.67</i>								
crushed intact rock: <i>0.62</i>								
FORMATION NAME:			<i>Curanilahue Formation sandstone</i>					
DESCRIPTION (BS 5930: 1989)								
colour	grain size	structure & texture	weathering	NAME				
<i>Yellowish grey</i>	<i>Fine-medium</i>	<i>Thinly-thickly bedded</i>	<i>Moderate</i>	<i>SANDSTONE (Curanilahue Formation)</i>				
INTACT ROCK STRENGTH (IRS) insert average value				sample number(s):		WEATHERING (WE)		
< 1.25 MPa	Crumbles in hand					insert value		
1.25 - 5 MPa	Thin slabs break easily in hand		<i>3.125</i>			unweathered	<i>1</i>	
5 - 12.5 MPa	Thin slabs broken by heavy hand pressure					slightly	<i>0.95</i>	
12.5 - 50 MPa	Lumps broken by light hammer blows					moderately	<i>0.9</i>	
50 - 100 MPa	Lumps broken by heavy hammer blows					highly	<i>0.62</i>	
100 - 200 MPa	Lumps only chip by heavy hammer blows (Dull ringing sound)					completely	<i>0.35</i>	
> 200 MPa	Rocks ring on hammer blows. Sparks fly							
DISCONTINUITIES			1	2	3	4	5	EXISTING SLOPE?
Discontinuity type: B=bedding C=cleavage J=joint			<i>B1</i>	<i>J1</i>	<i>J2</i>			dip-direction (°) dip (°)
Dip direction (degrees)			<i>111</i>	<i>210</i>	<i>171</i>			<i>176</i> <i>80</i>
Dip (degrees)			<i>70</i>	<i>55</i>	<i>82</i>			
Spacing (DS) (m)			<i>0.05</i>	<i>0.10</i>	<i>0.20</i>			height (m): <i>5.0</i>
Persistence								Stability (tick)
along strike (m)			<i>1</i>	<i>0.5</i>	<i>2.5</i>			stable: <i>1</i>
along dip (m)			<i>5</i>	<i>1.5</i>	<i>1</i>			small problems in near future: <i>2</i>
CONDITION OF DISCONTINUITIES								large problems in near future: <i>3</i>
Roughness large scale (R1) (on an area between 0.2x0.2 and 1x1 m ²)	wavy:	1.00						small problems: <i>4</i>
	slightly wavy:	0.95						large problems: <i>5</i>
	curved:	0.85			<i>0.80</i>			
	slightly curved	0.80	<i>0.80</i>	<i>0.80</i>				
	straight	0.75						
Roughness small scale (Rs) (on an area of 0.2x0.2 m ²)	rough stepped	0.95						notes: 1) For infill 'gouge' irregularities' and 'flowing material' small scale roughness = 0.55. 2) If roughness is anisotropic (e.g. ripple marks, striation, etc.) roughness should be assessed perpendicular and parallel to the roughness and directions noted on this form. 3) Non-fitting of discontinuities should be marked in roughness columns.
	smooth stepped	0.90						
	polished stepped	0.85						
	rough undulating	0.80	<i>0.80</i>	<i>0.80</i>				
	smooth undulating	0.75			<i>0.75</i>			
	polished undulating	0.70						
	rough planar	0.65						
	smooth planar	0.60						
polished planar	0.55							
Infill material (Im)	cemented/cemented infill	1.07						
	no infill- surface staining	1.00		<i>1.00</i>	<i>1.00</i>			
	non-softening & sheared material, coarse	0.95						
	medium	0.90						
	fine	0.85						
	e.g. free of clay, soft sheared coarse	0.75	<i>0.75</i>					
	medium	0.65						
	talca, etc. fine	0.55						
gouge < irregularities	0.42							
gouge > irregularities	0.17							
flowing material	0.05							
Karst (Ka)	none	1.00	<i>1.00</i>	<i>1.00</i>	<i>1.00</i>			
	karst	0.92						

LOGGED BY:	<i>P.Lamens</i>	DATE:	<i>23/12/2016</i>	exposure no:	<i>1</i>	
REFERENCE UNIT NAME	<i>Curanilahue Formation sandstone</i>					
INTACT ROCK STRENGTH (RIRS)						
If IRS (<i>3.13</i>) > 132 MPa then RIRS=132 otherwise RIRS = IRS (in MPa) / WE (WE= <i>0.9</i> , correction for weathering) <i>3</i>						
DISCONTINUITY SPACING (RSPA)						
DISCONTINUITIES	1	2	3	4	5	SPA (see figure)=
Discontinuity type: B=bedding C=cleavage	<i>J1</i>	<i>J2</i>	<i>J3</i>			factor 1 * factor 2 * factor 3 =
Dip direction (degrees)	<i>111</i>	<i>210</i>	<i>171</i>			<i>0.48 * 0.50 * 0.53 = 0.128</i>
Dip (degrees)	<i>70</i>	<i>55</i>	<i>82</i>			corrected for weathering and method of excavation:
Spacing (DS) (m)	<i>0.05</i>	<i>0.10</i>	<i>0.20</i>			RSPA = SPA / (WE*ME) (with a maximum of 1.00)
The spacing parameter (SPA) is calculated based on the three discontinuities with the minimum spacing based on the figure below:						RSPA = <i>0.13</i> / <i>0.9</i> * <i>1.00</i> = <i>0.142</i>
CONDITION OF DISCONTINUITIES (RTC & RCD)						
DISCONTINUITIES	1	2	3	4	5	
Roughness large scale (Rl)		0.80	0.80	0.80		
Roughness small scale (Rs)		0.8	0.8	0.75		
Infill material (Im)		0.75	1	1		
Karst (Ka)		1	1	1		
Total (Rl*Rs*Im*Ka=TC)		0.48	0.6400	0.6000		
RTC=TC/√(1.452-1.228e ^{-WE})		0.491763	0.65568	0.61470362		RTC = TC / sqrt(1.452-1.228*exp(-WE))
Weighted by spacing:						
				TC1 TC2 TC3		<i>0.48 0.64 0.60</i>
				DS1 DS2 DS3		<i>0.05 0.10 0.20</i>
				CD=		<i>0.54</i>
				DS1 DS2 DS3		<i>0.05 0.10 0.20</i>
corrected for weathering; RCD (with maximum of 1.0165)= CD/WE <i>0.543</i> / <i>0.90</i> = <i>0.60</i>						
REFERENCE UNIT FRICTION and COHESION (RFRI) & (RCOH)						
Rock mass friction: RFRI = RIRS*0.2417 + RSPA * 52.12 + RCD*5.779						
				3 * 0.2417 +		0 * 52.12 + 0.60 * 5.78 = <i>12°</i>
Rock mass cohesion RCOH = RIRS*94.27 + RSPA * 28629 + RCD*3593						
				3 * 94.27 +		0 * 28629 + 0.60 * 3593 = <i>6572.13</i>

1. Determination ORIENTATION INDEPENDENT STABILITY											
(SLOPE) INTACT ROCK STRENGTH SIRS =							RIRS	SWE	SIRS		
RIRS (from reference rock mass) * SWE (weathering slope) =								3	0.90	3	
DISCONTINUITY SPACING SSPA =							RSPA	SWE	SME	SSPA	
RSPA (from reference rock mass) * SWE (weathering slope)* SME (method excavation of slope) =							0.14	0.90	1.00	0.128	
CONDITION OF DISCONTINUITIES SCD =							RCD	SWE	SCD		
RCD (from reference rock mass) * SWE (weathering slope) =								0.603	0.90	0.543	
SLOPE UNIT FRICTION SFRI =				SIRS	coeff	SSPA	coeff	SCD	coeff	SFRI	
Rock mass friction = SIRS*0.2417 + SSPA *52.12 + SCD*5.779				2.81	0.24	0.13	52.12	0.54	5.78	10°	
SLOPE UNIT COHESION SCOH =				SIRS	coeff	SSPA	coeff	SCD	coeff	SCOH	
Rock mass cohesion= SIRS*0.09427 + SSPA *28.629 + SCD*3.593				2.81	0.09	0.13	28.63	0.54	3.59	6kPa	
MAXIMUM SLOPE HEIGHT (Hmax) = if SFRI>slope dip=slope height otherwise =							coeff	SCOH	SDIP	SFRI	Hmax
0.16*SCOH*sin(slope dip)*cos(SFRI)/(1-cos(slope dip -SFRI))							0.16	5.89	80.00	10	1.4
ratios:				SFRI / slope dip =			10.50	° /	80.00	° =	0.1
				Hmax/Hslope			1.40	m /	5.00	m =	0.3
Probably stable: if SFRI> slope dip, stability probability = 100%. Otherwise use figure for orientation independent stability											
ORIENTATION DEPENDENT STABILITY											
DISCONTINUITIES						SKIERS					
Type: B=bedding C=cleavage J=joint	B ₁	J ₁	J ₂	N	E	W					
Dip direction °	111	210	171								
Dip °	70	55	82								
With, Against, Vertical or Equal											
AP = arctan (cos δ * tan β) °	49.3	49.8	82.0								
RTC (from reference form)	0.49	0.66	0.61								
STC = RTC * sqrt(1.452-1.22*e^(-S))	0.48	0.64	0.60								
Probably stable:	5%	100%	100%								

K.1.5 MITIGATION MEASURES

The Chilean Ministeria de Minería has several recommendations for mitigation of slope failure. As precautionary measures, construction of non-resilient or sensitive buildings is discouraged in zones of high slope failure risk. Also, altering relief for construction is not recommended in sensitive areas, as well as deforestation or alteration of water bodies and streams. For existing unstable slopes, also measures are suggested. In highly cracked zones of rock slopes, induced by the earthquake event, water management measures in the form of drains, for example, are necessary to avoid debris flows due to infiltrating rain water. To avoid erosion by the tsunami at the toe of the slope, mass could be added here.

L STRUCTURAL DRAWINGS

L.1 3D IMPRESSIONS

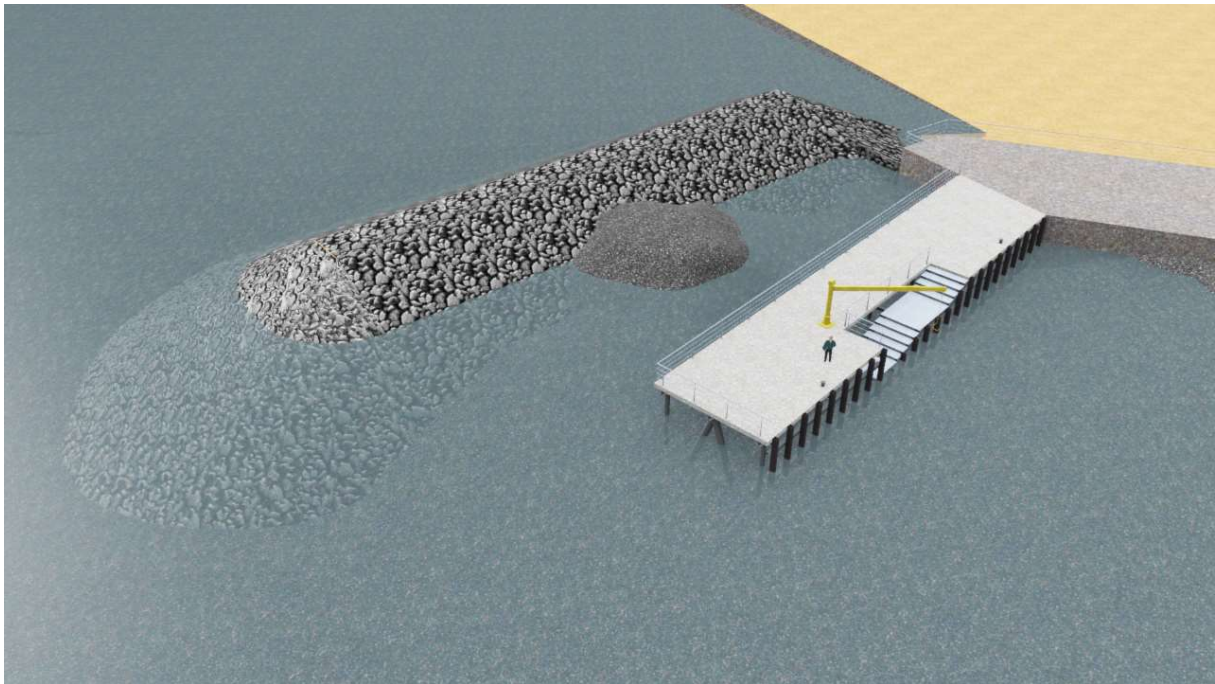


Figure L-1: Jetty and breakwater

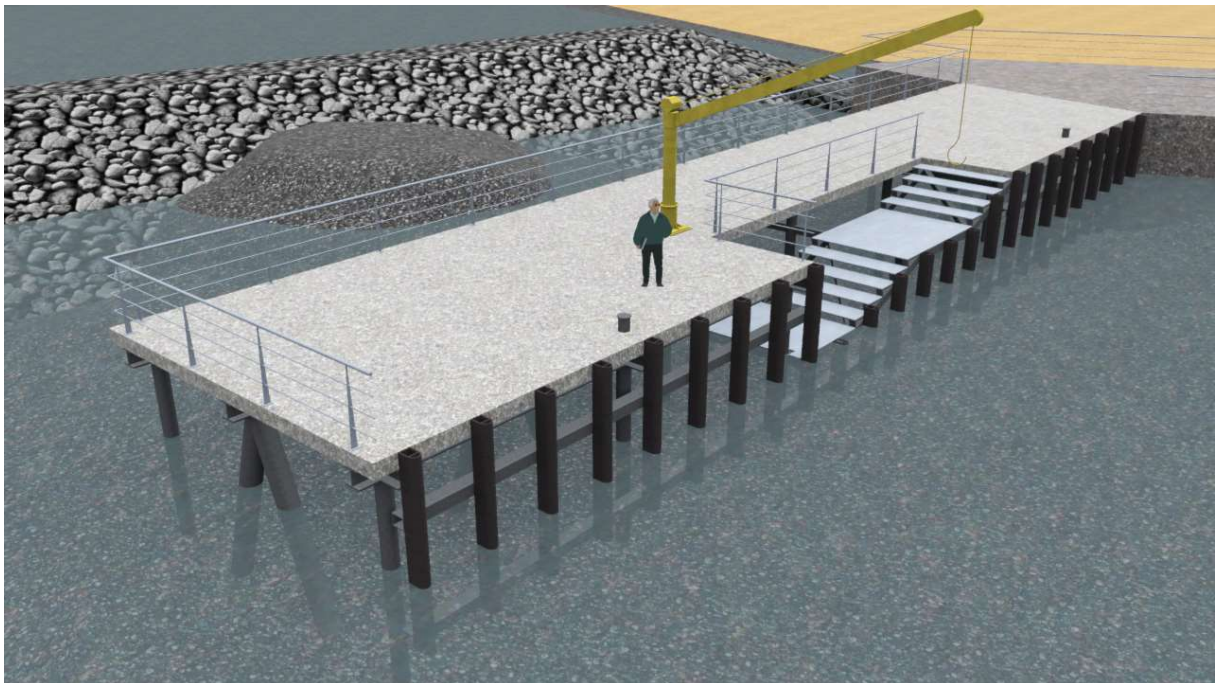


Figure L-2: Jetty in close-up



Figure L-3: Mooring side



Figure L-4: Structural framework

REFERENCES

- (2017). Retrieved from SWAN: <http://swanmodel.sourceforge.net/>
- AASHTO, L. (1998). *Bridge design specifications*.
- Acero, I. C. (2000). *Manual de diseño para estructuras de acero*. Instituto Chileno de Acero S.A.
- ACI Committee 318. (2008, January). Building Code Requirements for Structural Concrete (ACI 318-08) and Commentary. American Concrete Institute.
- American Institute of Steel Construction. (2010, June 22). Specification for Structural Steel Building. American Institute of Steel Construction.
- Aranguiz, R., & Martinez, C. (2016). Riesgo de tsunami y planificación resiliente de la costa chilena. *Revista de Geografía Norte Grande*, 33-54.
- Archila, M. e. (2013). Modal Testing of a Repaired Building After 2010 Chile Earthquake. *Topics in Dynamics of Civil Structures*, 119-125.
- Awad, A., & Ayoub, A. (1976). Ultimate uplift capacity of vertical and inclined piles in cohesionless soil. *Proceedings of the 5th international conference on soil mechanics and foundation engineering, Budapest*.
- Baeriswyl, S. (2015). Nuevos desafíos urbanos y nuevas herramientas de planificación. *Urbano 9*.
- BMT Argoss. (2016, May). Wave Climate.
- BMT Argoss. (2016, 05). www.waveclimate.com. (BMT Argoss) Retrieved 12 2016, from www.bmtargoss.com.
- BREAKWAT*. (2017, 01 10). Retrieved from Deltares: <https://www.deltares.nl/en/software/breakwat/>
- Brinkgreve, R. (2016). *PLAXIS 2016*. The Netherlands: Plaxis bv.
- Brzev, S. e. (2010). *Performance of confined masonry buildings in the February 27, 2010 Chile earthquake*. Oakland, California: Earthquake Engineering Research Institute (EERI).
- Bustos, A. (2016, December 22). Lecture on Seismically Isolated Structures. UdeC, Concepcion.
- Canam Group. (2016). *Seismic Isolators: GOODCO Z-TECH*. Quebec.
- Central Intelligence Agency. (2013). *The World Factbook 2012-2013*. Central Intelligence Agency.
- Chavez, J., Khemici, O., Khater, M., & Keshishian, P. (2010). *Building Codes and Relative Seismic Vulnerability in Latin American Countries*.

- De Jong, R. (1996). *Wave transmission at low-crested structures. Stability of tetraods at front, crest and rear of a low-crested breakwater*. Delft University of Technology.
- Eldeberky, Y. (1996). *Nonlinear transformation of wave spectra in the nearshore zone*. Delft University of Technology.
- ETABS. (2016, 12 19). ETABS (2016) [Software].
- FEMA. (2008). *Guidelines for Design of Structures for Vertical Evacuation from Tsunamis*. NOAA, FEMA. California: FEMA.
- FEMA. (2011). *Coastal Construction Manual P-55; Principles and Practices of Planning, Siting, Designing, Constructing, and Maintaining Residential Buildings in Coastal Areas (Fourth Edition)*. FEMA, Washington.
- Gerdau AZA S.A. (2010). *Identificación y calidades del acero de refuerzo AZA para hormigon*.
- Hackley, P. e. (2006). World coal quality inventory: Chile. *World coal quality inventory: South America, USGS*, 90-131.
- Haigh, S. K. (2000). Lateral spreading during centrifuge model earthquakes. *ISRM International Symposium*. International Society for Rock Mechanics.
- Hasselmann, S., Hasselmann, K., Allender, J., & Barnett, T. (1985). Computations and parameterizations of the nonlinear energy transfer in a gravity wave spectrum. *J. Phys. Oceanogr.*, pp. 1378-1391.
- Heerkens, E. (2014). *De bouwkundige uitdaging in het noorden*. Ermelo: NAM.
- Hidalgo, O. P. (1986). Norma Chilena Oficial Nch1537.Of86. *Diseño estructural de edificios - Cargas permanentes y sobrecargas de uso*. Instituto Nacional de Normalización.
- Holthuijsen, L. (2007). *Waves in oceanic and coastal waters*. TU Delft and UNESCO-IHE. Cambridge: Cambridge.
- Humire Guarachi, F., Saez Robert, E., & Leyton Florez, F. (2015). *Manual de Aplicacion de Tecnicas Geofisicas Basadas en Ondas de Superficie para la Determinacion del Parametro Vs30*. Instituto de la Construccion.
- Ilic, S. (1994). *The role of offshore breakwaters in the coastal defence: Comparison of two measurement systems*. University of Plymouth School of Civil and Structural Engineering.
- Immervoll, H. (2011). *Redistribution policy and inequality reduction in OECD countries: what has changed in two decades?*
- INN. (1996). *Earthquake Resistant Design of Buildings, NCh433.Of96*. Santiago, Chile: Instituto Nacional de Normalizacion.

- INN. (2008). *Reinforced Concrete*. Santiago, Chile: Instituto Nacional de Normalizacion.
- Instituto Chileno del Acero. (2000). Manual de diseño para estructuras de acero. *Metodo de factores de carga y resistencia*. Instituto Chileno del Acero S.A.
- Ishiyama, Y., Takada, T., Fukushima, S., & Inoue, T. (2006). Seismic Loads. In *Recommendations for Loads on Buildings*. Architectural Institute of Japan.
- Islam, A., Jameel, M., & Zamin Jumaat, M. (2011). Seismic isolation in buildings to be a practical reality: behaviour of structure and installation technique. *Journal of Engineering and Technology Research*, 3(4), 99-117.
- Lagos, R., Kpuffer, M., Lindenberg, J., & Bonelli, P. (2012). Seismic Performance of High-Rise Concrete Buildings in Chile. *International Journal of High-Rise Buildings*, 1(3), 181-194.
- Lomnitz, C. (2004). Major earthquakes of Chile: a historical survey 1535-1960. *Seismological Research Letters*, 368-378.
- Martínez, C., Rojas, O., Villagra, P., Arañguiz, R., & Salazar-Carrillo, K. (2016). *Risk Factors and Perceived Restoration in a Town Destroyed by the 2010 Chile Tsunami*. Nat. Hazards Earth Syst. Sci., Santiago.
- Melnick, D. e. (2009). Segmentation of megathrust rupture zones from fore-arc deformation patterns over hundreds to millions of years, Auraco peninsula, Chile. *Journal of Geophysical Research: Solid Earth*.
- Moreno, M., Rosenau, M., & Oncken, O. (2010). 2010 Maule earthquake slip correlates with pre-seismic locking of Andean subduction zone. *Nature*, 198-202.
- NEHRP Consultants. (2012). *Comparison of U.S. and Chilean building code requirements and seismic design practice 1985-2010*. U.S. Department of Commerce.
- NEHRP Consultants. (2012). *Comparison of U.S. and Chilean building code requirements and seismic design practice 1985-2010*. U.S. Department of Commerce.
- Nishenko, S. (1985). Seismic potential for large and great interplate earthquakes along the Chilean and southern Peruvian margins of South America: a quantitative reappraisal. *Journal of Geophysical Research: Solid Earth* 90.B5, 3589-3615.
- NPR9998. (2015). *Normcommissie 351 001: Assessment of buildings in case of erection, reconstruction and disapproval -Basic rules for seismic actions: induced earthquakes*. Retrieved March 15, 2016
- OCAD. (2009). *Technical standards and commentaries for port and harbour facilities in Japan*. Overseas Coastal Area Development Institute of Japan.

- Okada, Y. (1985). Surface deformation due to shear and tensile faults in a half-space. *Bulletin of the seismological society of America* 75.4, 1135-1154.
- PDCA. (2001). Recommended design specifications for driven bearing piles. Pile Driving Contractors Association.
- Pender, M. (1995). Earthquake resistant design of foundations. Melbourne: Pacific Conference on Earthquake Engineering.
- Precolombino, C. (2016). *Indigenous Stories of Mapuche: Kai Kai y Treng Treng*. Retrieved from Museo Chileno de Arte Precolombino: <http://chileprecolombino.cl/en/arte/narraciones-indigenas/mapuche/kay-kay-tren-tren/>
- Research, C. I. (2007). *The Rock Manual: The use of rock in hydraulic engineering*. Ciria.
- SAFE. (2016). SAFE (2016) [Software].
- Sandoval Munoz, C. A. (2010). *Diseno del Atracadero para la Estacion Biologia Marine en Dichato*. Concepcion: Universidad de Concepcion.
- Santander, A. (2016, 12 16). Obras maritimas y costeras para el pais. UdeC, Concepcion.
- Schiereck, G. (2003). *Introduction to bed, bank and shore protection*. CRC Press.
- Soloviev, S., & Go, N. (1975). *Catalog of Tsunamis on the Eastern Shore of the Pacific Ocean*. Academy of Science of the USSR.
- Steel Flooring Products Co. (n.d.). *Straight flight staircases*. Retrieved 12 19, 2016, from Steel Flooring Products: <http://www.steelflooring.ie/index.html>
- Thenoux, G., & al, e. (2002). *Guía de diseño estructural de pavimentos para caminos de bajo volumen de tránsito*. Dirección de Vialidad, Ministerio de Obras Públicas de Chile.
- Tokimatsu, K., & Hiroshi, A. (2004). S-wave velocity profiling by inversion of microtremor H/V spectrum. *Bulletin of the Seismological Society of America*, 53-63.
- Tol, A. (2006). *CTB1410(67) Funderingstechnieken*. Delft, The Netherlands: Delft University of Technology.
- Tugrul Tankut, A. (2009). *Earthquakes and Tsunamis: Civil Engineering Disaster Mitigation Activities*. Middle east technical university, Geotechnical, Geological and earthquake engineering. Ankara: Springer.
- Udias, A. e. (2012). The large Chilean historical earthquakes of 1647, 1657, 1730 and 1751 from contemporary documents. *Bulletin of the Seismological Society of America*, 1639-1653.

- Verhagen, H. J., d'Angremond, K., & van Roode, F. (2009). *Breakwaters and closure dams*. TU Delft. Delft: VSSD.
- Verhagen, H., d'Angremond, K., & van Roode, F. (2009). *Breakwaters and closure dams*. TU Delft, Coastal engineering. Delft: VSSD.
- Vucetic, M. (1992). Soil properties and seismic response. Rotterdam: Earthquake Engineering, Tenth World Conference.
- Waltham, T. (2009). *Foundations of engineering geology*. CRC Press.
- Wijdeven, B. (2015). *Marinas and cruise terminals (Ports and Waterways 2)*. Presentatie, TU Delft, Hydraulic engineering, Delft.
- Yamazaki, Y. (2010). Depth-integrated, non-hydrostatic model with grid nesting for tsunami generation,. *International Journal for Numerical Methods in Fluids*, 2081–2107.
- Youd, T., Idriss, I., Andrus, R., & Arango, I. (2001). "Liquefaction resistance of soils: summary report from the 1996 NCEER and 1998 NCEER/NSF workshops on evaluation of liquefaction resistance of soils. *Journal of geotechnical and geoenvironmental engineering* 127.10, 817-833.